

**INVESTIGATION OF SOIL ARCHING STABILITY UNDER  
STATIC AND CYCLIC SURFACE LOADING USING  
TRAPDOOR MODEL TESTS**

By

**Mahdi Abbas Mahdi Al-Naddaf**

Submitted to the graduate degree program in the Department of Civil, Environmental, and Architectural Engineering and the Graduate Faculty of the University of Kansas in partial fulfillment of the requirements for the degree of Master of Science.

---

Dr. Jie Han, Chairperson

---

Dr. Anil Misra

---

Dr. Robert L. Parsons

Date Defended: 03/10/2017

The Thesis Committee for Mahdi Al-Naddaf certifies that this is the approved version of the  
following thesis:

**INVESTIGATION OF SOIL ARCHING STABILITY UNDER  
STATIC AND CYCLIC SURFACE LOADING USING  
TRAPDOOR MODEL TESTS**

---

Dr. Jie Han, Chairperson

Date Approved: 03/10/2017

## ABSTRACT

Soil arching is a phenomenon describing pressure redistribution due to relative movement between adjoining portions. It commonly exists when soil interacts with structure elements, for example, tunnels, retaining walls, buried structures, and piles in pile-supported embankments. Therefore, soil arching is a key mechanism of load transfer in these geotechnical applications. The performance of these applications, where differential settlement, complete loss of support, or differential stiffness occurs, highly depends on the stability of the soil arching.

Trapdoor tests have been widely used by researchers to demonstrate and investigate the soil arching phenomenon. However, most trapdoor tests have been conducted under soil self-weight or soil self-weight plus uniform static surface load. In other words, the soil arching was investigated focusing on particle-particle interaction instead of stress transfer due to localized external loading. In addition, earth structures are often subjected to cyclic surface loading (due to moving vehicles and railroad crossings) and dynamic-in-depth loading (due to pile driving, blast waves, and earthquakes). Unfortunately, limited research of cyclic or dynamic loading on soil arching stability was conducted. Moreover, current design methods for geosynthetic-reinforced earth structures involving soil arching, such as geosynthetic over voids and geosynthetic-reinforced pile-supported embankments, were mostly based on the findings from trapdoor studies without any geosynthetic. This extrapolation lacks appropriate theoretical and experimental justifications.

This study is to address the aforementioned points by conducting a series of physical model tests under a plane strain condition. Fourteen model tests were conducted including two baseline tests and twelve other tests. The two baseline tests were carried out under only footing loading, one with static loading and another with cyclic loading. The remaining twelve tests consisted of

both trapdoor and loading tests to evaluate the stability of the soil arching. Kansas River sand was used as a granular fill material. Both unreinforced and geosynthetic-reinforced embankments were investigated. Fully mobilized soil arching was first reached by lowering the trapdoor, and then a footing load was applied on the surface. Both static and cyclic loads were applied to simulate traffic loading. Pressure distribution, footing and trapdoor displacements, geosynthetic strains, and embankment soil movement were monitored during each test.

The trapdoor test results show that the progressive displacement of the trapdoor affected the mobilization of the soil arching. Soil arching started to mobilize as the pressure on the trapdoor decreased and then deteriorated as the pressure on the trapdoor increased under soil self-weight after the trapdoor displacement increased to more than 2.5% of its width. However, the use of geosynthetic reinforcement prevented the deterioration of the soil arching and lowered the equal settlement plane height, although the trapdoor was lowered more than 4% of its width. The loading test results show that soil arching was not stable under surface loading without a geosynthetic, and the geosynthetic stabilized soil arching. To evaluate the progressive change of soil arching, soil arching ratio is defined as the ratio of the measured pressure on the trapdoor at a trapdoor displacement to the measured pressure on the trapdoor at no displacement. Soil Arching Degradation Pressure (SADP) is defined as an applied footing pressure required to eliminate soil arching (i.e., the soil arching ratio equal to 1.0). In the unreinforced embankment tests under static and cyclic loading, the SADPs were the same and equal to 54.0 kPa. Also, mobilizing soil arching under static and cyclic footing load (i.e., lowering the trapdoor under footing load) further decreased the SADPs to 45.0 kPa. The SADPs under static footing loading were increased from the unreinforced embankment to the reinforced embankment by 38.2% and 99.6% with the use of uniaxial and biaxial geogrids, respectively. Geosynthetic reinforcement further increased the

SADPs under cyclic footing loading as compared to those under static footing loading by 17.5% and 9.13 % with the use of uniaxial and biaxial geogrids, respectively. Finally, the SADPs in the double layer of geosynthetic reinforcement tests were lower than those in the single layer of geosynthetic reinforcement tests.

## **DEDICATION**

To my beloved parents, *Mr. Abbas Al-Naddaf* and *Mrs. Zainab Al-Dahhan*.

## **ACKNOWLEDGEMENTS**

I would like to express my gratitude to the Higher Committee for Education Development in Iraq (HCED) for offering me such an indispensable opportunity to complete my Master of Science degree at the University of Kansas. Also, this research study was partially sponsored by the National Natural Science Foundation of China (No. 51478349).

Also, I would like to express my sincere appreciation for my advisor prof. Jie Han, who gave priceless time and efforts to help me finish this research. His advice and encouragement during the period that I spent in my study will always be in my memory, and his instructions will be a guide for the rest of my career. I also would like to thank Prof. Anil Misra and Prof. Robert L. Parsons for serving as members of my final examining committee.

Furthermore, I would like to express my gratitude to the lab technicians, Matthew Maksimowicz and Kent Dye, in the Department of Civil, Environmental, and Architectural Engineering at the University of Kansas for their outstanding technical help in building the test box, modifying the loading system, and providing the necessary laboratory equipment. In addition, I would like to thank all the members of the Geotechnical Society at the University of Kansas (KUGS), especially Ghaith Abdulrasool and Saif Jawad, for their help and support in conducting the experimental work of this research.

Finally, my sincere gratitude goes to my beloved parents and lovely wife for their unlimited support, encouragement, and sacrifices during my study.

# TABLE OF CONTENTS

<b>ABSTRACT.....</b>	<b>III</b>
<b>ACKNOWLEDGEMENTS .....</b>	<b>VII</b>
<b>TABLE OF CONTENTS .....</b>	<b>VIII</b>
<b>LIST OF TABLES .....</b>	<b>XI</b>
<b>LIST OF FIGURES .....</b>	<b>XII</b>
<b>CHAPTER 1 INTRODUCTION.....</b>	<b>1</b>
1.1 BACKGROUND .....	1
1.2 PROBLEM STATEMENTS.....	3
1.3 OBJECTIVE OF THIS RESEARCH .....	4
1.4 METHODOLOGY .....	5
1.5 THESIS ORGANIZATION .....	6
<b>CHAPTER 2 LITERATURE REVIEW.....</b>	<b>7</b>
2.1 DEFINITION AND OVERVIEW OF SOIL ARCHING.....	7
2.2 RELEVANCE AND APPLICATIONS RELATED TO SOIL ARCHING.....	11
2.2.1 Reinforced Fill Systems over Cavities.....	13
2.2.2 Pile-Supported Embankments.....	14
2.3 LOAD TRANSFER MECHANISM .....	17
2.3.1 Soil Arching Theories .....	17
2.3.2 Tensioned Membrane Theories.....	23

2.4 SOIL ARCHING INVESTIGATIONS UNDER LOADING .....	27
2.4.1 Arching Under Self-Weight and Static Surface Loading.....	27
2.4.2 Arching Under Cyclic or Dynamic Loading.....	28
<b>CHAPTER 3 EXPERIMENTAL TESTS.....</b>	<b>32</b>
3.1 MODEL TEST SETUP .....	32
3.2 MATERIAL PROPERTIES .....	37
3.2.1 Fill Material .....	37
3.2.2 Reinforcement.....	39
3.3 METHOD OF MEASUREMENT.....	40
3.4 TEST PROCEDURE .....	46
3.5 LOADING TYPE .....	49
<b>CHAPTER 4 ANALYSIS OF TRAPDOOR TEST RESULTS.....</b>	<b>51</b>
4.1 TRAPDOOR TEST UNDER SOIL SELF-WEIGHT .....	51
4.1.1 Unreinforced Embankment Fill .....	51
4.1.2 Single Geosynthetic-Reinforced Embankment Fill .....	56
4.1.3 Double Geosynthetic-Reinforced Embankment Fill.....	69
4.2 TRAPDOOR TEST UNDER SOIL SELF-WEIGHT AND FOOTING LOAD .....	76
4.3 SUMMARY ON THE TRAPDOOR TESTS.....	81
<b>CHAPTER 5 ANALYSIS OF LOADING TEST RESULTS.....</b>	<b>85</b>
5.1 BASELINE TESTS .....	85

5.2 UNREINFORCED EMBANKMENT FILL .....	90
5.3 SINGLE GEOSYNTHETIC-REINFORCED FILL.....	98
5.4 DOUBLE GEOSYNTHETIC-REINFORCED FILL.....	107
5.5 SUMMARY ON THE LOADING TESTS .....	114
<b>CHAPTER 6 CONCLUSIONS AND RECOMMENDATIONS .....</b>	<b>118</b>
6.1 CONCLUSIONS .....	118
6.2 RECOMMENDATIONS FOR FUTURE STUDY .....	121
<b>REFERENCES.....</b>	<b>122</b>
<b>APPENDICES .....</b>	<b>130</b>

## LIST OF TABLES

Table 3.1 Test Plan .....	34
Table 3.2 Geosynthetic properties .....	40
Table 4.1 Soil arching ratios and equal settlement planes in the single geosynthetic-reinforced embankment tests (T5, T6, T11, and T12).....	60
Table 4.2 Soil arching ratios and heights of equal settlement plane in the double geosynthetic-reinforced tests (T7a, T7b, and T13) .....	72
Table 5.1 Soil arching ratios and degradation pressures in the unreinforced embankment tests .	98
Table 5.2 Soil arching ratios and degradation pressures in the single geosynthetic-reinforced tests and T2 .....	104
Table 5.3 Soil arching ratio and degradation pressure in the double geosynthetic-reinforced tests as well as T2, T6, and T12.....	114

## LIST OF FIGURES

Figure 1.1 Schematic of a typical trapdoor test setup.....	2
Figure 2.1 Schematic of soil arching phenomenon above a yielding base .....	8
Figure 2.2 Schematics of two different types of soil arching: (a) active or positive soil arching and (b) passive or negative soil arching (Han et al. 2016).....	8
Figure 2.3 Soil arching phenomena in various applications (Han, personal communication) .....	12
Figure 2.4 Typical cross-sections of PS and GRPS embankments (Han 2015) .....	15
Figure 2.5 Load transfer mechanisms in GRPS embankments (Han 2015) .....	16
Figure 2.6 Soil arching models: (a) vertical slip surface, (b) semispherical dome, and (c) triangular wedge (Han 2015) .....	18
Figure 2.7 Terzaghi's investigation of arching effect in sand: (a) proposed failure of downward movement in a trapdoor test; (b) free body diagram for a slice of soil within the yielding zone (Terzaghi 1943).....	19
Figure 2.8 Soil arching in (a) Plane strain condition (above continuous supports); (b) Three-dimensional condition (above the grid of piles in a square pattern) (Hewlett and Randolph 1988) .....	21
Figure 2.9 Delmas's tensioned membrane method: (a) before deflection and (b) after deflection (Gourc and Villard 2000).....	25
Figure 2.10 Deflected circular geosynthetic layer (Giroud et al. 1990) .....	26
Figure 2.11 Chen et al. (1991) dynamic soil arching experimental setup (Han, personal communication) .....	29
Figure 2.12 Contact force distribution for: (a) unreinforced and (b) reinforced embankment after 25 cycles of loading (Bhandari 2010).....	31

Figure 3.1 Test setup for the unreinforced fill (unit: mm).....	33
Figure 3.2 Test setup for the single geosynthetic-reinforced fill (unit: mm).....	33
Figure 3.3 Test setup for the double geosynthetic-reinforced fill (unit: mm) .....	34
Figure 3.4 Test setup: (a) test box, (b) embankment fill, (c) trapdoor mounted on electrical jack, and (d) footing on top of the fill.....	36
Figure 3.5 Particle size distribution curve for the Kansas River sand .....	37
Figure 3.6 Manual steel compactor.....	38
Figure 3.7 Two types of geogrid: (a) customized uniaxial geogrid and (b) biaxial geogrid .....	40
Figure 3.8 Earth pressure cell layout in the unreinforced fill tests .....	41
Figure 3.9 Earth pressure cell layout in the reinforced fill tests: (a) below the geosynthetic and (b) above the geosynthetic .....	42
Figure 3.10 Displacement transducer: (a) in display, (b) below the trapdoor and (c) above the footing.....	42
Figure 3.11 Materials for strain gauge installation: (a) strain gauge and (b) plastic bonding agent. .....	43
Figure 3.12 Strain gauge locations on the uniaxial geogrid.....	44
Figure 3.13 Strain gauge locations on the biaxial geogrid.....	44
Figure 3.14 Marked aluminum plates and black colored sand lines between sand lifts.....	45
Figure 3.15 Data acquisition systems: (a) smart, dynamic strain recorder and (b) CR-1000 data logger and multiplexers.....	46
Figure 3.16 Example of the monotonic static loading .....	49
Figure 3.17 Example of the incremental cyclic loading: (a) during the whole loading period, (b) from cycles No. 210 to 220, and (c) from cycles No. 810 to 820.....	50

Figure 4.1 Measured pressures on and besides the trapdoor during the fill construction in: (a) T2 and (b) T3.....	52
Figure 4.2 Measured pressures on and besides the trapdoor versus the trapdoor displacement in the unreinforced test T2 .....	53
Figure 4.3 Measured pressures on and besides the trapdoor versus the trapdoor displacement in the unreinforced tests: (a) T3 and (b) T9 .....	54
Figure 4.4 Equal settlement plane: (a) T2 and (b) T9.....	55
Figure 4.5 Measured pressures on and besides the trapdoor during the fill construction in the single geosynthetic-reinforced tests: (a) T5 and (b) T12 .....	57
Figure 4.6 Measured pressures on and besides the trapdoor versus the trapdoor displacement in the single geosynthetic-reinforced tests with uniaxial geogrid: (a) T5 and (b) T11 .....	58
Figure 4.7 Measured pressures on and besides the trapdoor versus the trapdoor displacement in the single geosynthetic-reinforced tests with biaxial geogrid: (a) T6 and (b) T12.....	59
Figure 4.8 Measured strains in the uniaxial geogrid during the trapdoor test in T5: (a) the cross-sectional distribution of the strains above the geogrid and (b) the measured strains above the geogrid versus the trapdoor displacement.....	61
Figure 4.9 Measured strains in the uniaxial geogrid during the trapdoor test in T5: (a) the measured strains above and below the geogrid at the distance of 90 mm away from the trapdoor centerline and (b) the measured strains above and below the geogrid at the distance of 173 mm away from the trapdoor centerline .....	62
Figure 4.10 Measured strains in the uniaxial geogrid during the trapdoor test in T11: (a) the cross-sectional distribution of the strains above the geogrid and (b) the measured strains above the geogrid versus the trapdoor displacement.....	63

Figure 4.11 Measured strains in the uniaxial geogrid during the trapdoor test in T11: (a) the measured strains above and below the geogrid at the distance of 90 mm away from the trapdoor centerline and (b) the measured strains above and below the geogrid at the distance of 173 mm away from the trapdoor centerline ..... 64

Figure 4.12 Measured strains in the biaxial geogrid during the trapdoor test in T6: (a) the cross-sectional distribution of the strains above the geogrid and (b) the measured strains above the geogrid versus the trapdoor displacement..... 65

Figure 4.13 Measured strains in the biaxial geogrid during the trapdoor test in T6: (a) the measured strains above and below the geogrid at the distance of 90 mm away from the trapdoor centerline and (b) the measured strains above and below the geogrid at the distance of 173 mm away from the trapdoor centerline ..... 66

Figure 4.14 Measured strains in the biaxial geogrid during the trapdoor test in T12: (a) the cross-sectional distribution of the strains above the geogrid and (b) the measured strains above the geogrid versus the trapdoor displacement..... 67

Figure 4.15 Measured strains in the biaxial geogrid during the trapdoor test in T12: (a) the measured strains above and below the geogrid at the distance of 90 mm away from the trapdoor centerline and (b) the measured strains above and below the geogrid at the distance of 173 mm away from the trapdoor centerline ..... 68

Figure 4.16 Measured pressures on and besides the trapdoor during the fill construction in the double geosynthetic-reinforced tests: (a) T7a and (b) T13 ..... 70

Figure 4.17 Measured pressures on and besides the trapdoor versus the trapdoor displacement in the double geosynthetic-reinforced tests: (a) T7a, (b) T7b, and (c) T13 ..... 71

Figure 4.18 Measured strains of the biaxial geogrid during the trapdoor test (T7a): (a) the strain distribution in the lower geogrid layer and (b) the measured strain in the lower geogrid layer versus the trapdoor displacement..... 73

Figure 4.19 Measured strains of the biaxial geogrids during the trapdoor test (T7a): (a) the strain distribution in the upper geogrid layer and (b) the measured strain in the upper geogrid layer versus trapdoor displacement..... 74

Figure 4.20 Measured strains of the biaxial geogrids during the trapdoor test (T7b): (a) the strain distribution in the lower geogrid layer and (b) the strain distribution in the upper geogrid layer 75

Figure 4.21 Measured strains of the biaxial geogrids during the trapdoor test (T13): (a) the strain distribution in the lower geogrid layer and (b) the strain distribution in the upper geogrid layer 76

Figure 4.22 Measured pressures on and besides the trapdoor during the fill construction in the tests: (a) T4 and (b) T10..... 77

Figure 4.23 Measured pressures on and besides the trapdoor versus the trapdoor displacement in tests: (a) T4 and (b) T10..... 78

Figure 4.24 Measured pressures on and besides the trapdoor versus number of cycles in the trapdoor test (T10) ..... 79

Figure 4.25 Cross-sectional distribution of the measured pressures during the trapdoor tests in: (1) T4 and (b) T10..... 80

Figure 5.1 Measured pressures on and besides the trapdoor in the loading test of T1: (a) the cross-sectional distribution of pressure and (b) measured pressure versus the monotonic static footing pressure..... 86

Figure 5.2 Applied and vertical pressures: (a) incremental cyclic footing pressure (b) measured pressures on and besides the trapdoor versus the number of cycles in the loading test of T8..... 87

Figure 5.3 Peak pressures on and besides the trapdoor in the loading test of T8: (a) along the trapdoor and the edges of the stationary supports and (b) the peak vertical pressure versus the applied pressure .....	88
Figure 5.4 Measured pressures at the trapdoor centerline (TC) versus the applied pressure in both T1 and T8.....	89
Figure 5.5 Measured footing settlements induced by static and cyclic footing pressures in T1 and T8 .....	89
Figure 5.6 Measured pressures on and besides the trapdoor versus the monotonic static footing pressure in the loading test of the unreinforced fill tests: (a) T2, (b) T3, and (c) T4 .....	91
Figure 5.7 Measured pressures on and besides the trapdoor in the loading test of the unreinforced fill test (T9): (a) the vertical pressure versus the number of cycles, (b) the results at the number of cycles from 420 to 440, and (c) the peak measured pressures versus the applied pressure .....	92
Figure 5.8 Measured pressures on and besides the trapdoor in the loading test of the unreinforced fill test (T10): (a) the pressure versus the number of cycles and (b) the measured peak pressure versus the applied pressure .....	93
Figure 5.9 Measured footing settlements induced by static and cyclic footing loads in the loading test of the unreinforced fill tests (T2, T3, T4, T9, and T10) to evaluate the effects of: (a) trapdoor displacement, (b) loading type, (c) application of the footing load during the trapdoor tests .....	95
Figure 5.10 Cross-sectional distribution of the measured pressures at the end of construction, the trapdoor test, and the static loading test of the unreinforced fill tests: (a) T2 and (b) T3 .....	97
Figure 5.11 Measured pressures on and besides the trapdoor versus the monotonic static footing pressure in the single geosynthetic-reinforced tests: (a) T5 and (b) T6.....	99

Figure 5.12 Measured pressures on and besides the trapdoor versus the incremental cyclic footing pressure in the single geosynthetic-reinforced tests: (a) T11 and (b) T12 .....	100
Figure 5.13 Cross-sectional distribution of the measured pressures at an applied static pressure of 50 kPa in T2, T5, and T6 .....	101
Figure 5.14 Measured footing settlements induced by the applied pressure in the single geosynthetic-reinforced tests (T5, T6, T11, and T12) to evaluate the effects of: (a) reinforcement type under static loading and (b) reinforcement type under cyclic loading.....	102
Figure 5.15 Measured footing settlements induced by the applied pressure in the single geosynthetic-reinforced tests (T5, T6, T11, and T12) to evaluate the effects of: (a) loading type with the uniaxial geogrid and (b) loading type with the uniaxial geogrid .....	103
Figure 5.16 Strain distribution along the geogrid during the static loading tests in the single geosynthetic-reinforced tests: (a) T5 and (b) T6.....	105
Figure 5.17 Strain distribution along the geogrid during the cyclic loading tests in the single geosynthetic-reinforced tests: (a) T11 and (b) T12.....	106
Figure 5.18 Measured pressures on and besides the trapdoor versus the monotonic static footing load in the double geosynthetic-reinforced tests: (a) T7a and (b) T7b .....	108
Figure 5.19 Measured pressures on and besides the trapdoor versus the incremental cyclic footing pressure in the double geosynthetic-reinforced test (T13) .....	109
Figure 5.20 Measured pressures at TC below the lower geosynthetic layer in T7a and T7b compared to that in T6 .....	109
Figure 5.21 Strain distribution along the biaxial geogrids during the loading test in T7a: (a) the lower geogrid layer and (b) the upper geogrid layer.....	110

Figure 5.22 Strain distribution along the biaxial geogrids during the loading test in T7b: (a) the lower geogrid layer and (b) the upper geogrid layer..... 111

Figure 5.23 Strain distribution along the biaxial geogrids during the loading test in T13: (f) the lower geogrid layer and (e) the upper geogrid layer..... 112

Figure 5.24 Measured footing settlement induced by the applied pressure in the double geosynthetic-reinforced tests (T7a, T7b, and T12) to evaluate the effects of: (a) reinforcement type under static loading and (b) reinforcement type and loading type..... 113

# CHAPTER 1 INTRODUCTION

This chapter provides general background about the soil arching phenomenon and its significance in the geotechnical applications as well as the importance of studying the stability of the soil arching. It also covers the problem statements, the objective of this research, and methodology adopted as well as the organization of this thesis.

## 1.1 BACKGROUND

Any structure, building or bridge, needs an adequate foundation that can withstand an exerted load and transfer it to the ground. In geotechnical applications such a load transfer mechanism is of considerable importance. In a soil mass forces are transferred from particle to particle and subsequently from one layer to another under normal conditions. In some applications, there is a differential settlement (e.g., piled embankments or local subsidence), complete loss of support (e.g., sinkholes or voids), or different stiffness between soil and structure (e.g., buried structure or conduit). The forces within the soil mass will transmit through a stress transfer mechanism that is called “Soil Arching.” Soil arching is a phenomenon describing stress re-distribution due to relative movement between adjoining soil masses.

When embankments are constructed for highways or railways, suitable ground is not necessarily available. Therefore, they have to be built on soft soils (e.g., alluvial soil and peats), which are considered technically unsuitable or challenging for construction because of their low shear strength and high compressibility (Demerdash 1996; Han 1999). In order to increase ground stability and reduce settlement, piles and geosynthetics have been increasingly used to support embankments on such problematic soils (Han and Gabr 2002). This technique is considered as a rapid solution for embankment construction and also applicable for handling the problems caused by existing large sinkholes under a planned highway or railway (Wang et al. 2009). In

Geosynthetic-Reinforced Pile-Supported (GRPS) embankments, load transfer mechanisms play an important role in the behavior of such a system. In this system, both soil arching and geosynthetic tensioned membrane effects are responsible for transferring the embankment load to the piles. The modulus difference between the soil and the piles under embankment loading causes differential settlement, which leads to the development of soil arching within the embankment fill and tension in the geosynthetic reinforcement. However, soil arching dominates the mechanisms, through which the embankment weight and the surface loading are transferred to the piles (Han et al. 2011). When highways and railways are built on GRPS embankments, surface traffic loading may have some effect on the stability of soil arching; however, this effect has not been well understood and investigated.

Researchers have commonly used trapdoor test to demonstrate and investigate the soil arching phenomenon. The trapdoor test setup shown in Figure 1.1 allows to induce differential settlement within the soil mass after the trapdoor being lowered; therefore, soil arching mobilizes.

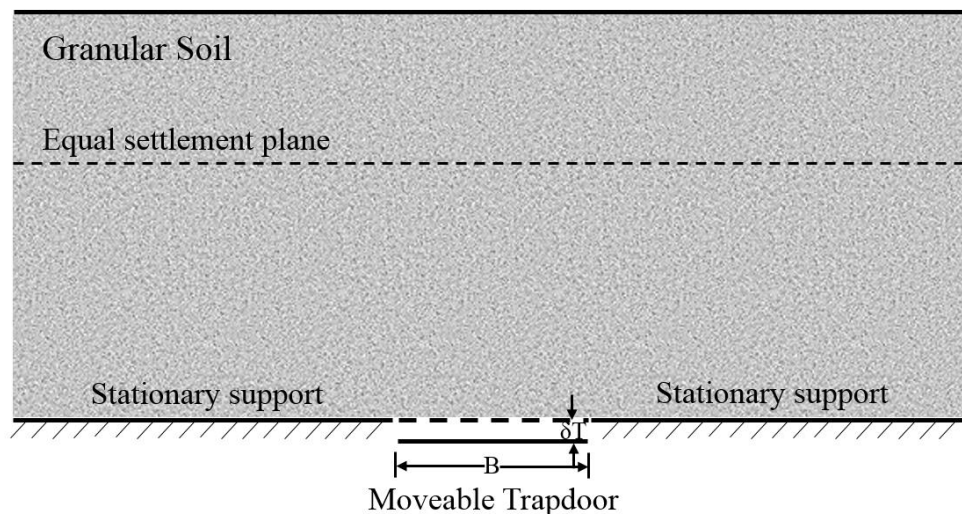


Figure 1.1 Schematic of a typical trapdoor test setup

## 1.2 PROBLEM STATEMENTS

Past research work has provided an essential level of knowledge of the soil arching phenomenon in geotechnical engineering, yet most studies have been conducted for specific applications. For example, researchers have used trapdoor tests to investigate the soil arching phenomenon (Terzaghi 1936; McNulty 1965; Ladanyi and Hoyaux 1969; Harris 1974). However, most trapdoor tests have been conducted in considerably small-scale models under soil self-weight or soil self-weight plus uniform static surface loading. Thus, this is a case where soil arching was investigated focusing on particle-particle interaction instead of stress transfer due to localized external loading (e.g., footings, vehicle tires, etc.). Scale effects of small model tests may have influenced the accuracy of the test results. In addition, a uniform surcharge may not be representative of most surface loading and the critical situation for soil arching stability since smaller differential settlement may develop in the soil under a uniform surcharge than a localized load.

Moreover, earth structures or buried structures are often subjected to cyclic surface loading (due to moving vehicles and railroad crossings) and dynamic-in-depth loading (due to pile driving, blast waves, and earthquakes). Unfortunately, the knowledge of cyclic or dynamic loading on soil arching stability lacks, even though Terzaghi (1943) pointed out that vibrations might have a significant impact on soil arching, and deterioration of soil arching would result in an increase of stresses applied on the buried structures and increase the chance of damaging these structures. Very limited research has been conducted to investigate the soil arching behavior under cyclic loading. Chen et al. (1991) studied soil arching based on impact loading on a flexible trapdoor, yet no true soil arching developed in their test because the flexible trapdoor deformed due to its flexibility.

Furthermore, current design methods for geosynthetic-reinforced earth structures involving soil arching, such as geosynthetic over voids and geosynthetic-reinforced pile-supported embankments, were mostly developed based on the findings from trapdoor studies without any geosynthetic. This extrapolation lacks appropriate theoretical and experimental justifications. The influence of geosynthetic reinforcement on soil arching phenomenon is not entirely understood. This study is expected to provide an insight into the effect of the geosynthetic on the mobilization of soil arching

### **1.3 OBJECTIVE OF THIS RESEARCH**

This research is conducted to fulfill the following tasks:

- To examine the load transfer mechanism of soil arching under soil self-weight as a result of differential movement without and with geosynthetic reinforcement,
- To study the progressive change of soil arching under static and cyclic footing load,
- To investigate the stability of mobilized soil arching under surface footing of static and cyclic loading, and
- To evaluate the benefit of geosynthetic in stabilizing soil arching under surface footing loading.

These objectives have been achieved throughout the research by conducting a series of physical model tests, each of which consisted of a trapdoor test and a loading test, under a plane strain condition to investigate the mobilization as well as the stability of soil arching under both surface static and cyclic footing loading.

## 1.4 METHODOLOGY

The methodology adopted in this research includes a literature review, which covers a brief summary of results and findings of past studies associated with soil arching and its applications, and two series of laboratory tests. These tests were performed inside a test box of the interior dimension of 1760×460× 1480 mm in the Geotechnical Engineering Laboratory at the University of Kansas with the following test plan:

(1) Trapdoor and static loading test series (totally eight tests)

(A) Unreinforced embankment fill

(i) Monotonic static loading test only (i.e., without trapdoor movement)

(ii) Trapdoor test followed by monotonic static loading (two tests)

(iii) Trapdoor test under constant surface static loading followed by monotonic static loading

(B) Reinforced embankment fill

(a) Single layer of geosynthetic reinforcement

(i) Uniaxial geogrid overlain by non-woven geotextile: trapdoor test followed by monotonic static loading

(ii) Biaxial geogrid overlain by non-woven geotextile: trapdoor test followed by monotonic static loading

(b) Double layers of geosynthetic reinforcement

(i) Double layers of biaxial geogrid overlain by non-woven geotextile: trapdoor test followed by monotonic static loading (two tests)

(2) Trapdoor and cyclic loading test series (totally six tests):

(A) Unreinforced embankment fill

- (i) Incremental cyclic loading test only (i.e., without trapdoor movement)
  - (ii) Trapdoor test followed by incremental cyclic loading
  - (iii) Trapdoor test under constant cyclic loading followed by incremental cyclic loading
- (B) Reinforced embankment fill
- (a) Single layer of geosynthetic reinforcement
    - (i) Uniaxial geogrid overlain by non-woven geotextile: trapdoor test followed by incremental cyclic loading
    - (ii) Biaxial geogrid overlain by non-woven geotextile: trapdoor test followed by incremental cyclic loading
  - (b) Double layers of geosynthetic reinforcement
    - (i) Double layers of biaxial geogrid overlain by non-woven geotextile: trapdoor test followed by incremental cyclic loading

## **1.5 THESIS ORGANIZATION**

This thesis consists of six chapters. Chapter 1 presents a brief introduction to this study followed by Chapter 2, which presents a literature review of soil arching and its applications, mechanisms of load transfer, and soil arching under static and cyclic loading. Chapter 3 discusses the test setup and apparatus, the materials, and the test procedure used in this study. Chapter 4 presents the trapdoor test results and discusses the effects of reinforcement and loading on the mobilization of soil arching. Chapter 5 investigates the stability of mobilized soil arching under footing loading. Chapter 6 provides the conclusions of this study and the recommendations for future research.

## CHAPTER 2 LITERATURE REVIEW

The primary objective of the literature review is to summarize the accumulated knowledge on the subject, draw attention to the areas where research is required, and subsequently define the aim of this study. This literature review covers the following subjects:

- Definition and overview of soil arching
- Applications related to soil arching
- Load transfer mechanism
- Soil arching investigations under static and cyclic loading

### 2.1 DEFINITION AND OVERVIEW OF SOIL ARCHING

Soil arching is a transfer of pressure from a yielding soil mass onto its adjoining stationary soil mass in response to a relative displacement between these two masses (Terzaghi 1943). If only a specific area of support for a soil mass yields, the soil above the yielding region would have a tendency to settle with the yielding support while the rest remains stationary. In the transition plane between the moving and stationary soil masses, shear stresses are developed to counteract the relative movement of the two masses. Since the shear resistance tries to keep the yielding mass in its original position, it reduces the pressure on the yielding part of the support and, subsequently, increases the pressure on the stationary part. Figure 2.1 shows a schematic of the soil arching phenomenon above a yielding base.

The mechanism in which the stresses are transferred and redistributed results from a series of shear stresses generated along the vertical planes that separate the yielding soil mass and the adjoining stationary mass as shown in Figure 2.1. These shear stresses are the counteracting forces depending on frictional characteristics of the soil to resist the relative movement. If the yielding soil moves downward, the induced frictional stresses have an uplift effect on the moving soil, so

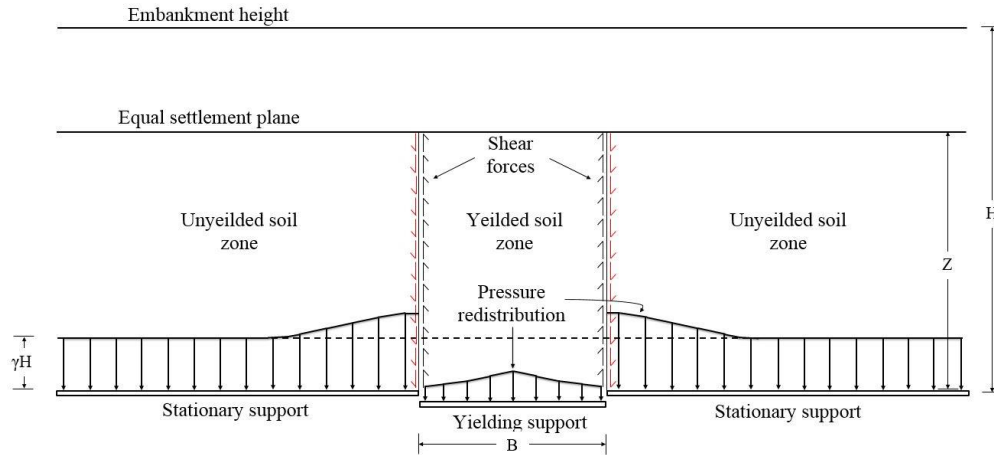


Figure 2.1 Schematic of soil arching phenomenon above a yielding base

it will reduce the pressure on the yielding mass and redistribute the pressure to the stationary mass as shown in Figure 2.2(a). This phenomenon is also called “active or positive” soil arching, and it can be generated with only a small movement (Terzaghi 1936). On the contrary, if the movement occurs in the reverse direction (i.e., the yielding soil mass moves upward with respect to other parts), frictional down-drag forces are generated to impede that movement. These down-drag forces will increase the stress on the yielding soil and reduce it on the surrounding soil. Such type of soil arching is referred to as “passive or negative” soil arching as shown in Figure 2.2(b).

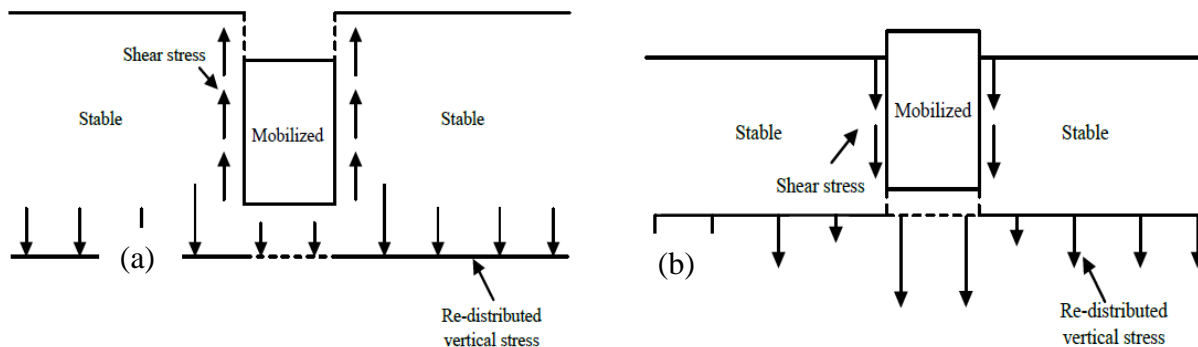


Figure 2.2 Schematics of two different types of soil arching: (a) active or positive soil arching and (b) passive or negative soil arching (Han et al. 2016)

Stress redistribution (i.e., soil arching) in a medium is also associated with the soil-structure interaction. Soil arching may cause a significant change in the stresses throughout the soil medium because the structure has different compressibility from the surrounding soil (McNulty 1965). McNulty (1965) stated that the main factors contributing to the level of pressure redistribution include: the physical properties of the structure (particularly its compressibility characteristics), the properties of the surrounding soil (mainly its ability to transfer loads through mobilization of shear stresses as a consequence of relative displacements); and the free field state of the stresses which would exist if the structure were not present.

The degree of load transfer can be evaluated by a soil arching ratio ( $\rho$ ) as proposed by McNulty (1965), which is defined as the average vertical stress above the yielding base ( $\sigma_v$ ) to the overburden pressure ( $\gamma H$ ) plus the surcharge ( $q$ ) if available, as expressed in Equation 2.1:

$$\rho = \frac{\sigma_v}{\gamma H + q} \quad \text{Equation 2. 1}$$

where  $\rho = 0$  represents complete soil arching while  $\rho = 1$  represents no soil arching.

Terzaghi (1943) stated that “arching effect is one of the most universal phenomena encountered in soils both in the field and in the laboratory.” The arching phenomenon has been investigated over a century in geotechnical and non-geotechnical fields. In France, military engineers found that silo base carried a fraction of grain weight while the silo walls carried more than one would expect (Feld 1948). The “Silo Theory” was proposed by Janssen (1895) to design silos based on the observed behavior.

In the United States, a large number of drainage projects were carried out in 1910, and many structural failures happened to the designed pipes after the installation and backfilling (Spangler and Handy 1973). These failures were believed related to load redistribution (i.e., the

arching phenomenon) on the underground conduits which were also investigated by Marston (1930) at Iowa State University. Depending upon the flexibility of conduits, the load on the conduit can vary from a portion of the overburden weight to several times the overburden weight (Marston 1930; Spangler 1964).

Engineers also observed arching around tunnels, i.e., the load carried by a tunnel was lower than the overburden pressure, and accurate predictions were necessary for a better design. Terzaghi (1943) developed a theoretical solution to quantify this load based on his experimental research (i.e., the use of trapdoor test) in 1936. Atkinson and Potts (1977) investigated soil arching related to the stability of tunnels. In 1960s when the US Defense Department sponsored considerable research for protection of infrastructures, soil-structure interaction gained great attention. Researchers showed that soil arching would contribute to the protection of underground facilities from nuclear attacks during war, which would demolish any surface building (Evans 1983).

Since 1960s, columns have used to support embankments over soft soils to control and reduce their settlement (Magnan 1994). Construction of embankments for highway applications on soft ground is hard to achieve without ground improvement techniques. Use of piles or columns is often an economical solution to reduce soft soil compressibility and enhance ground stability (Han and Gabr 2002). In these piled embankments, there exist two distinct supports – rigid pile caps and soft soil. Differential settlement easily develops between these two supports. Soil arching develops between the pile caps as a result of this differential settlement. Thus, embankment weight can be transferred to an adequate stratum below the soft soil through piles as pointed out by Holtz and Massarsch (1976), Holmberg (1979), Broms and Wong (1985) and studied by Hewlett and Randolph (1988); and Low et al. (1994).

Trapdoor test has been commonly used to evaluate soil arching developed above the yielding support. Terzaghi (1936) conducted the first trapdoor test to investigate the arching effect. Many researchers (McNulty 1965; Ladanyi and Hoyaux 1969; Harris 1974; Evans 1983) replicate Terzaghi's trapdoor tests. These trapdoor studies have been performed under soil self-weight or soil self-weight plus uniform static surface loading. A uniform surcharge configuration may not be the critical situation for soil arching stability as compared with the locally loaded situation since less differential settlement may develop in the soil.

## **2.2 RELEVANCE AND APPLICATIONS RELATED TO SOIL ARCHING**

Soil arching is considered as a universal phenomenon in geotechnical engineering because it is encountered in many geotechnical applications including sinkholes, mining subsidence, tunneling, landfill liner systems over voids, buried conduits and structures, piled embankments, fill behind retaining walls, slope stabilizing piles, and soil tunnel by animals or insects. Figure 2.3 depicts some of these applications.

In the above applications, soil arching is developed as a result of relative movement between soil and support in either vertical or lateral direction. Sinkholes, mining subsidence, tunneling, and landfill liner systems over voids are examples of relative vertical movement. While lateral movement of support, such as outward yielding of retaining walls, results in soil arching which forms a semi-arch between the wall and a slip plane and significantly reduces lateral earth pressures. Soil arching in retaining walls initiates from a rough wall when rotation of principal stresses at the wall takes place (Handy 1985). A slope stabilizing pile system is another example of lateral movement where soil arching develops as the soil tends to move through between the stabilizing piles, which are often embedded in firm foundations (Bosscher and Gray 1986).

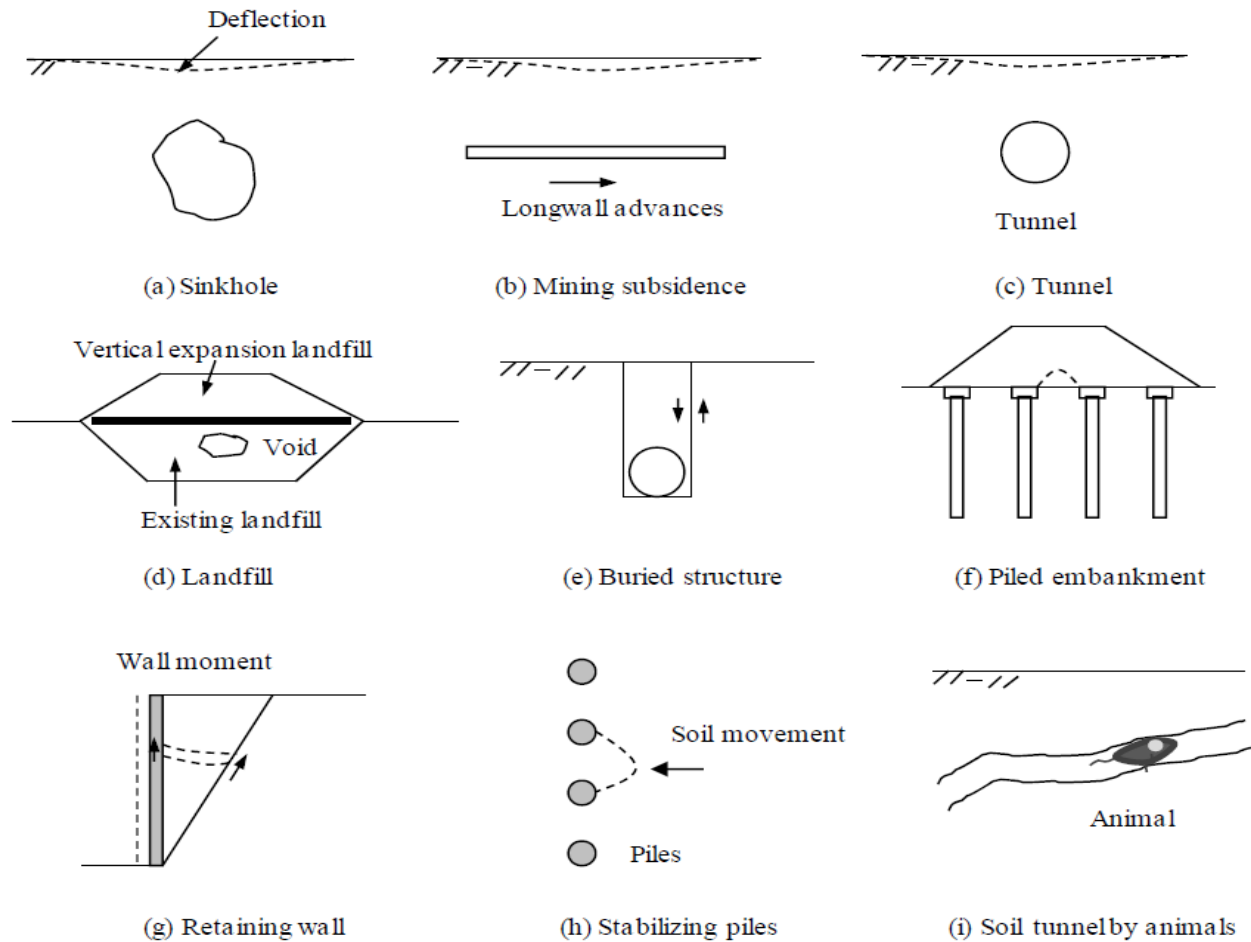


Figure 2.3 Soil arching phenomena in various applications (Han, personal communication)

In addition to the relative movement, a relative stiffness difference between the support and the surrounding soil may also mobilize soil arching which results in transfer of the load to a stiffer support. Buried conduits were one of the early applications considering soil arching as a result of relative stiffness (Marston 1930). Wu and Leonards (1985) indicated that soil arching above buried pipes (conduits) could be positive or negative depending on the stiffness of the pipe relative to that of the surrounding backfill. Also, Einstein and Schwartz (1979) presented a simplified analysis to account for the load redistribution on tunnel supports as subsequence to the relative stiffness difference.

In the following sections, two most common geotechnical applications involving soil arching will be further discussed.

### **2.2.1 Reinforced Fill Systems over Cavities**

Construction takes place on the natural ground that may include mining areas, karstic terrains, landfills, and non-saturated cohesive soils, which are susceptible to the danger of collapse because these areas more likely develop cavities or sinkholes during their lifetime. Ground water flows through soil masses that contain limestones, or gypsum contents can create significantly large sinkholes of a diameter ranging from one to several meters (Giroud et al. 1990). Sinkholes may develop when collapsible soils, which are dry or partially-saturated cemented soils, lose their cementation upon wetting and under loading (Agaiby and Jones 1996). In addition, some cavities are formed during the progress of longwall mining or tunnels excavated by animals or insects. Thus subsidence likely develops during such process (Tsur-Lavie et al. 1988; Reichman and Smith 1990). Also, vertical expansions to existing landfills have become an attractive alternative for expanding usable space. However, there is a concern that overstretching of liners and leachate collection systems may occur above voids in the old landfill areas created by progressive degradation of waste and collapse of large objects (Jang and Montero 1993). Agaiby and Jones (1996) pointed out that the term “cavity” is relative. For example, a thin compressible layer of very soft soil embedded in a much stiffer stratum can be considered as a cavity due to its incapability to provide the same support to loads as its surroundings.

The existence of a cavity, in general, in soil would induce either differential settlement or complete loss of support. Thus soil arching would transfer the loads above (i.e., fill soil self-weight and surface loading) onto the sides of the cavity. However, if the shear resistance of the soil forming the roof and the sides of a cavity is not strong enough to support the exerted loads, sudden

collapse may occur. Therefore, geosynthetic reinforcement may be used to bridge over a cavity and carry the loads to reduce the risks of collapse. Geosynthetics have been used to stabilize the soil above cavities (Giroud et al. 1990; Agaiby and Jones 1995; Wang et al. 1996). Depending on the cavity size and the geosynthetic stiffness, the geosynthetic may touch the bottom of the cavity (especially for a small cavity) and transfer some of the load to the soil underneath it or support the load without touching the bottom of the cavity (especially for a large cavity and a strong and stiff geosynthetic) (Giroud et al. 1990).

Much research, related to the load transfer mechanisms of such systems, has been done, including theoretical derivations, analytical methods, and experimental investigations. Terzaghi (1943) and Kezdi (1975) derived theoretical solutions for the soil arching over an infinitely long trench and circular voids, respectively. These solutions were adopted by Giroud (1984) and Giroud et al. (1990) as well as the tensioned membrane theory to assess the load-carrying capacity and to provide a design method for soil-layer geosynthetic systems spanning voids, such as sinkholes, tension cracks, dissolution cavities, and depressions.

### **2.2.2 Pile-Supported Embankments**

Piles have been used to enhance soft soil bearing capacity and minimize post-construction settlements in many embankments since early 1960s (Magnan 1994). When piles are used, they carry a large percent of the embankment weight up to 60% with as little as 10% of pile coverage area, by virtue of soil arching induced from the differential settlements between piles and soft soil (Hewlett and Randolph 1988). Therefore, a single stage of embankment construction is possible without the risk of soft soil undrained failure. Another advantage of piles during installation is that they may densify and stiffen soil, thus reducing the settlement of the foundation soil (Hewlett and Randolph 1988). These embankments are mainly used to support highway or railway systems.

Geosynthetics have been introduced in pile-supported (PS) embankments as basal reinforcement to assist the load transfer and to reduce the differential settlement (Han and Gabr 2002). Figures 2.4(a) and (b) show typical cross-sections of PS and GRPS embankments, respectively. Moreover, by introducing geosynthetic in a PS embankment, piles can be constructed with larger spacing and smaller caps, thus reducing the cost of piling (Jones et al. 1990). Bell et al. (1994) pointed out that primary and long-term secondary settlements can be minimized by using geosynthetic. Consequently, thick embankments to prevent the differential settlements at the base being reflected to the crest is not vital (Broms and Wong 1985).

Due to these advantages, many GRPS embankments have been built. In Scotland 1983, the first GRPS embankment was constructed with a single layer of geomembrane for a bridge approach embankment (Reid and Buchanan 1984). Also, multiple layers of geosynthetic were used to support a roadway embankment in London, England 1989 (Card and Carter 1995). In Philadelphia, PA in 1994, a large diameter storage tank was built on a geosynthetic reinforced column supported platform (Collin 2003).

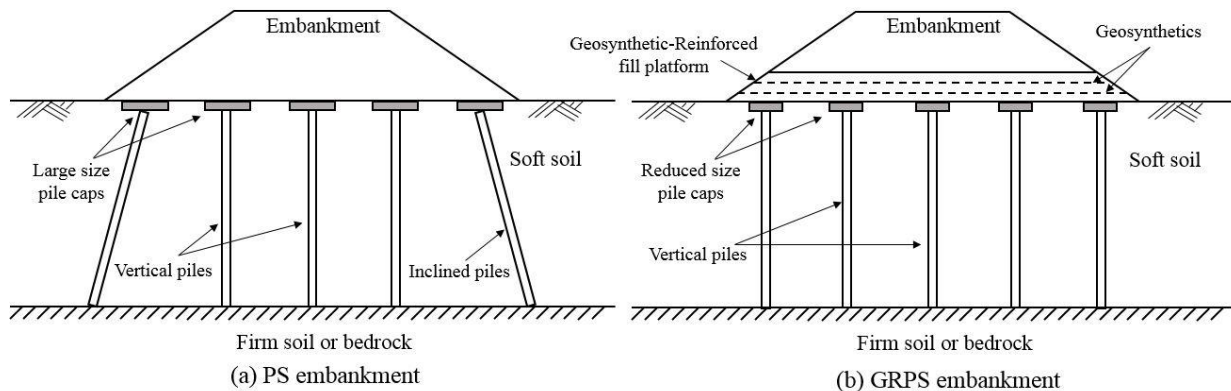


Figure 2.4 Typical cross-sections of PS and GRPS embankments (Han 2015)

In GRPS embankments, the geosynthetic-reinforced fill platform acts as a unit to reduce the load on soft soil (i.e., foundation soil) and transfer it to stiffer piles through soil arching and

tensioned membrane effects. Figure 2.5 illustrates these two mechanisms under a plane strain condition. If there are no piles within the foundation soil, the embankment soil should settle evenly, and the vertical pressure at the embankment base is equal to the total overburden stress ( $\gamma H$ ). When piles are incorporated, the embankment fill above the soft soil would have a tendency to settle relative to the stationary adjoining fill above the piles. As the differential settlement ( $\Delta S$ ) generates, soil arching mobilizes and transfers the embankment load to the piles.

Simultaneously, the geosynthetic sheet extending across the span of the two piles deforms as the soil mass moves downwards. A tangential tensile force ( $T$ ) develops within the geosynthetic sheet. The vertical component of the tensile force will counteract the downward moving soil mass and apply additional load on the piles. As the tension develops in the geosynthetic sheet, the embankment weight is transferred from the foundation soil to the piles. This is called the tensioned membrane effect. The load transfer mechanism in GRPS embankments is a combination of soil arching and tensioned membrane effects. However, soil arching dominates the mechanisms through which the embankment weight and the surface loadings are transferred to the piles (Han et al. 2011). Soil arching is the only mechanism which is responsible for the load transfer in PS embankments.

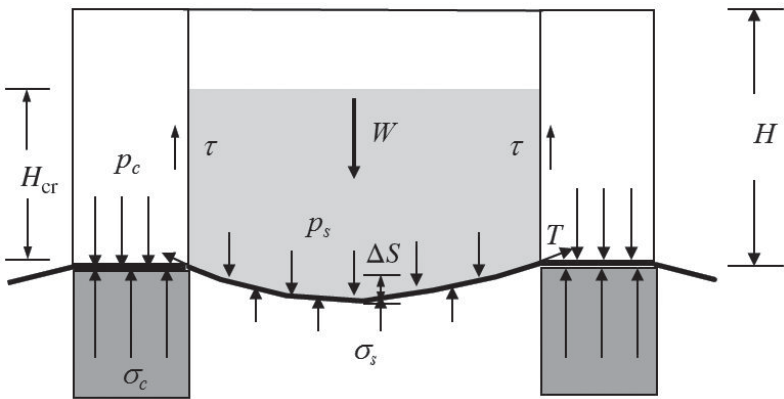


Figure 2.5 Load transfer mechanisms in GRPS embankments (Han 2015)

## **2.3 LOAD TRANSFER MECHANISM**

As pointed out in the previous sections, soil arching is a key mechanism in many geotechnical applications. However, soil arching does not act alone as a load transfer mechanism in many of these applications, such as GRPS embankments and geosynthetic over cavities. Therefore, both soil arching and geosynthetic tensioned membrane effects are studied and explained in the following section to have a better understanding of the load transfer mechanism.

### **2.3.1 Soil Arching Theories**

Soil arching theories are essential for discussing the arching effect and providing a path for further development in related arching studies. Soil arching phenomenon has been studied for decades; many experimentally and analytically-based theories have been proposed (Janssen 1895; Terzaghi 1936; Finn 1963; Hewlett and Randolph 1988; Low et al. 1994). Similar to many geotechnical problems, soil arching has been investigated by scholars in two distinctly different methods: limit equilibrium and continuum mechanics-based methods (Agaiby and Jones 1995). These two approaches are different in their assumptions, formulations, and consequences.

The formulations for the behavior of any geotechnical problems are either indeterminate or complex to some extent; therefore, commonly a simplified constitution for the soil behavior is favorable. Limit equilibrium methods facilitate the soil arching problem by assuming a failure state with certain shapes and ranges of slip surfaces, which make the problems easily solved (Agaiby and Jones 1995). The presumed shape of soil arching is the primary difference among all the limit equilibrium methods, such as a flat arch acting like a lintel or a curved mode like an arch, a ring or a dome (Getzler et al. 1968; Handy 1985; Hewlett and Randolph 1988).

Han (2015) classifies soil arching theories according to the proposed models by researchers in the following to study GRPS embankments: (a) vertical slip surfaces (Russell and Pierpoint

1997; Chen et al. 2008; British Standard 8006 2010); (b) semispherical dome (Hewlett and Randolph 1988; Kempfert et al. 2004); and (c) triangular wedge (Carlsson 1987; Miki 1997; Collin 2003). An illustration of these different models is shown in Figure 2.6.

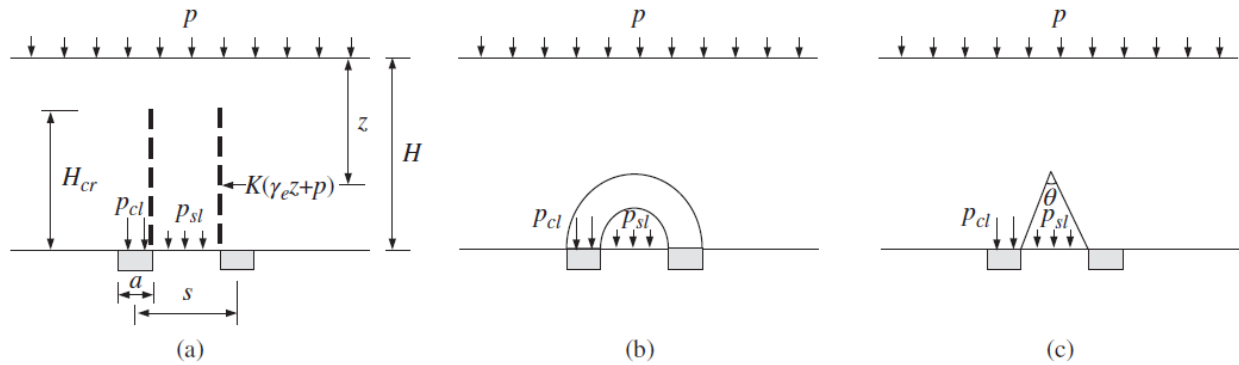


Figure 2.6 Soil arching models: (a) vertical slip surface, (b) semispherical dome, and (c) triangular wedge (Han 2015)

### ***Terzaghi's Investigation of Soil Arching***

A series of trapdoor tests were conducted by Terzaghi (1936) as the first experimental investigation of the arching phenomenon. Terzaghi's trapdoor tests were performed under a plane strain condition. Based on his results and observations, he proposed a theoretical solution to describe the soil arching phenomenon in 1943. He also developed an equation to calculate vertical stress above a yielding trapdoor.

In Terzaghi's experimental work, a trapdoor of 73 mm wide and 463 mm long was fixed on the base of a 310 mm sand container. It was allowed to move downwards gradually. Meanwhile, the total load on the trapdoor and its displacement were measured. As the displacement was just started, the load on the trapdoor decreased rapidly as indicated by the test results, and the shear stresses induced by soil arching increased with an increase in the displacement. Subsequently, the pressure on the trapdoor reached a constant value at a displacement of 10% of the trapdoor width.

The adopted model in Terzaghi's investigation is similar to the one proposed by Janssen (1895) to study the pressure distribution in silos. As shown in Figure 2.7 (a), Terzaghi (1943) observed that the real surfaces of sliding are curved (i.e., **ac** and **bd** curves) when the trapdoor was lowered. However, he assumed for the simplification and calculation purposes that two vertical planes passing through the outer edges of the trapdoor (i.e., **ae** and **bf** planes) restrained the yielding soil and a horizontal plane (**e<sub>1</sub>f<sub>1</sub>**), above which no relative displacement happened. Such a plane is called the equal settlement plane. The soil mass above the equal settlement plane was treated as a surcharge (i.e., no arching effect available above that plane).

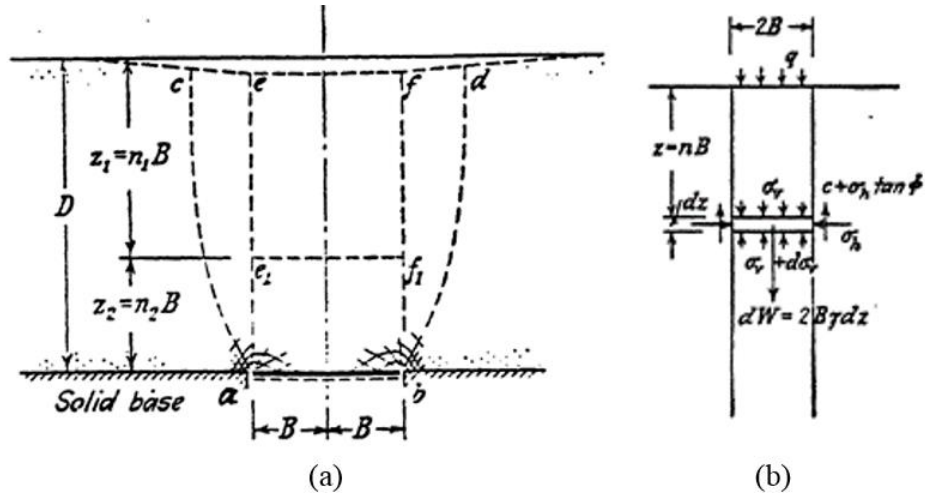


Figure 2.7 Terzaghi's investigation of arching effect in sand: (a) proposed failure of downward movement in a trapdoor test; (b) free body diagram for a slice of soil within the yielding zone (Terzaghi 1943)

Figure 2.7(b) shows the free body diagram for a slice of soil within the yielding zone examined by Terzaghi (1943), in which he assumed that normal stresses were uniform across the horizontal sections and the coefficient of lateral stress ( $K$ ) was a constant. Cohesion ( $c$ ) was assumed to exist along the sliding surfaces. By satisfying the force equilibrium vertically for the

free body diagram as in Equation 2.2, he derived the following equations to estimate the vertical stress ( $\sigma_v$ ) as in Equation 2.3 and the soil arching ratio as in Equation 2.4.

$$2B\gamma dz = 2B(\sigma_v + d\sigma_v) - 2B\sigma_v + 2cdz + 2\sigma_h dz \tan \phi \quad \text{Equation 2. 2}$$

$$\sigma_v = \frac{B(\gamma - c/B)}{K \tan \phi} \left(1 - e^{-Kz \tan \phi/B}\right) + qe^{-Kz \tan \phi/B} \quad \text{Equation 2. 3}$$

$$\rho = \frac{\sigma_v}{\gamma H + q} = \frac{B(\gamma - c/B)}{(\gamma H + q) K \tan \phi} \left(1 - e^{-Kz \tan \phi/B}\right) + \frac{qe^{-Kz \tan \phi/B}}{\gamma H + q} \quad \text{Equation 2. 4}$$

where  $2B$  = width of the trapdoor;  $\gamma$  = unit weight of soil;  $z$  = depth from the equal settlement plane;  $\sigma_v$  = vertical stress;  $\sigma_h$  = horizontal stress ( $\sigma_h = K\sigma_v$ );  $K$  = coefficient of lateral earth pressure;  $c$  = cohesion of soil;  $\phi$  = friction angle of soil; and  $q$  = surcharge at the soil surface.

### ***Hewlett and Randolph's Soil Arching Theory***

Hewlett and Randolph (1988) studied the mechanism by which the load is carried by a square grid of piles and continuous walls and is transferred from a granular embankment fill based on laboratory model tests. They suggested a model of arched shape based on their observations of deformations within the fill as in Figure 2.8. Then, an analysis of the soil arching effect, by considering limiting equilibrium of stresses within the arch, was proposed for a plane-strain and three-dimensional conditions.

For the plane strain condition, as shown in Figure 2.8(a), Hewlett and Randolph (1988) considered that long arches are formed within the arching zone and supported by continuous walls. These arches are responsible for transferring the embankment weight to the supports in a similar action to that of the masonry arches in cathedrals. They assumed that arches are semi-circular and have the same thickness, and no overlap of arches happens above the supports to satisfy the static equilibrium requirement. Also, they ignored the self-weight of the soil within the soil arching zone

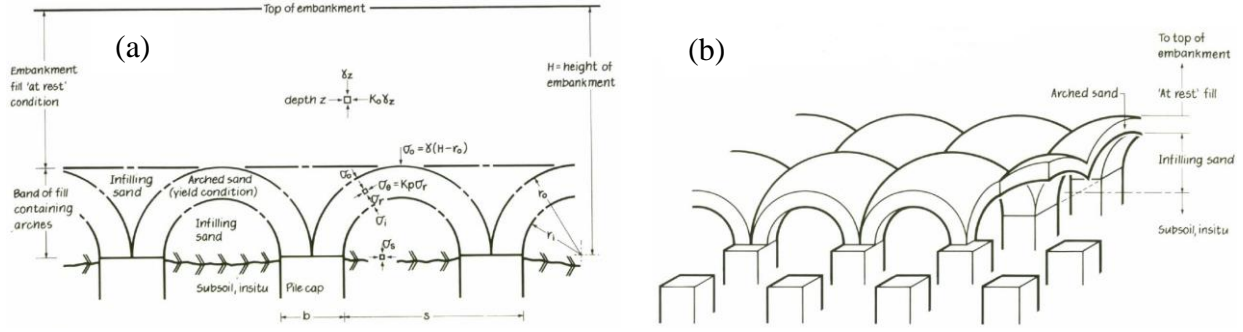


Figure 2.8 Soil arching in (a) Plane strain condition (above continuous supports); (b) Three-dimensional condition (above the grid of piles in a square pattern) (Hewlett and Randolph 1988)

and considered no mobilization of the shear stresses for the soil below and between the formed arches. Considering that the limit equilibrium would reach first at the crown, a differential equation in terms of equilibrium in the radial direction was obtained as in Equation 2.4. By satisfying the boundary conditions at the crown of the arch, the stress just below the inner boundary of the arch is as in Equation 2.5:

$$\frac{d\sigma_r}{dr} - \frac{(\sigma_r - \sigma_\theta)}{r} = 0 \quad \text{Equation 2. 5}$$

$$\sigma_i = \gamma \left( H - \frac{s}{2} \right) \left( \frac{s-b}{s} \right)^{(K_p-1)} \quad \text{Equation 2. 6}$$

$$\rho = \frac{\sigma_i}{\gamma H} = \frac{1}{H} \left( H - \frac{s}{2} \right) \left( \frac{s-b}{s} \right)^{(K_p-1)} \quad \text{Equation 2. 7}$$

where  $\sigma_r$  = the radial stress,  $\sigma_\theta$  = the tangential stress,  $r$  = the arch radius,  $\sigma_i$  = the vertical stress on the inner side of the arch, which equals to the vertical stress at  $r = (s-b)/2$ ,  $\gamma$  = the soil unit weight,  $H$  = the height of the embankment,  $s$  = the center to center spacing of the support,  $b$  = the width of the support, and  $K_p$  = Rankine's passive earth pressure coefficient.

Hewlett (1984) considered the self-weight of soil within the arching zone and obtained the differential equation in the radial direction as in Equation 2.6. By solving the differential equation

and applying the boundary conditions, the inner stress ( $\sigma_i$ ) below the boundary of the arch is as in Equation 2.7. This analysis is only valid for embankments of a height more than half the spacing of the supports (i.e.,  $H > s/2$ ):

$$\frac{d\sigma_r}{dr} - \frac{(\sigma_r - \sigma_\theta)}{r} = -\gamma \quad \text{Equation 2. 8}$$

$$\sigma_i = \gamma \left( \frac{s-b}{2(K_p-2)} \right) + \gamma \left( H - \frac{s-b}{4} - \frac{s}{2(K_p-2)} \right) \left( \frac{s-b}{s} \right)^{(K_p-1)} \quad \text{Equation 2. 9}$$

$$\rho = \frac{\sigma_i}{\gamma H} = \left( \frac{s-b}{2H(K_p-2)} \right) + \left( 1 - \frac{s-b}{4H} - \frac{s}{2H(K_p-2)} \right) \left( \frac{s-b}{s} \right)^{(K_p-1)} \quad \text{Equation 2. 10}$$

For the embankments that are supported by piles, the most representative analysis for studying the soil arching is a three-dimensional analysis. In a three-dimensional condition and when piles are in a grid of square pattern, Hewlett and Randolph (1988) found that soil arching would form in a series of domes based on their experimental tests as shown in Figure 2.8 (b). They also observed that the vaults do not necessarily fail only at the crown of the domes, but also they might fail at the pile cap location as an inverted bearing capacity failure because of the high concentrated stresses above the limited area of the caps. Therefore, either location failing first will determine the arching capacity, and the analysis should be done for both locations to determine which has the lower capacity. By considering the equilibrium at the crown of the arch and satisfying the boundary conditions into the following differential equation (Equation 2.11), the inner stress ( $\sigma_i$ ) below the boundary of the arch is as in Equation 2.12.

$$\frac{d\sigma_r}{dr} + \frac{(\sigma_r - \sigma_\theta)}{r} = -\gamma \quad \text{Equation 2. 11}$$

$$\sigma_i = \left[ \gamma \left( 1 - \frac{b}{s} \right)^{2(K_p-1)} \right] \times \left[ H - \frac{s}{\sqrt{2}} \left( \frac{K_p-2}{2K_p-3} \right) \right] + \gamma \frac{s-b}{\sqrt{2}(2K_p-3)} \quad \text{Equation 2. 12}$$

$$\rho = \frac{\sigma_i}{\gamma H} = \left( 1 - \frac{b}{s} \right)^{2(K_p-1)} \times \left[ 1 - \frac{s}{\sqrt{2}H} \left( \frac{K_p-2}{2K_p-3} \right) \right] + \frac{s-b}{\sqrt{2}H(2K_p-3)} \quad \text{Equation 2. 13}$$

The soil arching ratio when failure happens at the pile cap location is given in Equation 2.14:

$$\rho = 1 / \left[ \left( \frac{2K_p (K_p \delta + 1 - (1-\delta)^{K_p})}{(K_p + 1)(\delta + 1)} - 1 \right) (\delta^2 - 1) \right] \quad \text{Equation 2. 14}$$

where:  $\delta = b/s$ .

### 2.3.2 Tensioned Membrane Theories

Geosynthetics have been widely used as a basal reinforcement in both pile-supported embankments and over existing sinkholes to better transfer the applied loads to the piles or surrounding soils, respectively. Thus, when a geosynthetic layer is extended over voids or compressible soils, the geosynthetic deforms and mobilizes some of its strength. This phenomenon is called a tensioned membrane effect. Gourc and Villard (2000) defined the membrane effect as “the ability of a geosynthetic sheet to be deformed, thereby absorbing forces initially perpendicular to its surface through tension.”

A few tensioned membrane theories have been proposed to count for the membrane effect. The available theories are based on a parabolic arc shape and a circular arc shape of the deformed geosynthetic. The stresses developing within the supported soil and applied on the geosynthetic are the reason behind these two shapes. A parabolic shape is a result of considering that the stresses acting on the geosynthetic are only vertical at all the locations across the void width. However, assuming the geosynthetic deformed shape as a circular arc indicates that the stresses acting on the

geosynthetic are normal to the geosynthetic surface even when it deforms. Thus, the stresses on the geosynthetic have vertical and horizontal components at all locations except in the center of the void. It is noteworthy to mention that most of these theories were originally developed for the design of soil-geosynthetic systems over voids, such as sinkholes, dissolution cavities, and localized depression. Even though, they have also been used for designing GRPS embankments. Two of the common methods that have been used in designing geotechnical problems are Delmas (1979), Giroud et al. (1990), will be presented below.

### ***Delmas' Method***

As described earlier, a parabolic arc shape was proposed by Delmas (1979) in an analytical method to predict the tension-deformation relationship of a horizontal geosynthetic sheet above a void (e.g., cavity or trench) subjected to a uniform distributed vertical load as shown in Figure 2.9. The assumptions behind Delmas' method as stated by Gourc and Villard (2000) are:

- the problem is under a plane-strain condition,
- the geosynthetic sheet of original length ( $L$ ) is fixed at each end, and is subjected to a uniformly distributed vertical load ( $q$ ),
- the stresses remain vertical and constant after deformation takes place,
- there is no horizontal displacement of any point on the geosynthetic during deflection,
- the geosynthetic is assumed to have a linear elastic behavior ( $T=J*\varepsilon$ , where  $T$  = the tensile force in the sheet,  $\varepsilon$  = the strain and,  $J$  = the tensile stiffness defined by a unit width of the sheet).

The geosynthetic vertical deformation ( $Z$ ) at any distance ( $y$ ) from the edge of the void can be estimated from Equation 2.15.

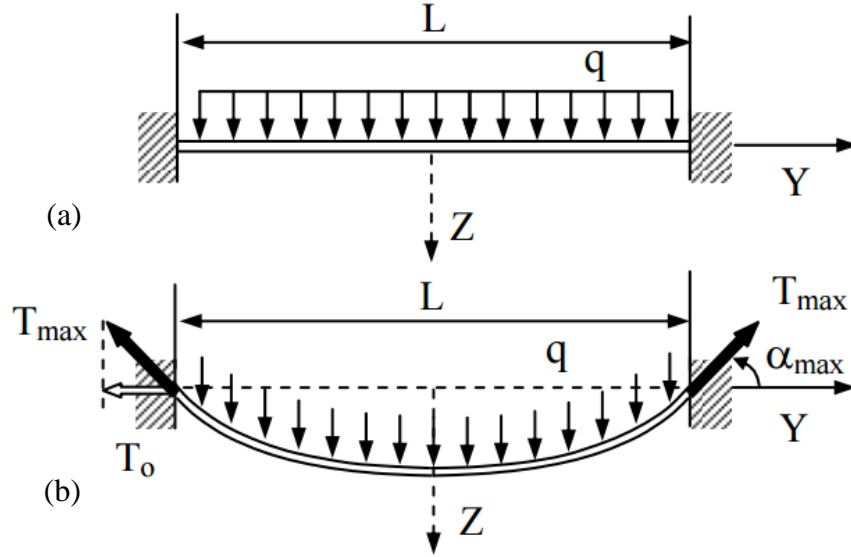


Figure 2.9 Delmas's tensioned membrane method: (a) before deflection and (b) after deflection  
(Gourc and Villard 2000)

$$Z(y) = \frac{qL^2}{8T_0} - \frac{qx^2}{2T_0} \quad \text{Equation 2. 15}$$

where  $T_0$  is the horizontal component of the maximum tension,  $T_{max}$ , and can be calculated from the following equations:

$$T_0 = \frac{qL}{2\beta} \quad \text{Equation 2. 16}$$

$$\frac{qL}{J} = \frac{3 \left[ \beta \sqrt{1 + \beta^2} + \text{ArgSh}(\beta) - 2\beta \right]}{3 + \beta^2} \quad \text{Equation 2. 17}$$

While the maximum tension,  $T_{max}$ , and the maximum deformation,  $Z_{max}$ , can be calculated as:

$$T_{max} = \frac{\sqrt{4T_0^2 + q^2L^2}}{2} \quad \text{Equation 2. 18}$$

$$Z_{max} = \frac{qL^2}{8T_0} \quad \text{Equation 2. 19}$$

***The Giroud et al. Method***

An analytical solution to estimate the tension in the geosynthetic that bridges over a void and deforms in a circular arc shape was presented in Giroud et al. (1990). In addition to assuming the deformed geosynthetic as a circular arc as shown in Figure 2.10, they considered that the load is normally applied to the geosynthetic, which only stretches within the void span with a uniform strain along the portion of the geosynthetic overlying the void.

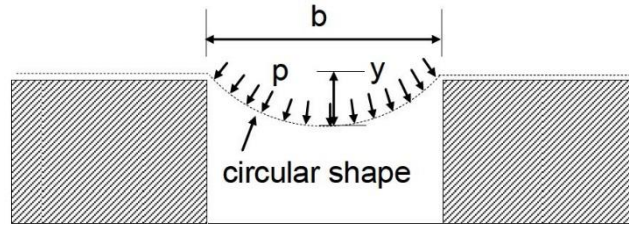


Figure 2.10 Deflected circular geosynthetic layer (Giroud et al. 1990)

The geosynthetic tensile force,  $T$ , over an infinitely long void, can be estimated using Equation 2.20.

$$T = pb\Omega \quad \text{Equation 2. 20}$$

where  $p$  = the pressure normal to the geosynthetic,  $b$  = the void width, and  $\Omega$  = a dimensionless factor, which can be determined by either Equation 2.21 or 2.22:

$$1 + \varepsilon = 2\Omega \sin^{-1} \left( \frac{1}{2\Omega} \right) \quad (y/b \leq 0.5) \quad \text{Equation 2. 21}$$

$$1 + \varepsilon = 2\Omega \left[ \pi - \sin^{-1} \left( \frac{1}{2\Omega} \right) \right] \quad (y/b \geq 0.5) \quad \text{Equation 2. 22}$$

where  $\varepsilon$  = the geosynthetic strain and  $y$  = the maximum deflection.

For a geosynthetic spanning a circular void, despite that the deflection shape is not a circular, Giroud et al. (1990) suggested using a diameter of,  $2r$ , instead of the width,  $b$ , in Equation 2.20 to calculate the tension,  $T$ , approximately.

## **2.4 SOIL ARCHING INVESTIGATIONS UNDER LOADING**

### **2.4.1 Arching Under Self-Weight and Static Surface Loading**

Soil arching has been commonly investigated using the trapdoor test approach since Terzaghi (1936), who conducted the first trapdoor test. Terzaghi's tests were performed in a two-dimensional "plane-strain" box by using a rectangular trapdoor mounted to the box base under soil self-weight only, while McNulty (1965) used a circular trapdoor inside a cylindrical chamber to investigate the arching phenomenon under an axisymmetrical test setup. In addition, McNulty (1965) applied air pressure on the surface of the soil. Terzaghi (1936) and McNulty (1965) found that the shear stress induced by soil arching increased with an increase of the trapdoor displacement based on their test results. The Terzaghi (1936) tests indicated that the pressure on the trapdoor became constant when the deflection reached 10% the width of the trapdoor, while McNulty (1965) studies showed a lower percentage of approximately 3% of deflection needed. They also found a plane of equal settlement, above which no soil arching or reduction of stress was developed, existed when the thickness of the soil mass was large enough. According to Terzaghi's observation, the equal settlement plane was at the height of 1.5 to 2.5 times the width of the trapdoor. However, McNulty (1965) found that the height of the equal settlement plane was from 1.0 to 1.5 times the trapdoor diameter under an axisymmetrical test condition.

Furthermore, trapdoor tests were carried out by Adachi et al. (1989) to investigate soil arching between piles that are used to stabilize landslide. Soil displacement and soil arching effect represented by the load applied on the piles were quantified by using displacement tracking marks buried in the soil and strain gauges attached to the piles, respectively. The soil arching phenomenon was observed by examining the pattern of soil particles' movement. Bertin (1978) conducted

centrifuge cavity collapse tests to investigate the effects of cavity diameter, soil properties, roof thickness, and surcharge on the collapse of the cavity.

Numerical methods have also been used to investigate soil arching behavior in different geotechnical problems. Koutsabeloulis and Griffiths (1989) simulated the trapdoor problem using a finite element method to study the stress distribution related to the active and passive modes of soil arching. In addition, plane strain finite element analyses were conducted by Gabr and Hunter (1994) to investigate the contribution of geogrid in reducing the tensile strains induced in landfill liners over subsurface cavities. Han and Gabr (2002) studied the soil arching effects associated with the geosynthetic-reinforced pile-supported embankments using the finite difference program - FLAC. They found that the soil arching ratio depends on the stiffness difference between piles and soil, the pile spacing, and the existence of geosynthetic reinforcement.

As a conclusion, all these trapdoor studies and numerical studies so far have been conducted with considerably small-scale model tests under soil self-weight or soil self-weight plus uniform static surface loading. Scale effects may have influenced the accuracy of the results, and a uniform surcharge configuration may not be the critical situation for soil arching stability as compared with the locally loaded situation since less differential settlement may develop in the soil. Even though, the load configuration effects have not yet been well investigated.

#### **2.4.2 Arching Under Cyclic or Dynamic Loading**

Several geotechnical applications are subjected to dynamic or cyclic surface loading, such as moving vehicles, railroad crossings, pile driving, impact due to falling of heavy objects, blast waves, and earthquakes.

Chen et al. (1991) performed simple impact tests using buried flexible plates as a trapdoor, acrylic plate, to evaluate the effects of impact or dynamic loading on the soil arching. In their test

setup shown in Figure 2.11, a small-scale cylindrical sand tank was used. By using a steel ball that was dropped from a high of 0.6 m on an aluminum plate placed on the top of sand, the impact loading was generated. Three different thicknesses of buried plates were used to represent different degrees of roof rigidity. In all the tests, the ratio of soil cover thickness to opening diameter was kept to be 0.5. The earth pressures above and accelerations below the buried plate were measured. The test results demonstrated significant soil arching effects, and these effects depended on the deflection of the plate and the interaction between the soil and the plate. However, it is believed that no true soil arching developed in Chen et al. (1991) tests because the trapdoor deflection was corresponded to the deflection of the acrylic plate itself due to its flexibility.

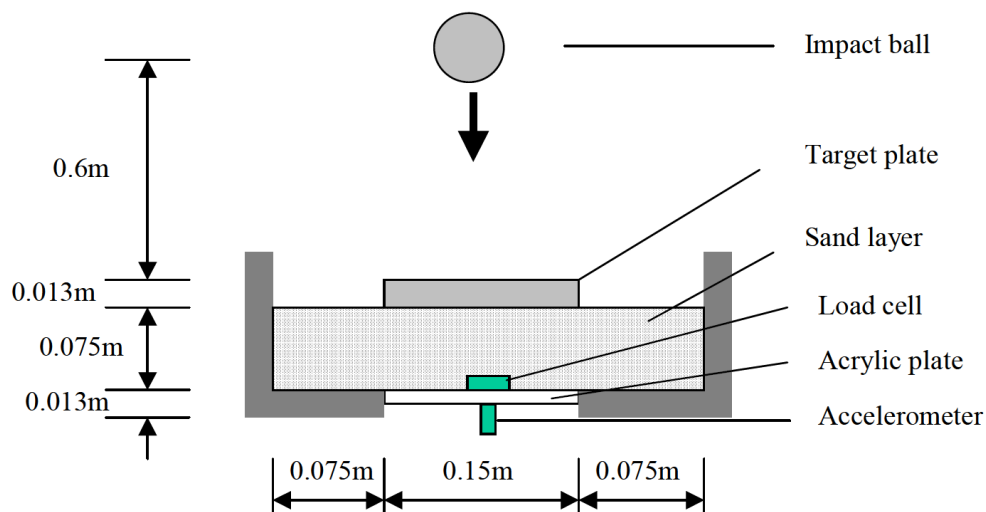


Figure 2.11 Chen et al. (1991) dynamic soil arching experimental setup (Han, personal communication)

Dancygier and Karinski (1999) also studied the soil arching contribution on the response of soil-buried structures under dynamic surface loading and proposed a simple, analytical model to evaluate the effect of shear stresses in soil. Their model assumed that the soil was subjected to a uniformly distributed surface dynamic or impact loading. The model also assumed the potential slip plane above the buried structure is vertical, which is the same as that proposed by Terzaghi

(1943). Dancygier and Karinski (1999) defined the “arching ratio” as the ratio of the shear stress to the vertical displacement, which is different from the ratio proposed by McNulty (1965). Furthermore, Helwany and Chowdhury (2000) performed experimental studies to assess the change of lateral earth pressures on buried structures under dynamic loading considering soil arching effects.

Han and Bhandari (2009) and Bhandari (2010) conducted a numerical study using a discrete element method (DEM) to investigate soil arching and geogrid tension in geogrid reinforced and unreinforced pile supported embankments under cyclic loading. In the unreinforced embankment shown in Figure 2.12 (a), the contact force was oriented randomly after 25 cycles of loading through the footing on the surface, suggesting the collapsing of soil arching. In the geosynthetic-reinforced embankment, however, the orientation and continuity of the contact force suggested a stable soil arching as shown in Figure 2.12 (b). Bhandari (2010) found that the vertical stresses over the pile caps and the soft soil were constant for the reinforced embankment irrespective of the load cycles. On the other hand, the stresses over the pile caps decreased and the stresses on the soil increased with the load repetition for the unreinforced embankment. Consequently, one can conclude that the stresses above the pile caps and the soil may eventually approach to the same value if a sufficiently large number of load repetitions is applied, which is a case of disappearance of soil arching due to the equal stress condition.

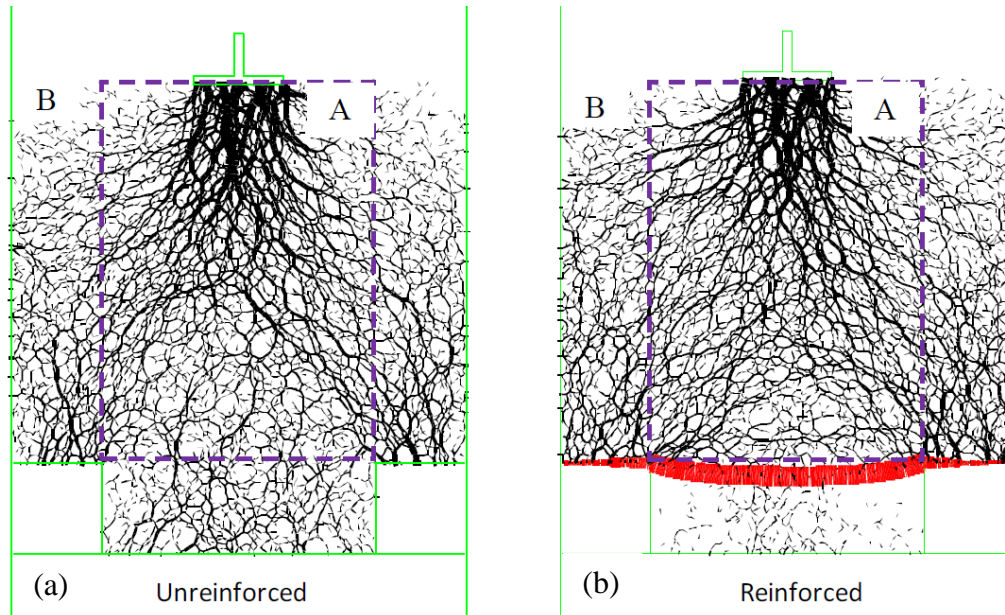


Figure 2.12 Contact force distribution for: (a) unreinforced and (b) reinforced embankment after 25 cycles of loading (Bhandari 2010)

In general, soil arching under static loading is formed by shear stresses, which depend on the contact stresses between soil particles as a result of the interactional frictional forces. Under dynamic loading, however, the interactional frictional forces and the contact stresses may be reduced due to vibration effects so that the soil arching tends to deteriorate leading to the progressive collapse of interactional forces transmitting shear stresses otherwise developing in the granular media. The factors that may affect the stability of the soil arching under dynamic or cyclic loading are, for example, the severity (i.e., number and intensity) of cyclic loading, the size of the load area, the distance between the load and the stable arch, and the presence of reinforcement.

## CHAPTER 3 EXPERIMENTAL TESTS

This chapter presents the test setup and describes the experimental work details including embankment material properties, reinforcement properties, instrumentation, test procedure, and loading types.

### 3.1 MODEL TEST SETUP

To address the points mentioned earlier in the problem statement section in Chapter 1, three different conditions were investigated, which include unreinforced fill, single geosynthetic-reinforced fill, and double geosynthetic-reinforced fill. Complete test setup for each condition is depicted in Figures 3.1, 3.2, and 3.3, respectively. Since the general focus of this research was to investigate the soil arching mobilization and to assess the stability of soil arching during surface loading, fully-mobilized soil arching developed first and was followed by the application of an incremental footing load. Therefore, in general, a complete test consisted of two test stages after the embankment fill had been constructed: (1) a trapdoor test stage and (2) a loading test stage. For the comparison purpose, two tests, though, were performed with a loading test stage without a trapdoor test stage. Table 3.1 outlines 14 tests that were carried out as part of this research, eight of which were performed under static loading after the trapdoor test had been completed, but ??? of which were conducted under cyclic loading. The trapdoor test stage was carried out under soil self-weight, soil self-weight plus static load, and soil self-weight plus a cyclic load for the unreinforced fill case, while for each case of the single and double geosynthetic-reinforced fill, the trapdoor test stage was performed under soil self-weight only. The loading test stage was performed using a rigid footing subjected to either monotonic static or incremental cyclic loading under all the three conditions.

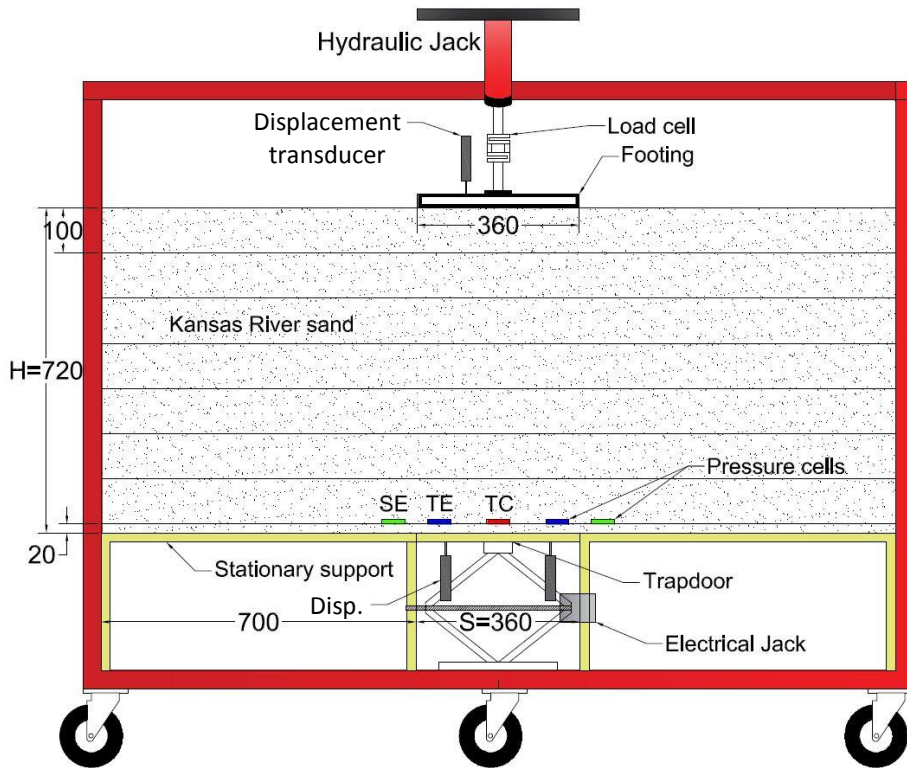


Figure 3.1 Test setup for the unreinforced fill (unit: mm)

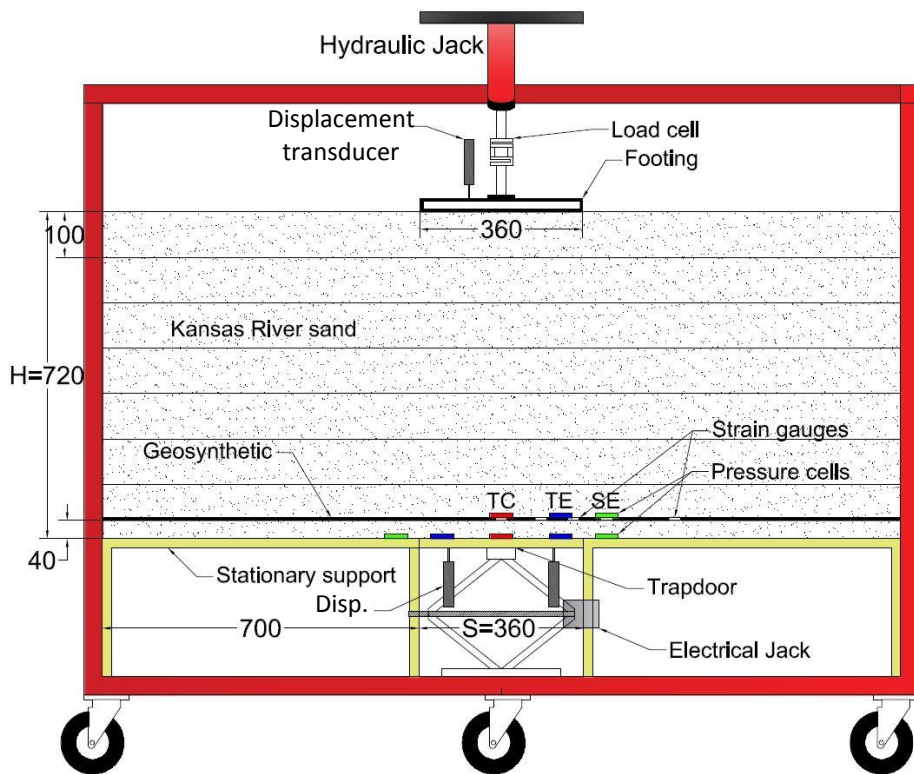


Figure 3.2 Test setup for the single geosynthetic-reinforced fill (unit: mm)

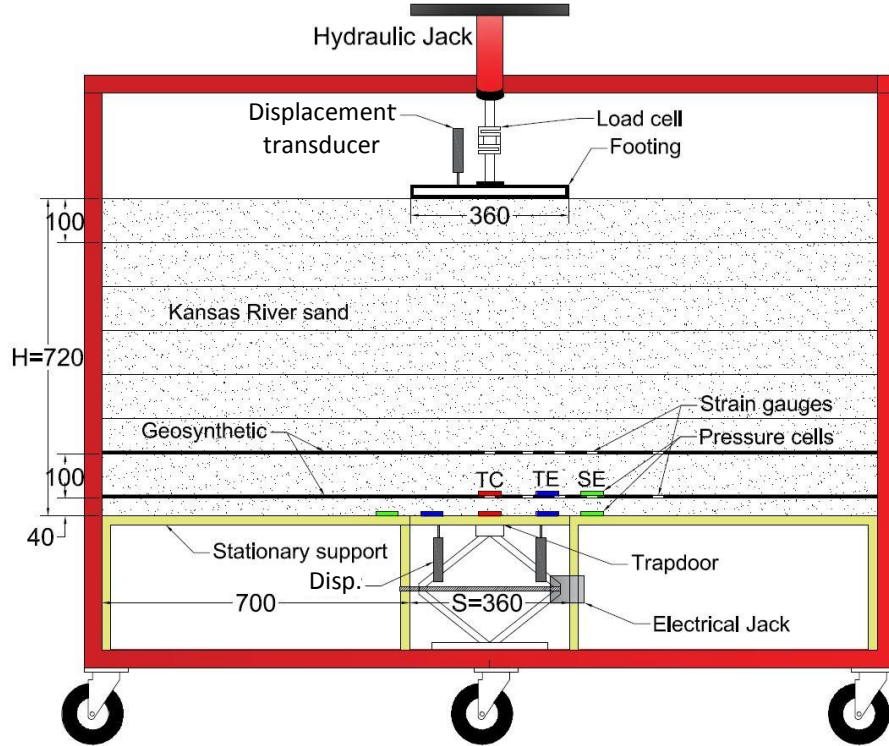


Figure 3.3 Test setup for the double geosynthetic-reinforced fill (unit: mm)

Table 3.1 Test Plan

Trapdoor and static loading test series (Eight tests)	Unreinforced fill (Four tests)	<b>Test No. 1</b> Loading test without trapdoor test (baseline test)	<b>Test No. 2 and No. 3</b> Different maximum displacements of a trapdoor test then a loading test	<b>Test No. 4</b> A constant static loading test then a trapdoor test
	Single layer of geosynthetic (Two tests)	<b>Test No. 5</b> A uniaxial geogrid overlain by a non-woven geotextile		<b>Test No. 6</b> A biaxial geogrid overlain by a non-woven geotextile
	Double layers of geosynthetic (Two tests)	<b>Test No. 7a and No. 7b</b> Double layers of biaxial geogrid overlain by a non-woven geotextile		
Trapdoor and cyclic loading test series (Six tests)	Unreinforced fill (Three tests)	<b>Test No. 8</b> Loading test without a trapdoor test (baseline test)	<b>Tests No. 9</b> A trapdoor test then a loading test	<b>Test No. 10</b> A constant cyclic loading then a trapdoor test
	Single layer of geosynthetic (Two tests)	<b>Test No. 11</b> A uniaxial geogrid overlain by a non-woven geotextile		<b>Test No. 12</b> A biaxial geogrid overlain by a non-woven geotextile
	Double layers of geosynthetic (One test)	<b>Test No. 13</b> Double layers of biaxial geogrid overlain by a non-woven geotextile		

All tests were carried out under a plane strain condition in the test box with an interior dimension of 1760×460×1480 mm (long×wide×high). This box was made of three sides of plywood and a Plexiglas on the front side to allow for monitoring of soil movement during the test and reinforced by steel tubes all around the box outside to minimize its lateral movement as shown in Figure 3.4 (a and b). Also, the Plexiglas was stiffened by two sections of steel angle in a size of 50×50×5 mm along the front side. All three sides of the plywood were covered by a plastic sheet to minimize the frictional effect of the box sides.

An embankment of granular fill was built using the Kansas River sand on the box base, which consisted of two wooden stationary supports and one moveable trapdoor. The trapdoor had a dimension of 360 mm wide and 460 mm long and could be moved vertically using an electrical jack as shown in Figure 3.4 (c). The length of the trapdoor was the same as the width of the box. The trapdoor width,  $S$ , was selected to be 1/5 of the test box width (i.e., 1760 mm) so that the boundary effect could be minimized. The trapdoor roof consisted of one piece of 19 mm thick plywood on a 6.35 mm thick steel plate, which was supported by an electrical jack. To ensure that the trapdoor would settle evenly, four springs were placed near the corners of the trapdoor. In addition, a plastic washer was placed all around the trapdoor and used to reduce the frictional resistance between the trapdoor and the stationary supports. The stationary supports had a dimension of 700 mm×460 mm and were made of one piece of 19 mm thick plywood.

On the top of the embankment fill, a load was applied during each loading test stage using a hydraulic jack attached to a rigid steel footing that had the same dimension as the trapdoor (i.e., 360 mm×460 mm) and was centered above the trapdoor as shown in Figure 3.4 (d). The hydraulic jack had a capacity of 25 tons and was modified to apply cyclic loading with a maximum frequency of 0.5 Hz as well as static loading. During the loading test, the applied load was monitored using

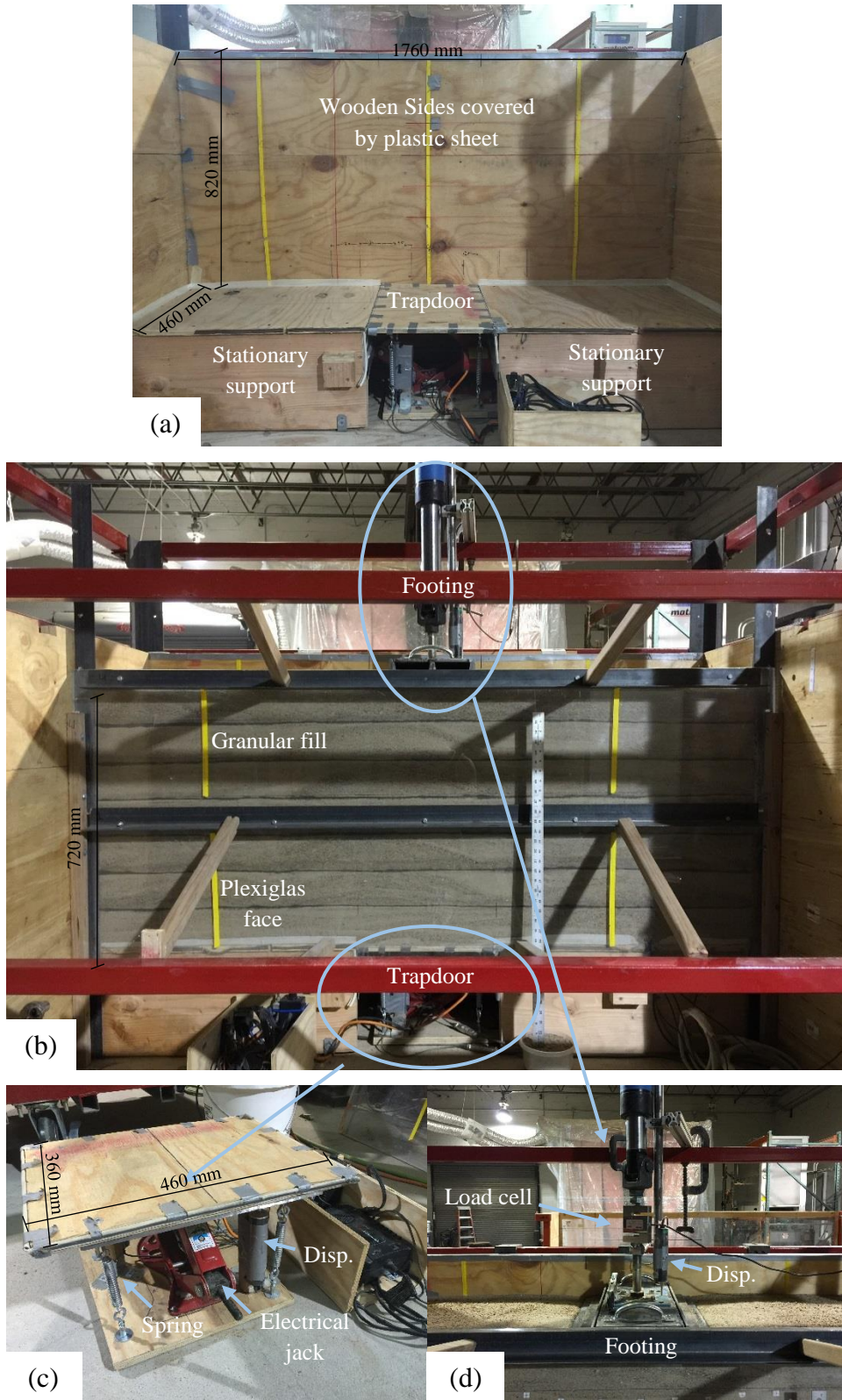


Figure 3.4 Test setup: (a) test box, (b) embankment fill, (c) trapdoor mounted on electrical jack, and (d) footing on top of the fill

of 0.5 Hz as well as static loading. During the loading test, the applied load was monitored using an S-shape load cell with a capacity of 22.3 kN.

### 3.2 MATERIAL PROPERTIES

#### 3.2.1 Fill Material

Granular material is commonly used as a fill material in most of the geotechnical applications, such as embankments, reinforced earth platforms, fill over buried pipes, and fill behind retaining walls, in which soil arching is an important mechanism of the load transfer. Therefore, Kansas River sand was selected as a granular fill material in this study to investigate the arching phenomenon. Based on the particle size distribution curve shown in Figure 3.5 and according to the Unified Soil Classification System (USCS), this sand was classified as a poorly graded sand (SP). The coefficients of uniformity ( $C_u$ ) and curvature ( $C_c$ ) were calculated to be equal to 3.18 and 0.99, respectively. The Kansas River sand had minimum and maximum dry unit weights of  $16.02 \text{ kN/m}^3$  and  $18.85 \text{ kN/m}^3$ , respectively, in accordance with ASTM D4254-14 and ASTM D4253-14.

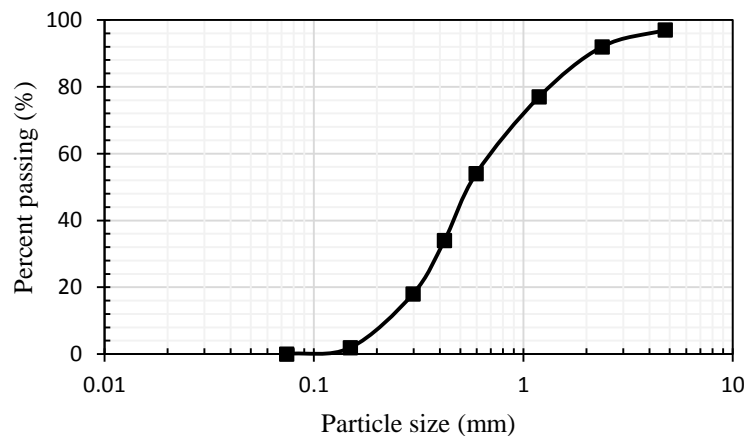


Figure 3.5 Particle size distribution curve for the Kansas River sand

For all tests, the embankment height (H) was selected to be twice the width of the trapdoor (i.e.,  $H=720$  mm,  $S=360$  mm, and  $H/S=2$ ) in order to ensure that the equal settlement plane was formed within the embankment. The embankment was constructed in seven lifts of 100 mm thick per lift using a mass-volume control method. During the construction of the embankment, the Kansas River sand was poured and then compacted until the required fill height was reached. Even though most studies related to the soil arching investigation were usually performed on a backfill that had been constructed using an air pluviation (or raining) method to ensure a uniform density, this method was believed to be unrepresentative for the actual construction followed in geotechnical practices. Therefore, a manual compactor, with a 150 mm drop height as shown in Figure 3.6, was used to compact each lift by evenly distributing 64 drops on the sand lift surface until a relative density of 75% was reached. The sand compacted at this density had a unit weight of  $18.04 \text{ kN/m}^3$  and a peak friction angle of  $38.6^\circ$  based on triaxial shear tests.



Figure 3.6 Manual steel compactor

### 3.2.2 Reinforcement

As pointed out in Chapter 2, geosynthetic reinforcement has been used in several geotechnical applications, such as GRPS embankments, geosynthetic bridging over cavities, and reinforced earth platforms. However, the effect of geosynthetic reinforcement on soil arching has rarely been investigated. Therefore, investigating the effects of the geosynthetic reinforcement on soil arching is valuable for practical applications.

In all the reinforced fill test sections, a non-woven geotextile layer was placed above a geogrid layer as a reinforcement layer. Because sand was used as a fill material, the non-woven geotextile was placed above the geogrid to prevent sand from flowing through the geogrid aperture and distribute the load from the embankment to the geogrid. Also, as outlined earlier in Table 3.1, two types of geogrids were utilized. They were biaxial geogrid and customized uniaxial geogrid as shown in Figure 3.7. The uniaxial geogrid was customized from the biaxial geogrid by removing two sequential transverse ribs. Because the tests in this study were carried out under a two-dimensional plane strain condition, the use of the uniaxial geogrid was considered in order to distinguish between the two-dimensional (2D) and three-dimensional (3D) behavior of the geosynthetic. Table 3.2 presents the properties of uniaxial geogrid, biaxial geogrid, and non-woven geotextile.

As shown in Figure 3.2, the single geosynthetic layer was placed over a sand cover of 40 mm thick over the trapdoor and stationary supports. Also, the same thickness of sand cover was used under the first reinforcement layer in the double geosynthetic reinforced fill tests, and a distance of 100 mm was left between the first and second layers of reinforcement as shown in Figure 3.3.

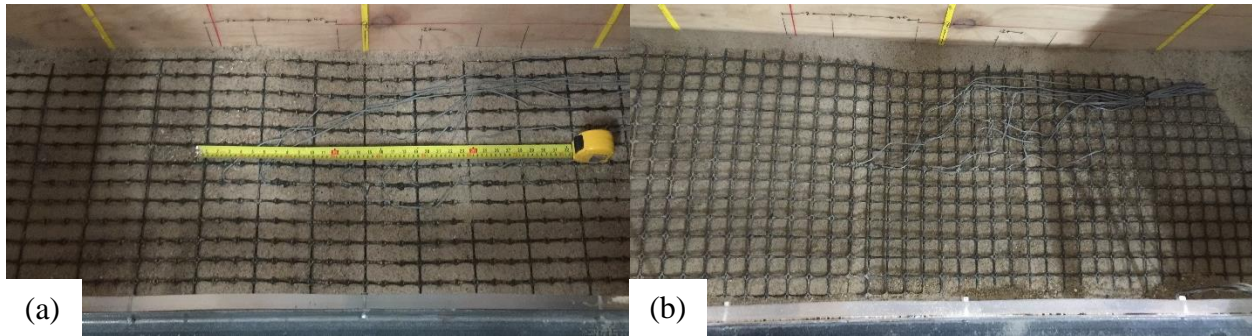


Figure 3.7 Two types of geogrid: (a) customized uniaxial geogrid and (b) biaxial geogrid

Table 3.2 Geosynthetic properties

Geosynthetic	Properties	Units	Values	
			MD values*	XMD values*
Uniaxial geogrid	Aperture dimensions	mm	Long.: 100	Tran.: 25
	Minimum rib thickness	mm	0.76	
	Tensile strength @ 2% strain	kN/m	6.4	
	Tensile strength @ 5% strain	kN/m	12.8	
	Ultimate tensile strength	kN/m	17	
			MD values*	XMD values*
Biaxial geogrid	Aperture dimensions	mm	25	33
	Minimum rib thickness	mm	0.76	0.76
	Tensile strength @ 2% strain	kN/m	4.1	6.6
	Tensile strength @ 5% strain	kN/m	8.5	13.4
	Ultimate tensile strength	kN/m	12.4	19
Non-woven geotextile	Unit mass	g/m <sup>2</sup>	119	
	Grab tensile strength	N	400	
	Grab elongation	%	50	
	Trapezoid tear	N	156	
	Puncture	N	245	
	Mullen burst	kN/m <sup>2</sup>	1276	

\*Note: MD refers to the machine direction, and XMD refers to the cross-machine direction.

### 3.3 METHOD OF MEASUREMENT

In this study, four types of measurements were made in each test, which include earth pressures, footing and trapdoor displacements, geosynthetic strains, and embankment fill movement.

To obtain the pressure distribution in each unreinforced fill test, eight earth pressure cells were used and placed over a 20 mm thick sand bed, which was placed over the trapdoor and the

stationary supports as shown in Figure 3.8. These pressure cells had an outside diameter of 50 mm, a sensing-surface diameter of 46 mm, a thickness of 11.3 mm, and a maximum capacity of 200 kPa. Five pressure cells, which are highlighted inside the ellipse shape in Figure 3.8, were installed symmetrically about the centerline of the trapdoor at the distances of 0, 130, and 230 mm, respectively, in all the tests. Three pressure cells located on the top of the trapdoor were used to measure the change of the vertical earth pressures with the vertical displacement of the trapdoor, while the other two cells were installed to measure the increase of the vertical earth pressures at the stationary supports. The pressure cell placed at the centerline of the trapdoor is noted as TC, and the other two cells near the edges of the trapdoor are noted as TE-R and TE-L (R stands for the right, and L stands for the left). Also, the two pressure cells near the edges of the stationary supports are noted as SE-R and SE-L.

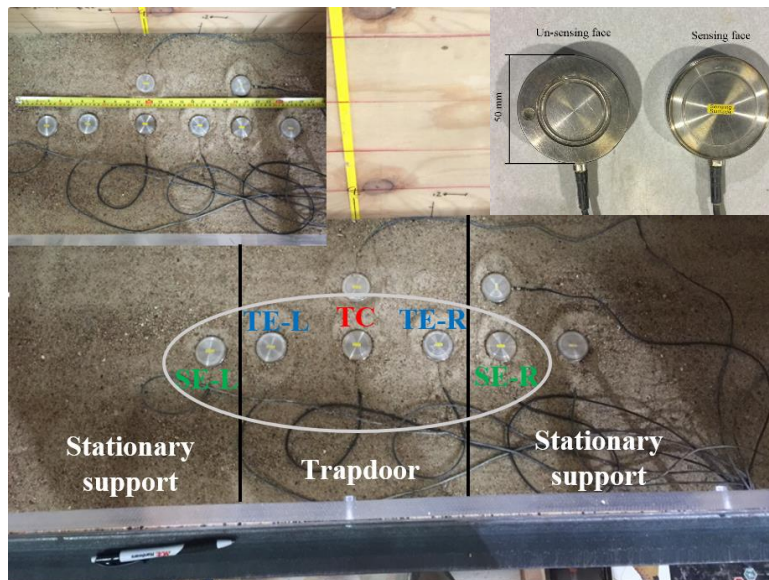


Figure 3.8 Earth pressure cell layout in the unreinforced fill tests

In the geosynthetic-reinforced tests, five pressure cells were placed over the trapdoor and the stationary supports directly with the same spacing mentioned earlier, and three pressure cells were placed over the first geosynthetic layer as shown in Figure 3.9.

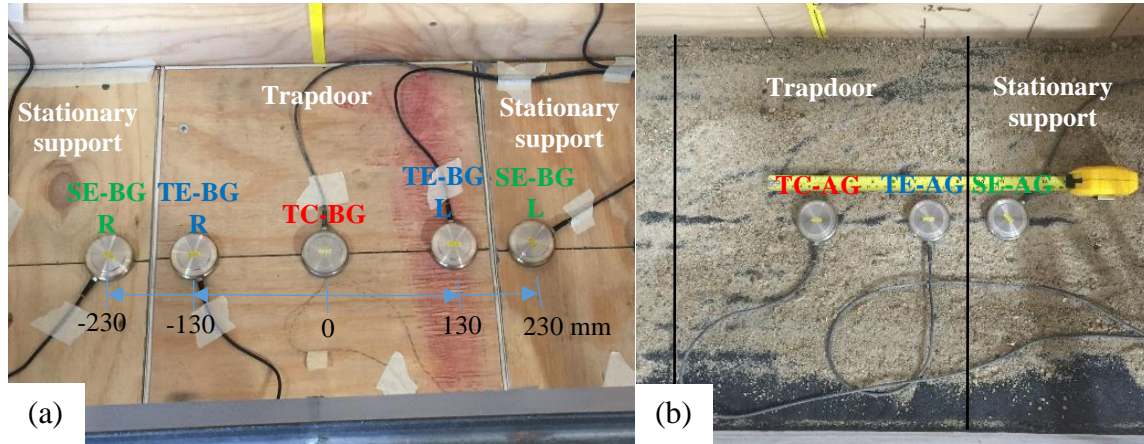


Figure 3.9 Earth pressure cell layout in the reinforced fill tests: (a) below the geosynthetic and (b) above the geosynthetic

For the clarity of the figures in next chapter, the average pressure from the pressure cells (TE-R and TE-L) and that from (SE-R and SE-L) will be presented instead of all the readings because they were essentially the same due to the symmetrical layout.

The displacements of the footing and the trapdoor were monitored using three displacement transducers (type TML CDP-50, manufactured by the Tokyo Sokki Kenkyujo Co., Ltd.) with a measuring capacity of 50 mm. Figure 3.10 shows that two displacement transducers were placed

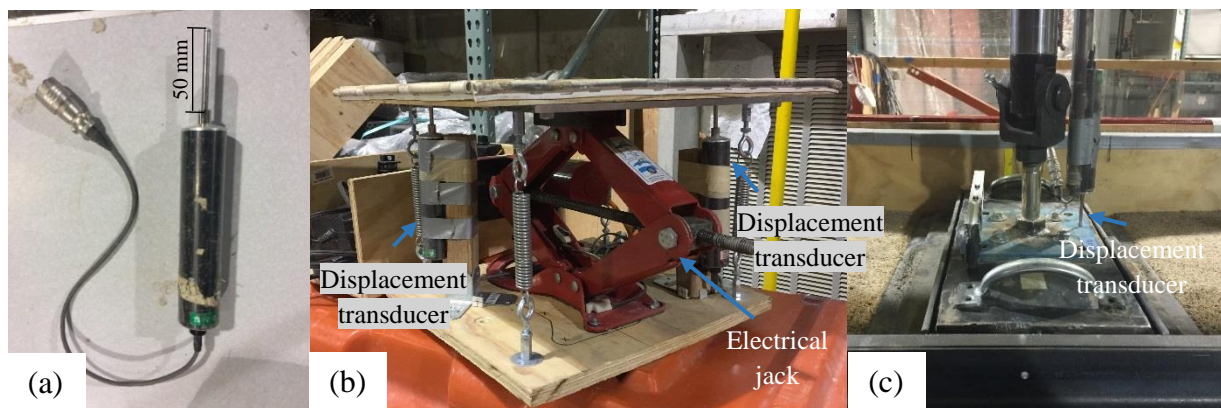


Figure 3.10 Displacement transducer: (a) in display, (b) below the trapdoor and (c) above the footing

under the trapdoor, along with the diagonal line and at 100 mm away from the sides of the trapdoor. Another displacement transducer was mounted above the footing to monitor the footing settlement during the loading test stage.

In the geosynthetics reinforced fill tests, 5-mm long strain gauges supplied by Tokyo Sokki Kenkyujo Co., Ltd., as shown in Figure 3.11(a), were attached to the geogrid at different locations. Plastics hard bonding agent was used to glue strain gauges to the geogrid as shown in Figure 3.11(b).

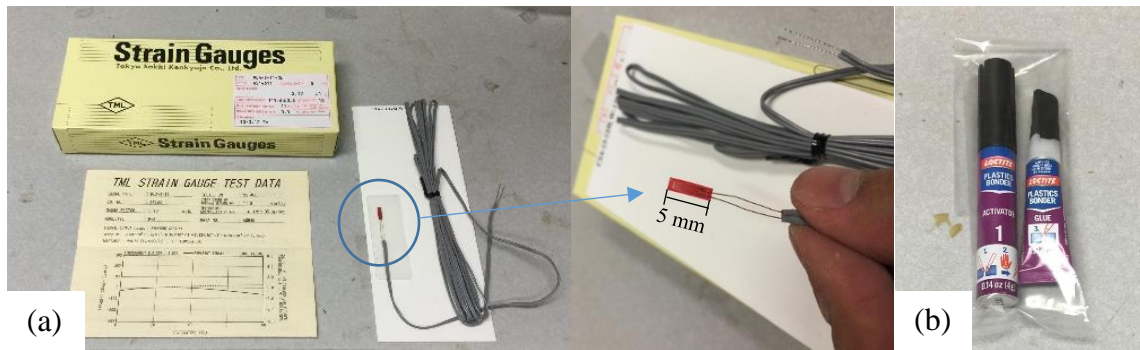


Figure 3.11 Materials for strain gauge installation: (a) strain gauge and (b) plastic bonding agent.

When the uniaxial geogrid was used, nine strain gauges were placed at five different locations along the middle rib as shown in Figure 3.12, seven of which were attached to the upper surface and the other two were attached to the lower surface of the geogrid. The strain gauges placed on double surfaces at the same location where the high tensile forces were expected to study the bending effect of the geogrid. When the biaxial geogrid was used, eleven strain gauges were attached at six different locations as shown in Figure 3.13. Among these strain gauges, six gauges were placed above and below the geogrid while the other five were attached to the upper surface of the geogrid only.

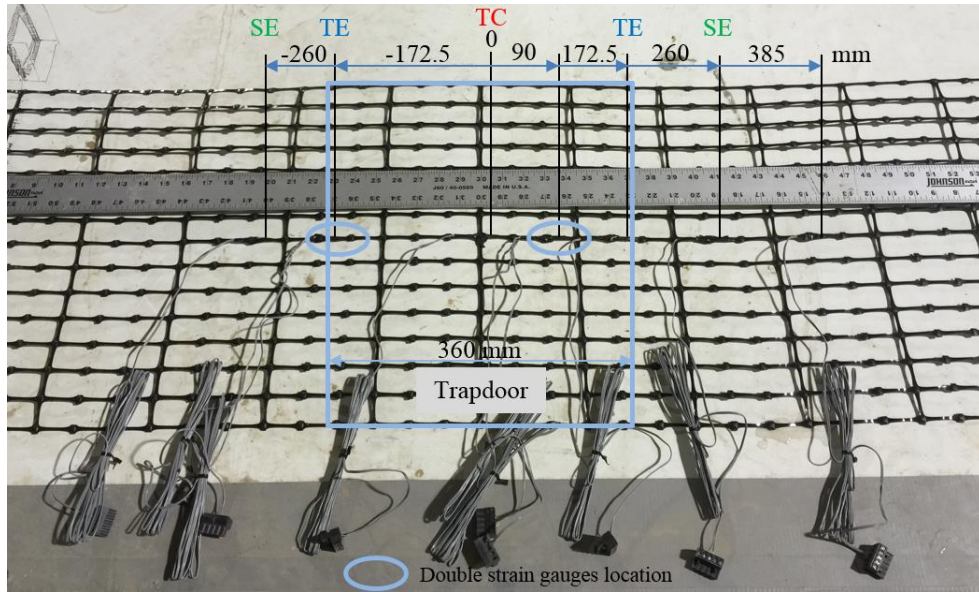


Figure 3.12 Strain gauge locations on the uniaxial geogrid

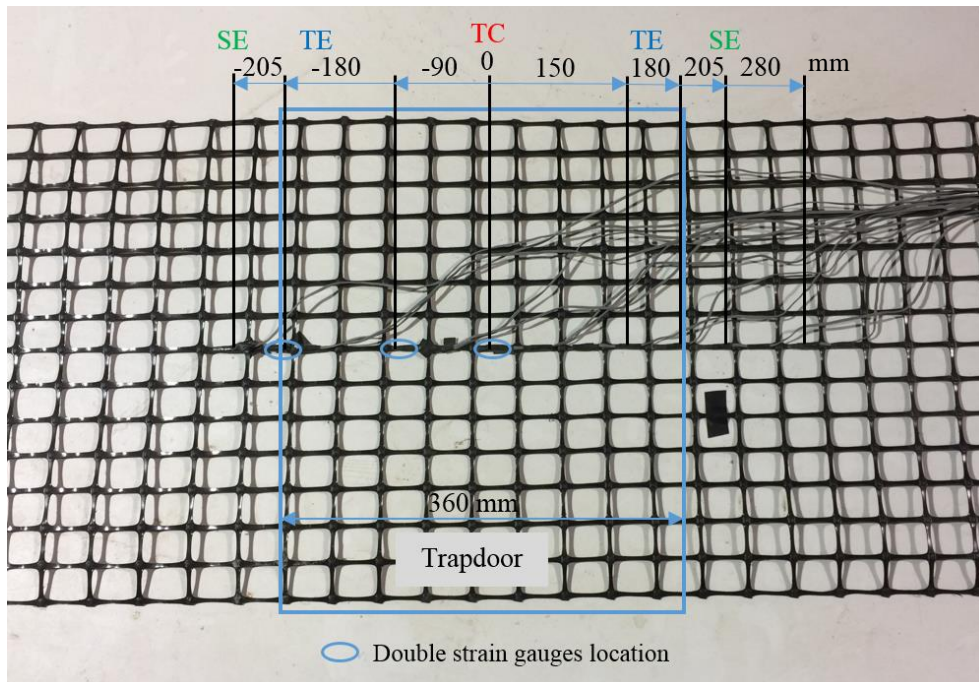


Figure 3.13 Strain gauge locations on the biaxial geogrid

To estimate the height of the equal settlement plane and monitor the fill movement, a photogrammetric method was used to trace the marked aluminum plates of 10 mm × 10 mm in size and the black colored sand lines, which were placed between the lifts of sand during the fill

placement. For the photogrammetric method, a camera was used and fixed in position during the trapdoor test to record the fill movement. Figure 3.14 shows the mark setup for tracing the fill movement during each test.

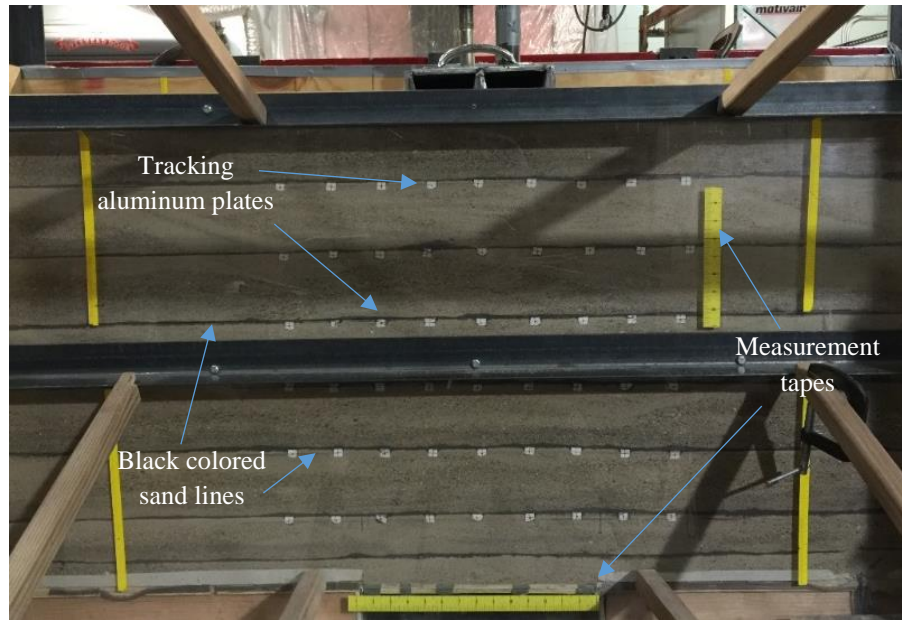


Figure 3.14 Marked aluminum plates and black colored sand lines between sand lifts

Two data acquisition systems were used to record the vertical pressures, the footing and trapdoor displacements, and the geosynthetic strains. Three Smart Dynamic Strain Recorders (type DC-204R, manufactured by Tokyo Sokki Kenkyujo Co., Ltd.) were connected to the pressure cells and the displacement transducers to record the pressure distributions and the displacements automatically with a scan frequency of 100 Hz. Another data acquisition system consisted of the CR-1000 Campbell Scientific data logger and two units of multiplexer, which were connected to the strain gauges. Figure 3.15 shows the data acquisition systems used in this study.

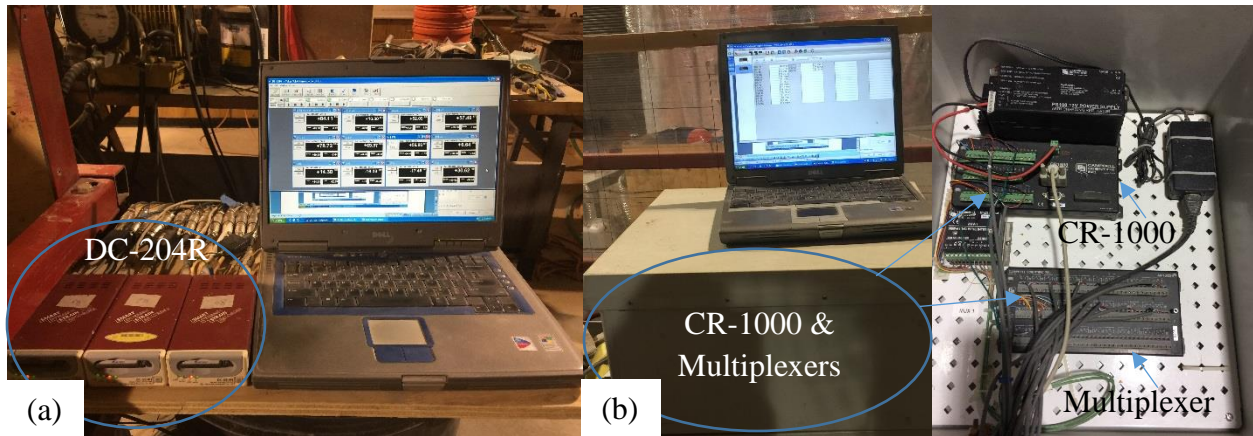


Figure 3.15 Data acquisition systems: (a) smart, dynamic strain recorder and (b) CR-1000 data logger and multiplexers

### 3.4 TEST PROCEDURE

As mentioned earlier, totally 14 tests were carried out in this study. Most tests consisted of embankment construction, trapdoor test, and loading test. However, two baseline tests were conducted just with a loading test stage after the embankment had been constructed. The general procedures for the embankment construction of these tests are summarized in the following steps:

In the unreinforced embankment tests:

1. Placing a sand bed of 20 mm over the box base which consisted of one middle trapdoor and two stationary supports.
2. Installing the earth pressure cells, as described earlier, and connecting them to the data acquisition system to record the pressures during the embankment fill construction.
3. Using the mass-volume control method to place 155 kg of the Kansas River sand inside the box with the pre-determined fill lift of 100 mm.
4. Compacting the sand lift using the steel manual compactor as described earlier with the even distribution of 64 drops on the surface of the sand lift in a square pattern until reaching the required thickness.

5. Placing the marked aluminum plates and the black colored sand lines, which were used during the trapdoor test to locate the equal settlement plane, behind the Plexiglass.
6. Recording the vertical pressures after the placement of each sand lift.
7. Repeating the above four steps from No. **3** to **6** six more times until the required height of the embankment was reached.

In the reinforced embankment tests with a single layer of geosynthetic reinforcement:

1. Placing five earth pressure cells directly over the box base symmetrically about the centerline of the trapdoor.
2. Placing a sand lift of 40 mm, a uniaxial geogrid or a biaxial geogrid, and a non-woven geotextile.
3. Installing three more pressure cells on the geotextile layer (one in the center of the trapdoor and the other two at the distances of 130 and 230 mm away from the centerline, respectively).
4. Placing the rest sand lifts and compacting each lift as described in Step No. **4** of the unreinforced test procedure.
5. Repeating Steps No. **3** to **6** as the unreinforced test procedure six more times until the required height of the embankment was reached.

In the reinforced embankment tests with double layers of geosynthetic reinforcement:

1. Following the same steps No. **1** to **4** from the procedure for the single geosynthetic-reinforced tests.
2. Adding the second geosynthetic layer within the second sand lift such that the distance between the first and second layers was equal to 100 mm.
3. Following Step No. **5** for the single geosynthetic-reinforced tests.

After the embankment had been constructed, the trapdoor test was initiated by slowly lowering the trapdoor at about 1 mm displacement increments until reaching fully mobilized soil arching. A period of five minutes was allowed after each displacement increment to ensure that the pressure cell readings were stable and the embankment deformations were measured. A photogrammetric method, by utilizing a fixed camera, was used to detect the embankment deformations by tracing colored sand lines which were placed between the sand lifts during the construction. The fully mobilized soil arching was determined when the earth pressure over the stationary supports reached a peak value.

To examine the stability of soil arching under a surface load, a footing static or cyclic load was utilized in the loading test stage. In this stage, the trapdoor was held in place, and no further displacement was allowed. Then, the footing load was applied and increased in increments with each incremental pressure of about 7 kPa. The loading test was ended when the pressure on the center of the trapdoor exceeded the pressure on the stationary supports. The static and cyclic loading details are further discussed in the next section.

### 3.5 LOADING TYPE

Throughout the experimental tests, both monotonic static and cyclic loads were adopted to investigate the effect of surface loading on the stability of soil arching. The load was applied using a rigid footing which had the same dimension as that of the trapdoor and was centered along the test box centerline, as described earlier in the test setup section. As outlined in Table 3.1, eight tests were performed on both unreinforced and geosynthetic-reinforced fill under a static footing load, which was applied in increments with each incremental pressure of about 7 kPa and was held for about seven minutes. Figure 3.16 shows a general example of the monotonic loading sequence that was used for the tests under static loading.

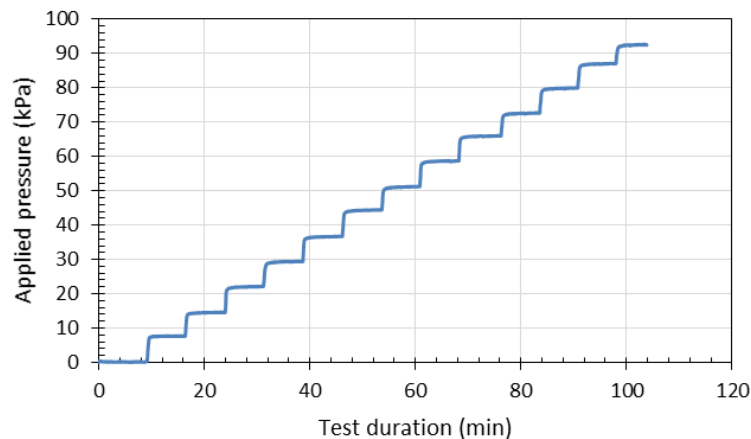


Figure 3.16 Example of the monotonic static loading

In the cyclic loading tests, the soil arching phenomenon was investigated under an incremental cyclic loading of a frequency of 0.1 Hz and with 100 cycles per each loading increment of 7 kPa. Figure 3.17 shows a general example of the incremental loading applied in the cyclic loading tests.

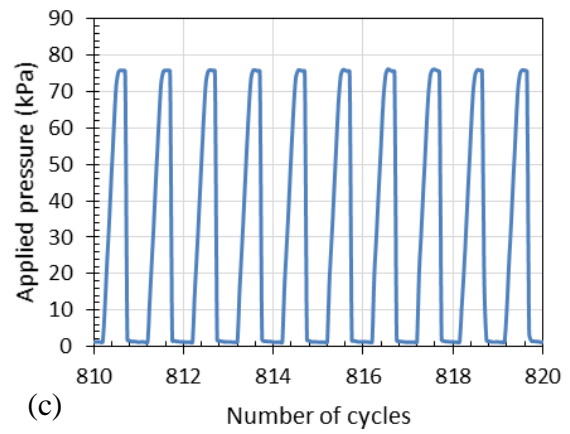
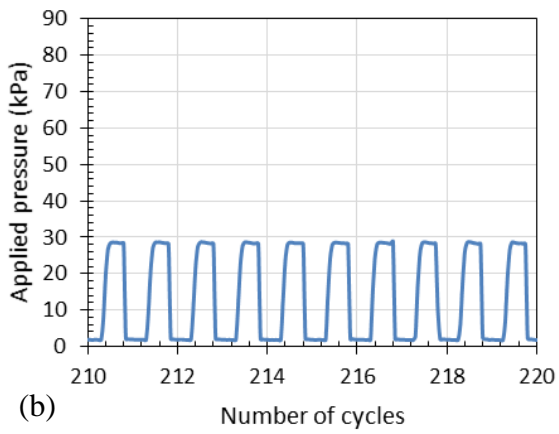
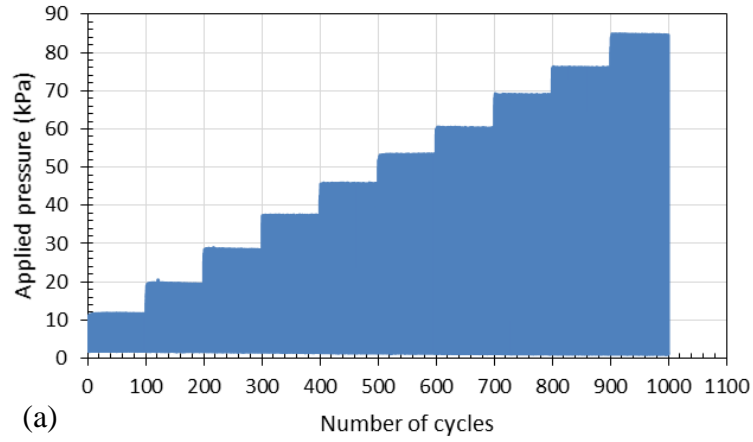


Figure 3.17 Example of the incremental cyclic loading: (a) during the whole loading period, (b) from cycles No. 210 to 220, and (c) from cycles No. 810 to 820

## **CHAPTER 4 ANALYSIS OF TRAPDOOR TEST RESULTS**

This chapter presents and discusses the results of twelve trapdoor tests that were carried out after the construction of embankment fill to investigate the mobilization of the soil arching under different conditions: soil self-weight, and soil self-weight plus static or cyclic footing load. Ten trapdoor tests were conducted under soil self-weight, three of which were performed with the unreinforced embankment fill (T2, T3, and T9), four with the single geosynthetic-reinforced fill (T5, T6, T11, and T12), and three with double geosynthetic-reinforced fill (T7a, T7b, and T13). The other two trapdoor tests were conducted under soil self-weight plus static footing load (T4) and soil self-weight plus cyclic footing load (T10) with the unreinforced embankment fill. All trapdoor tests on the reinforced embankment fill and T2 were performed to a maximum trapdoor displacement of about 15.0 mm, while the trapdoor tests with the unreinforced embankment fill were conducted with a maximum trapdoor displacement of about 8.0 mm. Each trapdoor test was followed by either static or cyclic surface loading to investigate the stability of the soil arching, which will be discussed in the next chapter. The description and number of the tests carried out in this study were summarized in Table 3.1.

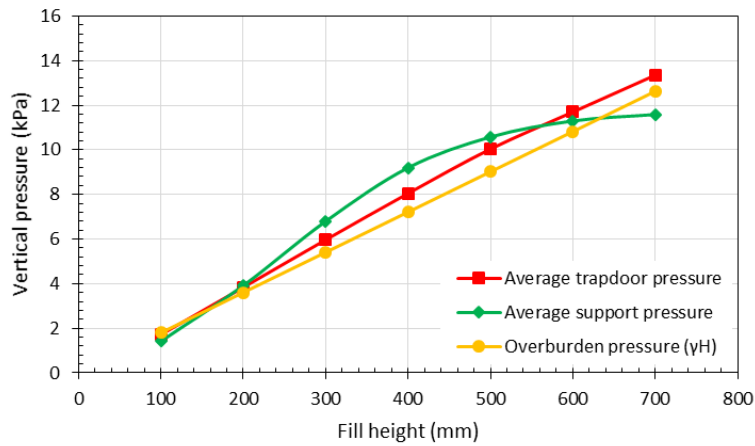
### **4.1 TRAPDOOR TEST UNDER SOIL SELF-WEIGHT**

#### **4.1.1 Unreinforced Embankment Fill**

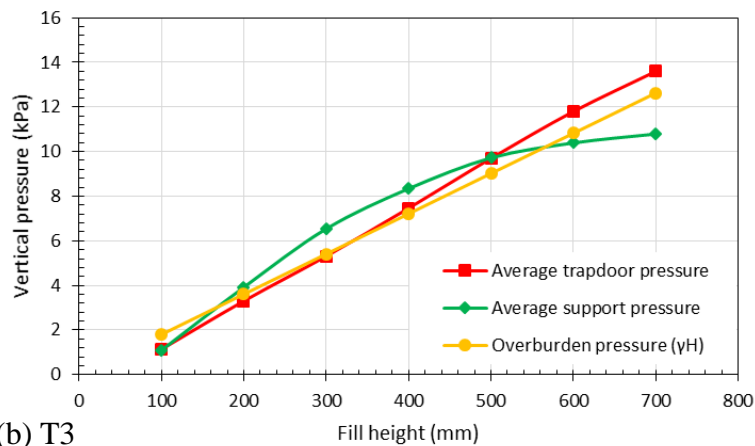
In the unreinforced embankment fill, three trapdoor tests (T2, T3, and T9) with two different maximum trapdoor displacements were performed to assess the displacement effect on the soil arching mobilization.

Figure 4.1 shows the measured pressures on the box base during the embankment construction for T2 and T3. This figure shows that during the construction of the embankment, the measured pressures increased on both the trapdoor and the stationary supports. At the end of the

construction, the vertical pressures over the trapdoor and the supports were almost equal to the overburden pressure ( $\gamma H$ ). However, the pressure on the trapdoor was slightly higher than that on the stationary supports. This difference could be attributed to the stiffness difference of the trapdoor and the stationary supports because of the presence of the steel plate underneath the trapdoor as described earlier in Chapter 3.



(a) T2



(b) T3

Figure 4.1 Measured pressures on and besides the trapdoor during the fill construction in: (a) T2 and (b) T3

Figure 4.2 shows the result of the trapdoor test in T2, which was conducted to a maximum trapdoor displacement of 15 mm and then followed by a loading test with a static footing load.

Figure 4.2 also shows that the measured pressures on the trapdoor (TC and TE) sharply decreased with a trapdoor displacement of about 2 mm. Meanwhile, the pressure at SE gradually increased as the trapdoor was progressively lowered due to the soil arching effect. However, the pressure at SE decreased after a trapdoor displacement of about 9 mm. The decrease of the pressure at SE was accompanied by an increase of the pressures at both TC and TE. In other words, soil arching started to deteriorate under soil self-weight as the trapdoor displacement increased to more than 2.5% of its width.

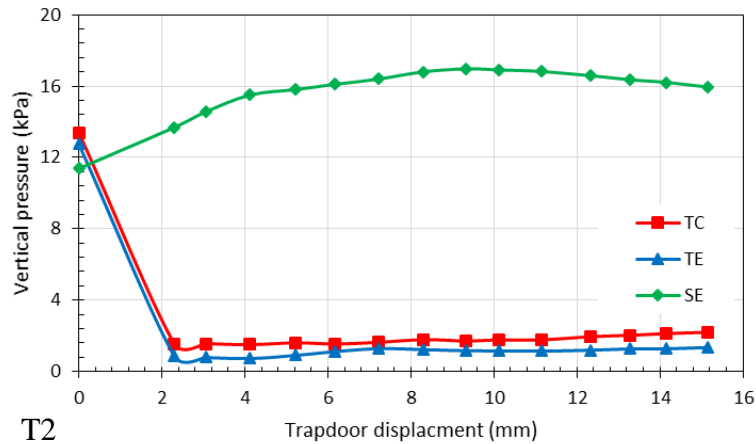


Figure 4.2 Measured pressures on and besides the trapdoor versus the trapdoor displacement in the unreinforced test T2

Figure 4.3 shows the results of two trapdoor tests in T3 and T9, which were conducted to a maximum trapdoor displacement of about 8 mm and were followed by a static and cyclic footing load, respectively. In these trapdoor tests, the trapdoor displacement was stopped at about 8 mm to eliminate any soil arching deterioration caused by the progressive settlement of the trapdoor and to study only the effect of the footing load on the stability of soil arching. Figure 4.3 shows a similar trend of the pressures at TC, TE, and SE to that in T2. In addition, a peak value of the measured pressure at SE in T2 was 17 kPa at the trapdoor displacement of 9 mm, while the peak

pressures at SE in T3 and T9 were 18 kPa and 19 kPa, respectively, at the trapdoor displacement of 8 mm.

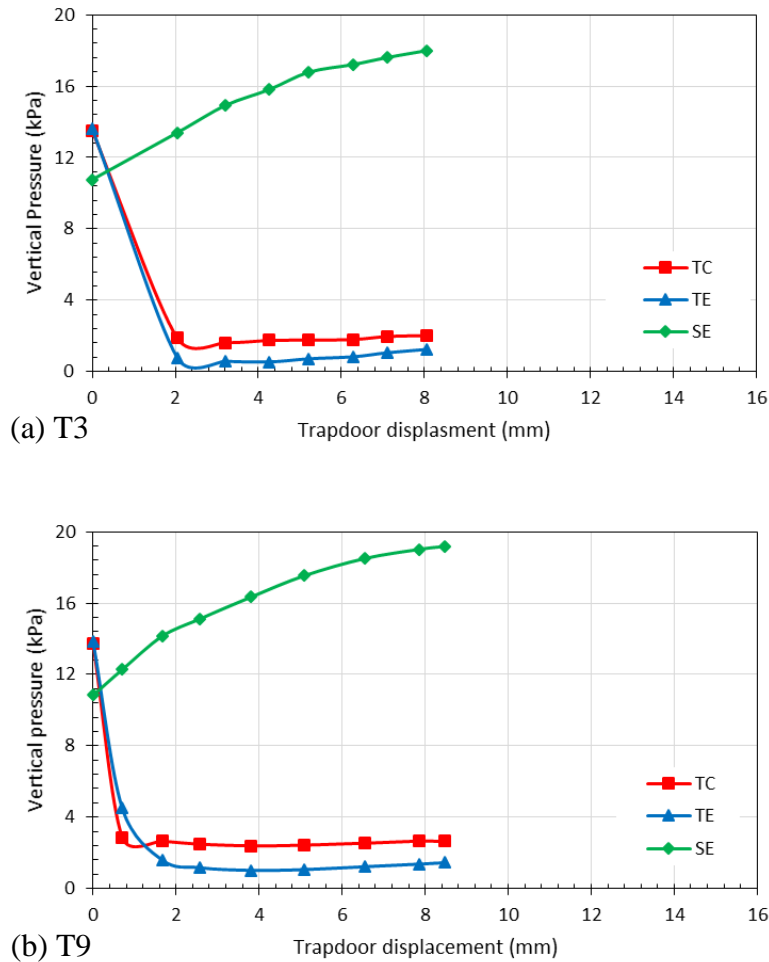
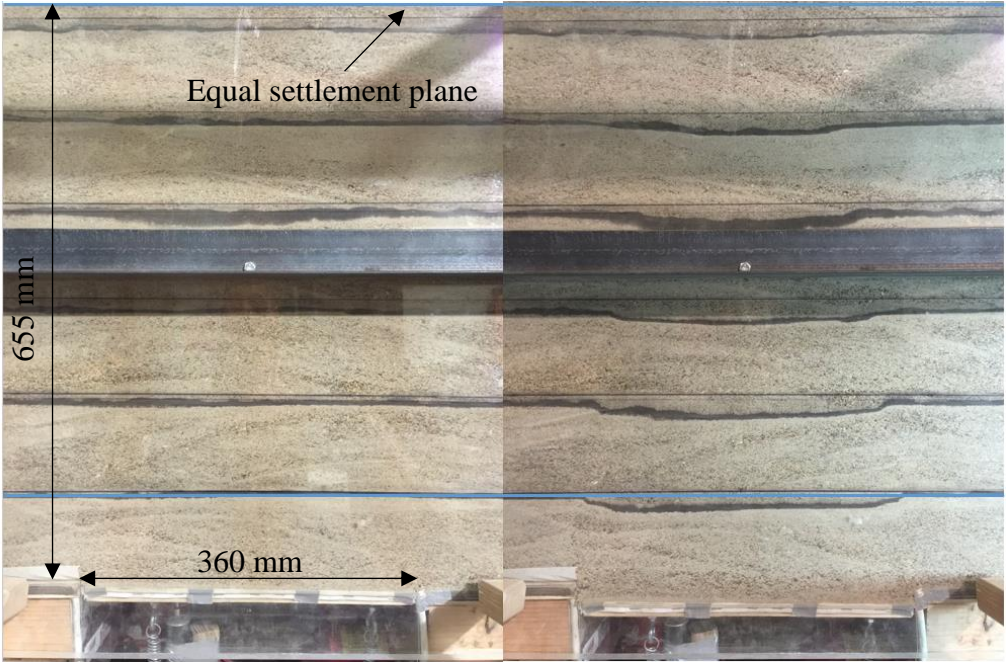


Figure 4.3 Measured pressures on and besides the trapdoor versus the trapdoor displacement in the unreinforced tests: (a) T3 and (b) T9

As mentioned earlier in Chapter 2, the degree of the soil arching mobilization is evaluated by the soil arching ratio. The soil arching ratios at the end of the trapdoor tests in T2, T3, and T9 were 0.14, 0.13, and 0.16, respectively. In other words, soil arching was fully mobilized in all three tests. Moreover, trapdoor displacement caused particle movement within the embankment fill and differential settlement between the yielding soil mass (i.e., the soil above the trapdoor) and the

unyielding soil mass (the soil above the stationary supports). An equal settlement plane existed at a height,  $Z$ , from the trapdoor, above which there was no obvious differential settlement and thus no effect on the soil arching as shown in Figure 2.1. It is preferred for actual applications that soil arching should be within the embankment fill. In other words, the equal settlement plane should



(a) T2 At 0 mm trapdoor displacement

At 15.15 mm trapdoor displacement



(b) T9 At 0 mm trapdoor displacement

At 8.47 mm trapdoor displacement

Figure 4.4 Equal settlement plane: (a) T2 and (b) T9

be within the embankment fill. In the trapdoor tests (T2, T3, and T9), the equal settlement planes were at 1.82S, 1.39S, and 1.44S, respectively, where S refers to the trapdoor width (360 mm in this study). Figure 4.4 depicts the equal settlement plane in trapdoor tests (T2 and T9).

#### **4.1.2 Single Geosynthetic-Reinforced Embankment Fill**

Four tests were carried out with single geosynthetic reinforcement in order to investigate the effects of geosynthetic inclusion on the soil arching mobilization and stability. Two different types of reinforcement were utilized, which were a layer of uniaxial geogrid overlain by a layer of non-woven geotextile (in T5 and T11) and a layer of biaxial geogrid overlain by a layer of non-woven geotextile (in T6 and T12), as described in Chapter 3. In all these tests, after the embankment fill had been constructed, trapdoor tests were performed to a maximum trapdoor displacement of 15 mm followed by a loading test of a static footing load in T5 and T6 and a loading test of a cyclic footing load in T11 and T12. The maximum trapdoor displacement of 15 mm was utilized in these tests due to the use of geosynthetic reinforcement, which required more geosynthetic displacement to mobilize some of its strength. Therefore, the benefit of geosynthetic inclusion in these tests was analyzed by comparing the trapdoor test results with that in T2.

Figure 4.5 shows the measured pressures on and besides the trapdoor during the embankment construction in the single geosynthetic-reinforced fill tests with both the uniaxial geogrid (in T5) and the biaxial geogrid (in T12).

Figures 4.6 and 4.7 depict the results of the trapdoor tests in T5, T6, T11, and T12. In all these tests, the measured pressures on the trapdoor above and below the geosynthetic reinforcement (TC and TE) sharply decreased with a trapdoor displacement of about 1 mm. Meanwhile, the pressure at SE above and below the geosynthetic reinforcement gradually increased as the trapdoor was progressively lowered due to the combined effect of the soil arching

and tensioned membrane effect. However, the pressure at SE above the geosynthetic decreased due to the increased pressures at TC and TE above the geosynthetic after a trapdoor displacement of about 12 mm, whereas the measured pressure at SE below the reinforcement continued to increase.

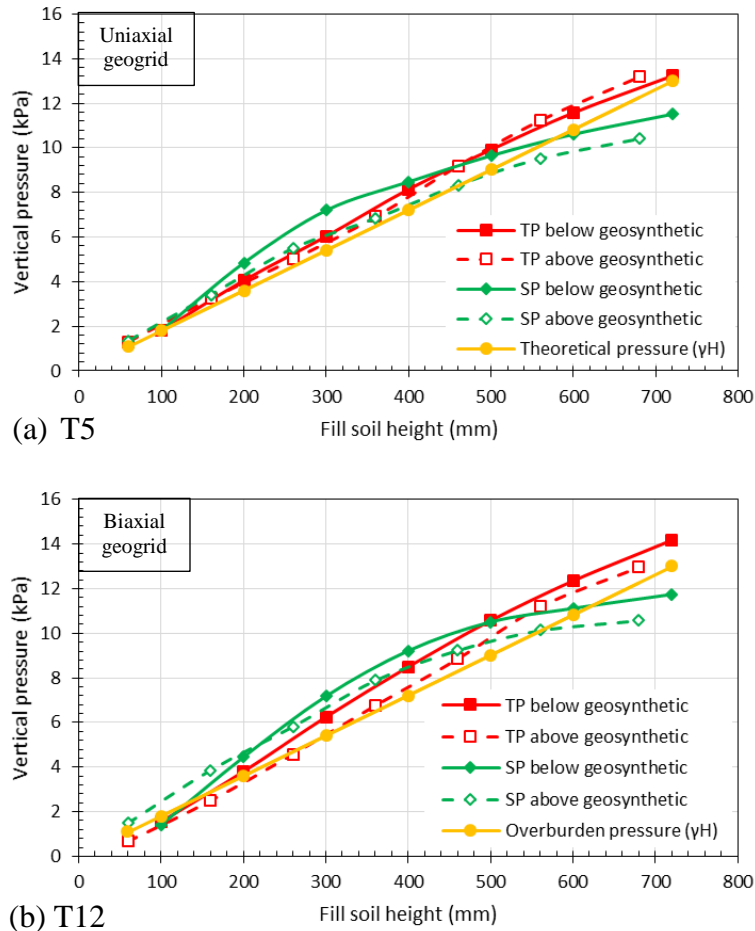


Figure 4.5 Measured pressures on and besides the trapdoor during the fill construction in the single geosynthetic-reinforced tests: (a) T5 and (b) T12

Moreover, the measured pressure at TE below the geosynthetic in all four tests decreased more after a trapdoor displacement of about 10 mm. The measured pressure at SE below the geosynthetic reinforcement in T5, T6, T11, and T12 can be compared to that at SE in T2, as shown

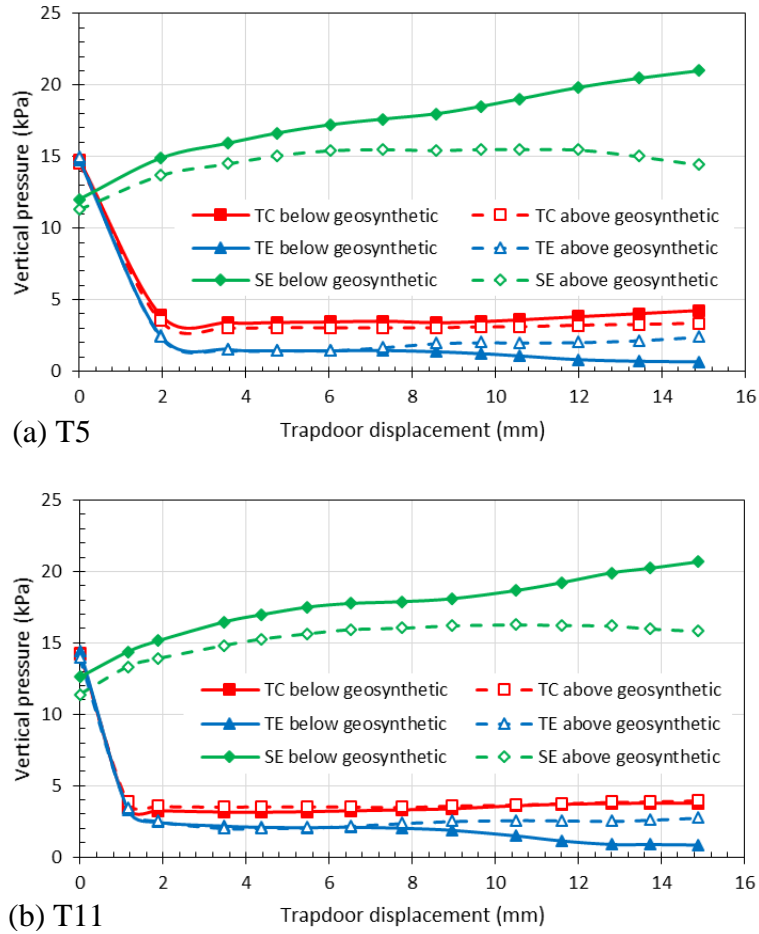


Figure 4.6 Measured pressures on and besides the trapdoor versus the trapdoor displacement in the single geosynthetic-reinforced tests with uniaxial geogrid: (a) T5 and (b) T11

in Figure 4.2, in which the pressure at SE decreased after trapdoor displacement of 9 mm. This result proves that the geosynthetics inclusion prevented the deterioration of the soil arching under soil self-weight. The mechanisms in which the geosynthetic helped stabilize soil arching were the tensioned membrane and lateral restraint. As the trapdoor was lowered, the geosynthetic was stretched and mobilized some of its strength. The vertical component of the tension in the reinforcement reduced the pressures on the trapdoor but increased the pressures on the stationary supports. In other words, the geosynthetics helped transfer the pressure from the foundation soil

to the stiffer supports, such as piles or columns. At the same time, the geosynthetic provided lateral restraint to particle movement, which increased the shear strength of the fill.

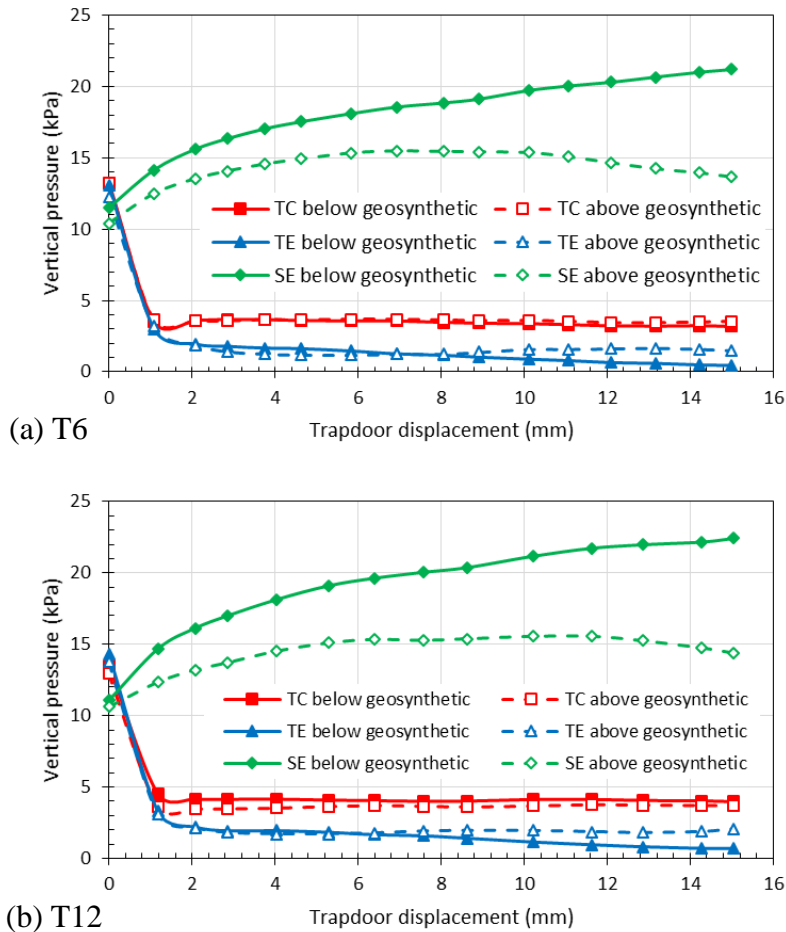


Figure 4.7 Measured pressures on and besides the trapdoor versus the trapdoor displacement in the single geosynthetic-reinforced tests with biaxial geogrid: (a) T6 and (b) T12

Two types of geosynthetic reinforcement were utilized in these four tests. In both T5 and T11, a layer of uniaxial geogrid overlain by non-woven geotextile was used, while in T6 and T12, a layer of biaxial geogrid overlain by non-woven geotextile was used. Biaxial geogrid helped transfer more pressure from the trapdoor to the stationary supports than that in the tests with the uniaxial geogrid. Also by comparing the pressure at SE in these four test, the tests with the biaxial

geogrid needed less trapdoor displacement to mobilize its strength than that with the uniaxial geogrid.

Table 4.1 presents the soil arching ratio and the equal settlement plane at the end of the trapdoor test in each of these tests. Soil arching ratios show that soil arching was fully mobilized in all these tests. In addition, Table 4.1 shows the effect of the geosynthetic reinforcement on lowering the equal settlement plane in T5, T6, T11, and T12 as compared with that in T2. Therefore, the geosynthetic not only helped stabilize the soil arching but also reduced the height of the equal settlement plane. In other words, the differential settlement existed at the depth below the surface of the embankment.

Table 4.1 Soil arching ratios and equal settlement planes in the single geosynthetic-reinforced embankment tests (T5, T6, T11, and T12)

Test number	Reinforcement type*	Soil arching ratio		Equal settlement plane	Loading type
		Below	Above**		
T5	Uniaxial geogrid	0.19	0.23	1.64 S	Static
T6	Biaxial geogrid	0.14	0.20	1.56 S	Static
T11	Uniaxial geogrid	0.18	0.27	1.67 S	Cyclic
T12	Biaxial geogrid	0.17	0.22	1.58 S	Cyclic

\* Each geogrid was overlain by a layer of non-woven geotextile

\*\* Soil arching ratios were calculated above and below the reinforcement

### ***Measured Strains in Single Geosynthetic-Reinforced Embankment Tests***

In the single geosynthetic-reinforced tests, geogrid strains were monitored and are presented in this section. In both T5 and T11, the strain gauges were attached to the uniaxial geogrid at five different locations: 0, 90, 173, 260, and 385 mm away from the trapdoor centerline. At the distances of 90 and 173 mm, the strain gauges were attached above and below the geogrid to study the bending effect on the geogrid. In both T6 and T12, however, the strain gauges were attached to the biaxial geogrid at six different locations: 0, 90, 150, 180, 205, and 280 mm away from the

trapdoor centerline. At the distances of 90 and 180 mm, the strain gauges were also attached above and below the geogrid. Figures 4.8 to 4.15 present the measured strain gauges during the trapdoor tests in T5, T11, T6, and T12, respectively.

As the trapdoor was lowered in both T5 and T11, the geogrid was stretched thus causing the maximum tensile strains of 0.5% and 0.35% at the distance of 173 mm away from the trapdoor centerline (i.e., at the edge of the trapdoor) at the trapdoor displacements of 11.99 and 8.96 mm as

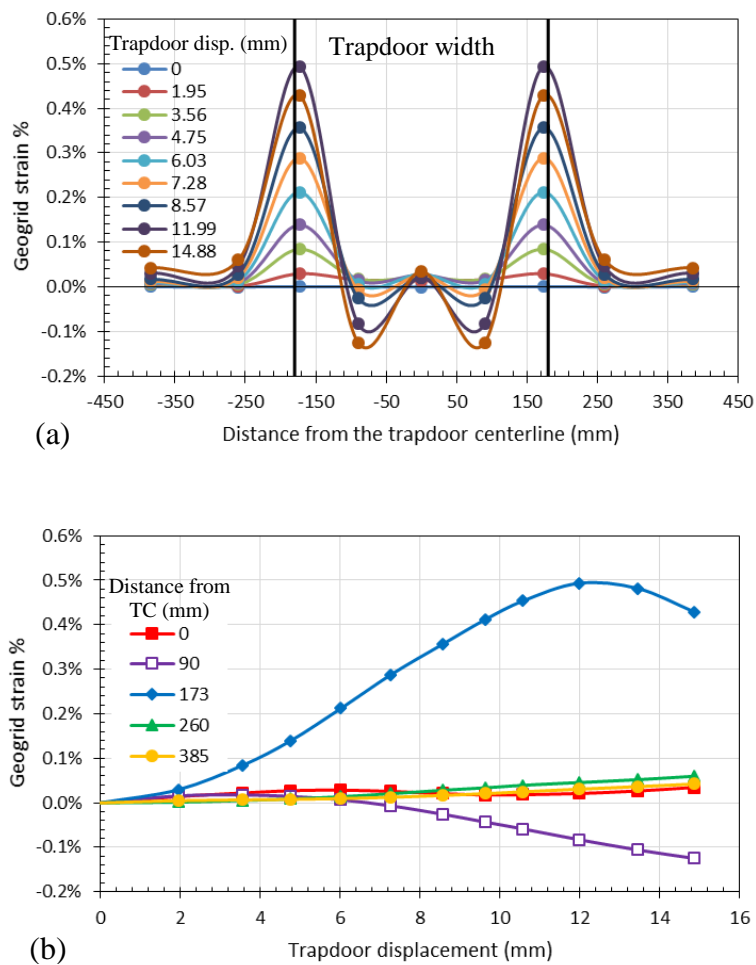


Figure 4.8 Measured strains in the uniaxial geogrid during the trapdoor test in T5: (a) the cross-sectional distribution of the strains above the geogrid and (b) the measured strains above the geogrid versus the trapdoor displacement

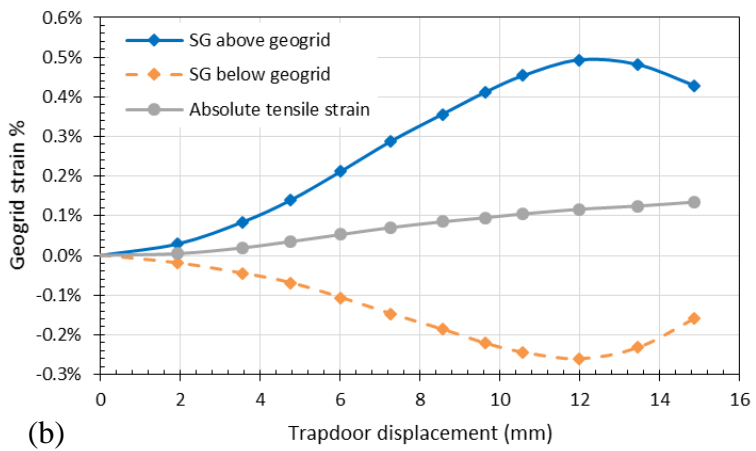
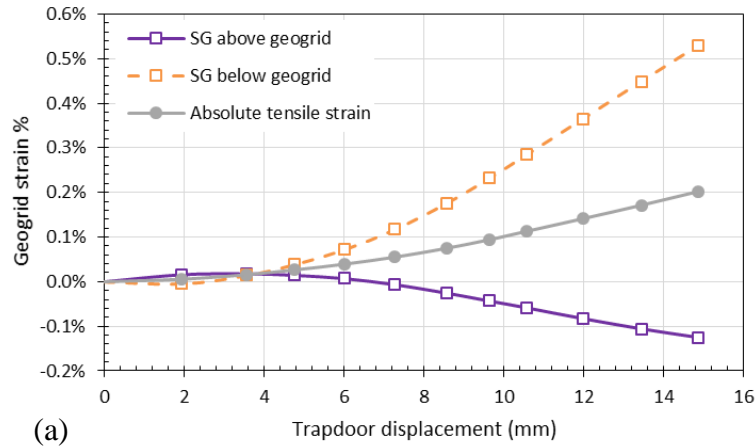


Figure 4.9 Measured strains in the uniaxial geogrid during the trapdoor test in T5: (a) the measured strains above and below the geogrid at the distance of 90 mm away from the trapdoor centerline and (b) the measured strains above and below the geogrid at the distance of 173 mm away from the trapdoor centerline

shown in Figures 4.8(a) and 4.10(a), respectively. However, the minimum tensile strain along the geogrid was found at the centerline of the trapdoor in both tests. At the distance of 90 mm away from the trapdoor centerline, the strain gauges above the geogrid experienced the maximum compressive strains of about 0.12% and 0.1% at the trapdoor displacements of 14.88 and 14.9 mm in both T5 and T11 as shown in Figures 4.8(b) and 4.10(b), respectively. However, the strain gauges attached at the same location below the geogrid experienced the tensile strains of about

0.52% and 0.45 % in T5 and T11, respectively. Therefore, in both tests, the geogrid experienced an absolute tensile strain of about 0.2% at the distance of 90 mm away from the trapdoor centerline as shown in Figures 4.9(a) and 4.11(a). An opposite behavior was observed at the distance of 173 mm away from the trapdoor centerline in both T5 and T11, at which the strain gauges attached below the geogrid underwent compressive strain with peak values of 0.27% and 0.18% at the trapdoor displacements of 11.99 and 8.96 mm as shown in Figures 4.9(b) and 4.11(b), respectively.

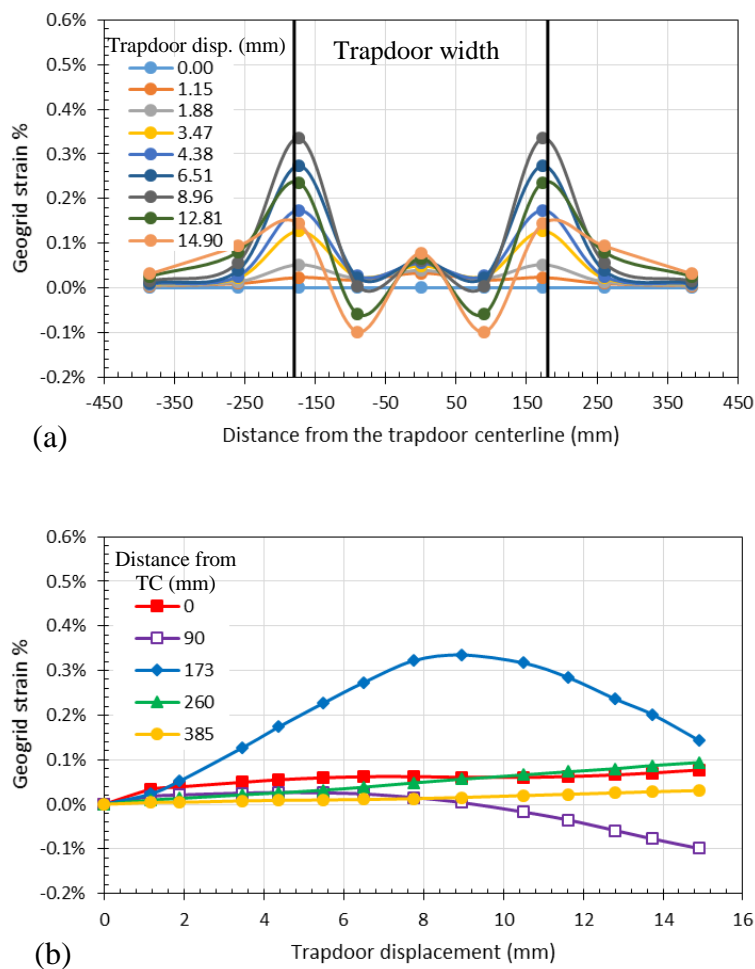


Figure 4.10 Measured strains in the uniaxial geogrid during the trapdoor test in T11: (a) the cross-sectional distribution of the strains above the geogrid and (b) the measured strains above the geogrid versus the trapdoor displacement

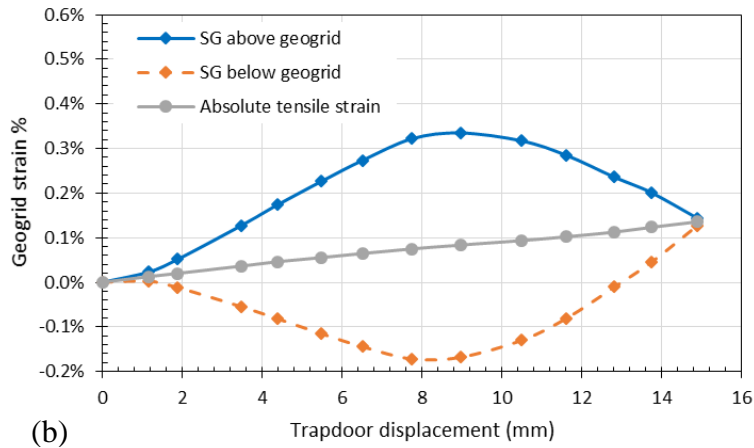
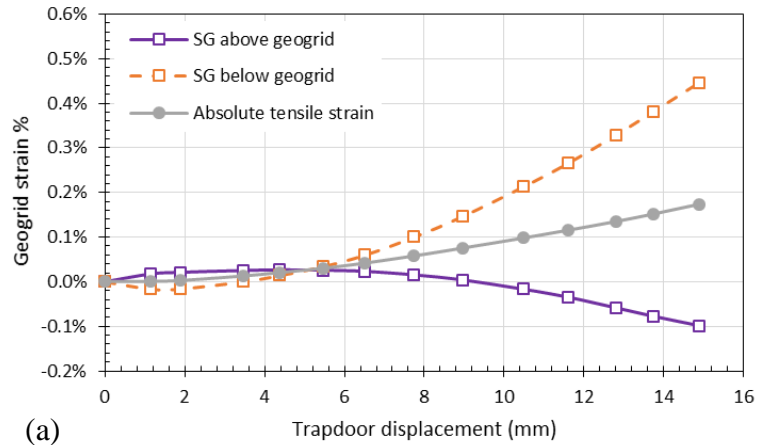


Figure 4.11 Measured strains in the uniaxial geogrid during the trapdoor test in T11: (a) the measured strains above and below the geogrid at the distance of 90 mm away from the trapdoor centerline and (b) the measured strains above and below the geogrid at the distance of 173 mm away from the trapdoor centerline

At the distances of 90 and 173 mm away from the trapdoor centerline, the tensile and compressive strains indicate that the geogrid was subjected not only to the axial forces (tensile forces) but also to the bending moments, which increased the tensile forces at either the upper or the lower surface of the geogrid so that the geogrid was more susceptible to failure at that location.

In both T6 and T12, the biaxial geogrid within the trapdoor underwent compressive strains at the beginning of the trapdoor tests, followed by tensile strains as the trapdoor displacement

increased as shown in Figures 4.12(b) and 4.14(b). Similar to the uniaxial geogrid tests (T5 and T11), the maximum tensile strain along the biaxial geogrid was located at the distance of 180 mm away from the trapdoor centerline (i.e., at the trapdoor edge) in both T6 and T12 with a value of about 0.62% at the trapdoor displacement of 15.0 mm as shown in Figures 4.12(a) and 4.14(a).

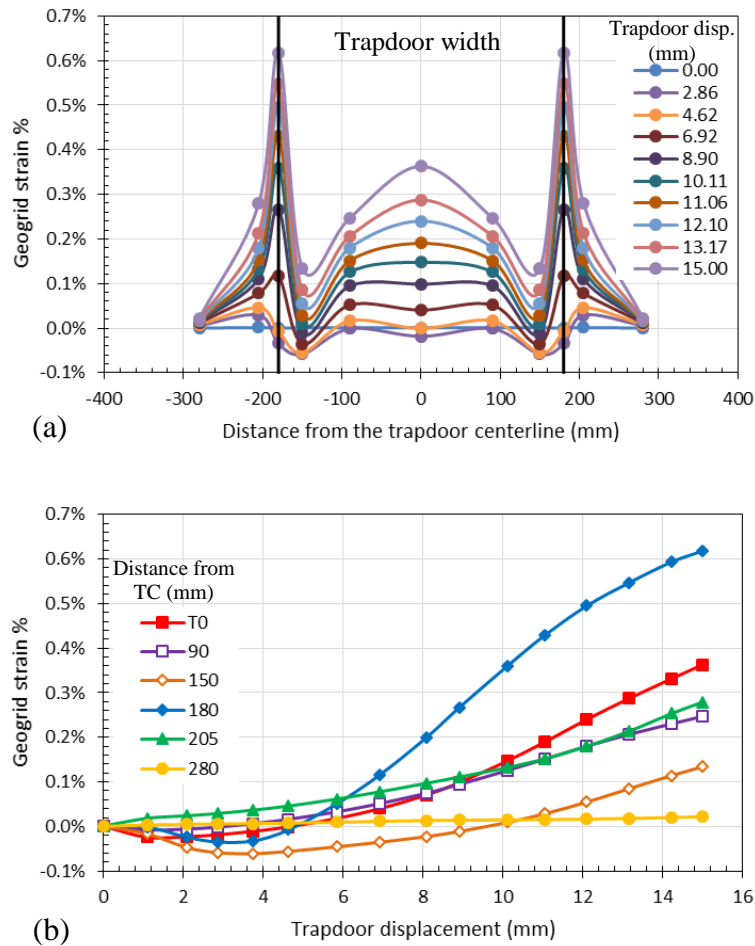


Figure 4.12 Measured strains in the biaxial geogrid during the trapdoor test in T6: (a) the cross-sectional distribution of the strains above the geogrid and (b) the measured strains above the geogrid versus the trapdoor displacement

Unlike the tests with the uniaxial geogrid, in which the minimum tensile strain of about 0.03% was found at the trapdoor centerline, the tests with the biaxial geogrid experienced a tensile

strain of about 0.35% at the trapdoor centerline as depicted in Figures 4.12(a) and 4.14(a). Also, the strain gauges above the biaxial geogrid at 90 mm away from the trapdoor centerline in both T6 and T12 underwent a tensile strain instead of a compressive strain above the uniaxial geogrid at the same location.

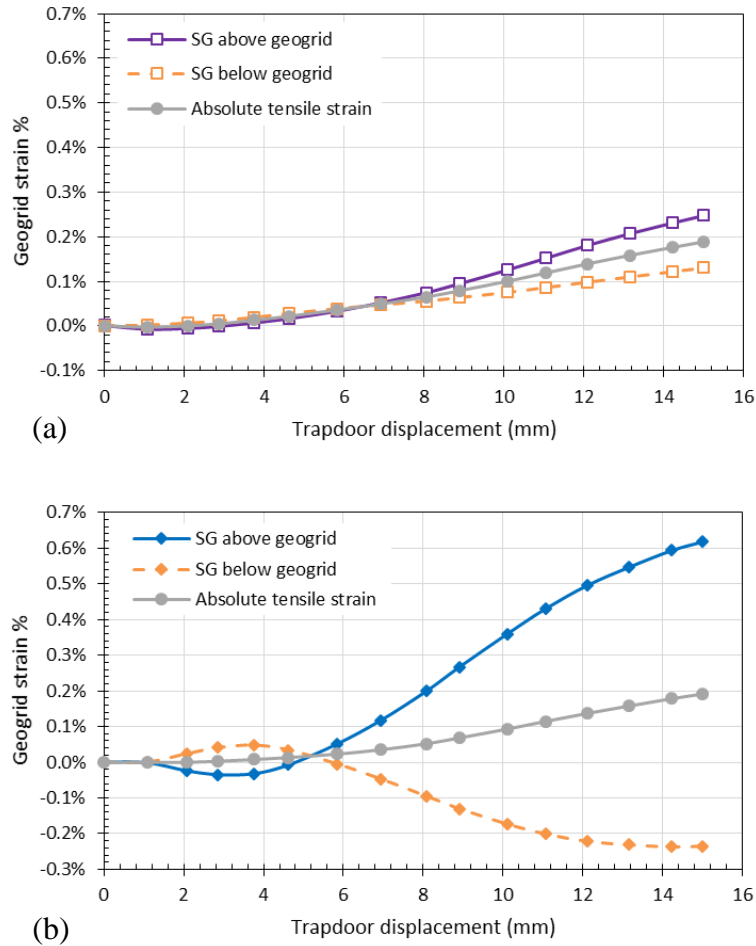


Figure 4.13 Measured strains in the biaxial geogrid during the trapdoor test in T6: (a) the measured strains above and below the geogrid at the distance of 90 mm away from the trapdoor centerline and (b) the measured strains above and below the geogrid at the distance of 173 mm away from the trapdoor centerline

Furthermore, the tensile strains continuously increased above the geogrid at the trapdoor edge as the trapdoor displacement increased in the tests with the biaxial geogrid as shown Figures

4.13(b) and 4.15(b), whereas in the tests with the uniaxial geogrid the tensile strains decreased after a trapdoor displacements of about 12.0 and 9.0 mm in both T5 and T11, respectively. Bending was also observed in the biaxial geogrid tests at the distance of 180 mm away from the trapdoor centerline where the strains above and below the geogrid experienced opposite tensile and compressive behavior, respectively. Consequently, the biaxial geogrid sustained an absolute tensile strain of about 0.2% as shown in Figures 4.13(b) and 4.15(b).

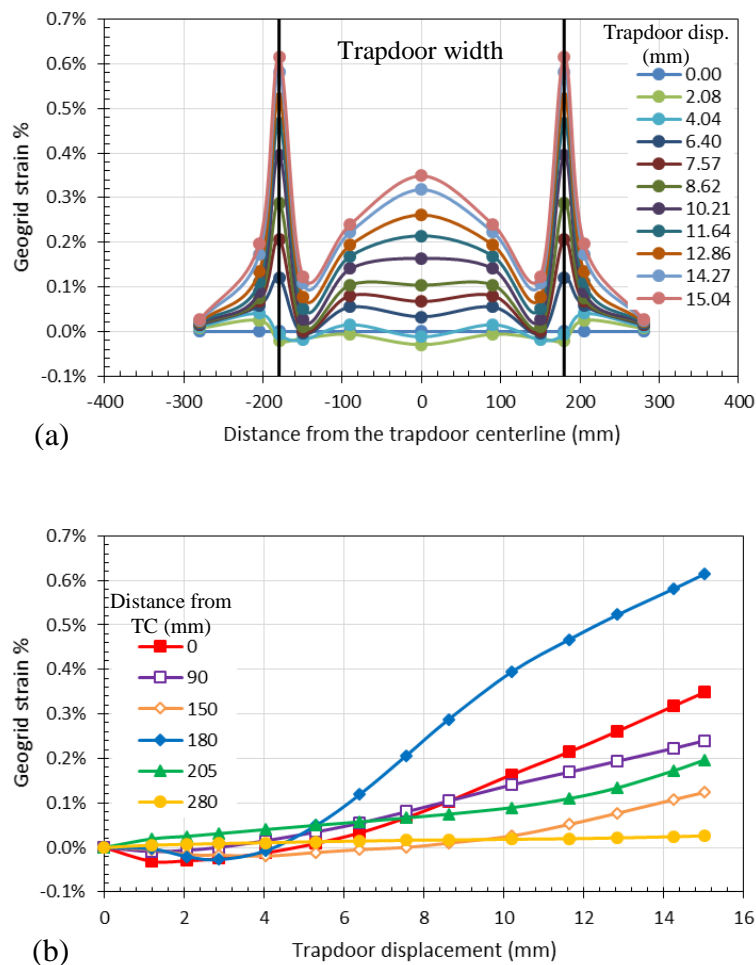
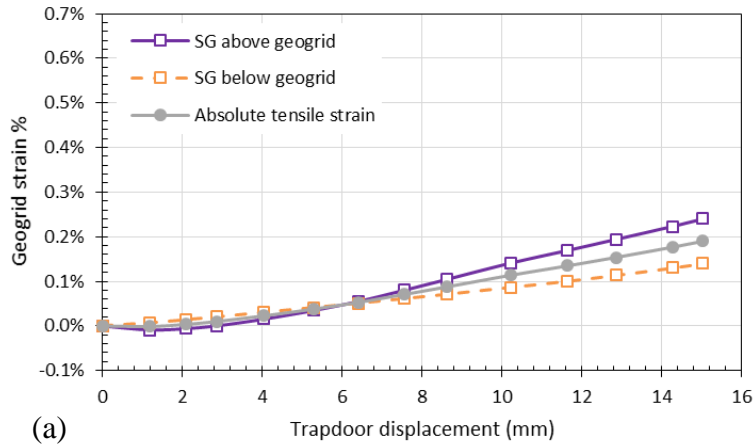
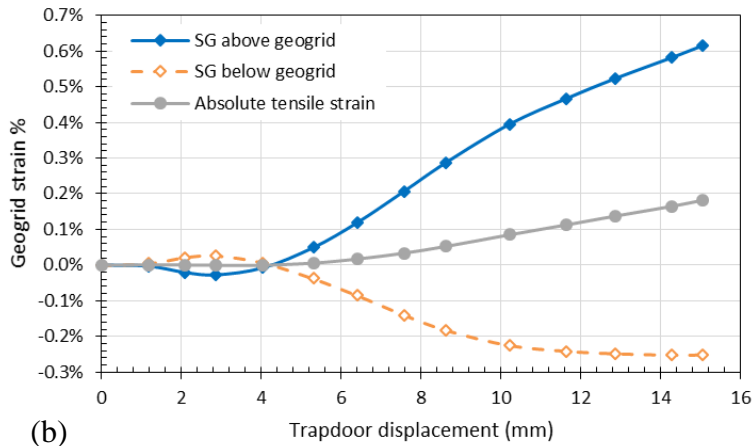


Figure 4.14 Measured strains in the biaxial geogrid during the trapdoor test in T12: (a) the cross-sectional distribution of the strains above the geogrid and (b) the measured strains above the geogrid versus the trapdoor displacement



(a)



(b)

Figure 4.15 Measured strains in the biaxial geogrid during the trapdoor test in T12: (a) the measured strains above and below the geogrid at the distance of 90 mm away from the trapdoor centerline and (b) the measured strains above and below the geogrid at the distance of 173 mm away from the trapdoor centerline

It is worth mentioning that the absolute strains (i.e., the average strains from the strain gauges above and below the geogrid) in the similar tests with uniaxial or biaxial geogrids were identical even though the measured strains from a single strain gauge were not necessarily comparable. Figures 4.9(b) and 4.11(b) show that in the tests with the uniaxial geogrid (T5 and T11), the absolute tensile strain was equal to 0.12% at the end of the trapdoor test in both tests

while the tensile strains were equal to 0.41% and 0.12% and the compressive strains were equal to 0.17% and 0.12% in T5 and T11, respectively.

#### **4.1.3 Double Geosynthetic-Reinforced Embankment Fill**

Gabr and Han (2005) suggested that further investigation be needed on the load transfer platform or the beam effects associated with the multiple layers of geosynthetic reinforcement. Therefore, in this study, double geosynthetic-reinforced embankments were chosen to investigate the effects of the second layer of geosynthetic on the soil arching mobilization and stability as compared with the single layer of geosynthetic reinforcement. For this purpose, three tests, T7a, T7b, and T13, were carried out by adding a double layer of biaxial geogrid overlain by a non-woven geotextile as detailed in Chapter 3. After the embankment had been constructed in each test, trapdoor tests were performed to the maximum trapdoor displacement of about 15.0 mm and followed by a static loading test in both T7a and T7b and a cyclic loading test in T13.

Figure 4.16 shows the measured pressures on and besides the trapdoor during the embankment construction for the double geosynthetic-reinforced fill tests, T7a and T13.

Figure 4.17 shows the measured pressure with the trapdoor displacement in the trapdoor tests (T7a, T7b, and T13). In all these tests, the earth pressure cells were placed below and above the lower layer of the geosynthetic reinforcement. Similar to the results of the trapdoor tests with the single layer of geosynthetic reinforcement, the measured pressures above and below the lower geosynthetic reinforcement layer within the trapdoor (TC and TE) sharply decreased with the trapdoor displacement of about 1 mm, and further decreased at a slightly reduced rate until reaching the minimum measured pressures at the end of the trapdoor tests. Meanwhile, the pressures above and below the lower geosynthetic reinforcement on the support (SE) gradually increased as the trapdoor was progressively lowered until reaching the maximum pressure at the

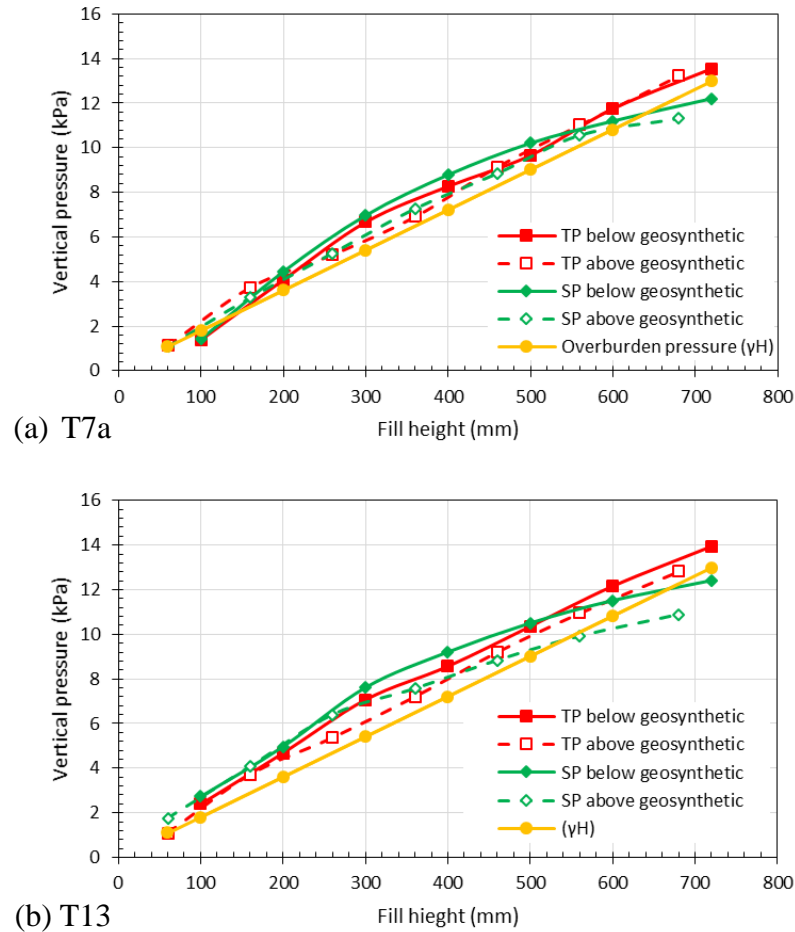


Figure 4.16 Measured pressures on and besides the trapdoor during the fill construction in the double geosynthetic-reinforced tests: (a) T7a and (b) T13

end of the trapdoor tests. Unlike the test results of the trapdoor tests with the single layer of geosynthetic reinforcement in which the pressure above the geosynthetic on the support (SE) decreased after the trapdoor displacement of about 12 mm, this pressure continuously increased in the double geosynthetic-reinforced fill. The same comparison existed for the measured pressures above and below the lower geosynthetic layer at TC, TE, and SE indicated that the platform formed by double layers of geosynthetic reinforcement as well as the sand in between acted as a stiffened member in minimizing the deterioration of soil arching under soil self-weight. In addition, this platform helped transfer more load to the stationary supports than that in the single layer of

geosynthetic reinforcement, which indicates that lower pressure would be applied onto the foundation soil (i.e., the soil in the trapdoor area) in real applications.

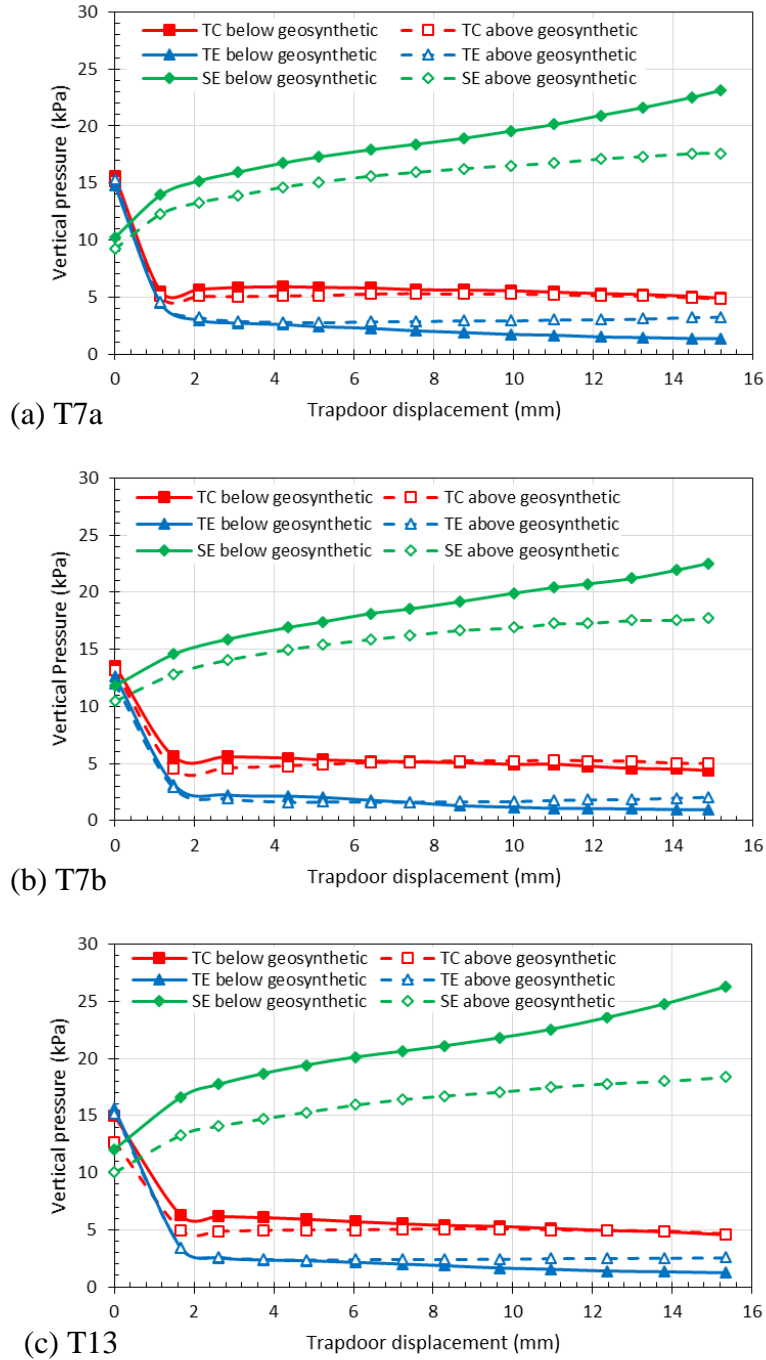


Figure 4.17 Measured pressures on and besides the trapdoor versus the trapdoor displacement in the double geosynthetic-reinforced tests: (a) T7a, (b) T7b, and (c) T13

Table 4.2 presents the soil arching ratio,  $\rho$ , and the equal settlement plane in the trapdoor tests (T7a, T7b, and T13). Two arching ratios were calculated at the trapdoor displacement of about 1.5 mm and the end of the trapdoor test for each test. Soil arching ratios show that as the trapdoor displacement increased, the soil arching ratio decreased for the locations both above and below the lower layer of geosynthetic reinforcement. In other words, soil arching was further mobilized. The use of double layers of geosynthetic reinforcement helped stabilize soil arching as well as allowed more settlement in the foundation soil (i.e., the trapdoor displacement). In addition, Table 4.2 shows the benefit of adding the second geosynthetic layer on further lowering of the equal settlement plane in each test as compared with the heights of the equal settlement planes in the single geosynthetic-reinforced tests (i.e., 1.56S in the T6 test and 1.58S in the T12 test).

Table 4.2 Soil arching ratios and heights of equal settlement plane in the double geosynthetic-reinforced tests (T7a, T7b, and T13)

Test number	$\rho$ @ 1.5 mm*		$\rho$ @ 15 mm**		Height of equal settlement plane	Loading type
	Below***	Above***	Below***	Above***		
T7a	0.38	0.39	0.24	0.33	1.42S	Static
T7b	0.34	0.30	0.21	0.29	1.39S	Static
T13	0.37	0.34	0.22	0.29	1.40S	Cyclic

Note: \* soil arching ratio at the trapdoor displacement of 1.5 mm; \*\* soil arching ratio at the trapdoor displacement of 15 mm; \*\*\*soil arching ratios were calculated above and below the lower reinforcement layer.

### ***Measured Strains in Double Geosynthetic-Reinforced Embankment Tests***

In the double geosynthetic-reinforced tests, the strains of the lower and upper geogrid layers, which were 100 mm apart, were monitored. Strain gauges were attached to the lower biaxial geogrids at six different locations: 0, 90, 150, 180, 205, and 280 mm and to the upper biaxial geogrids at five different locations: 0, 90, 160, 205, and 280 mm away from the trapdoor centerline. Figures 4.18

and 4.19, 4.20, and 4.21 present the measured geogrid strains during the trapdoor tests (T7a, T7b, and T13), respectively.

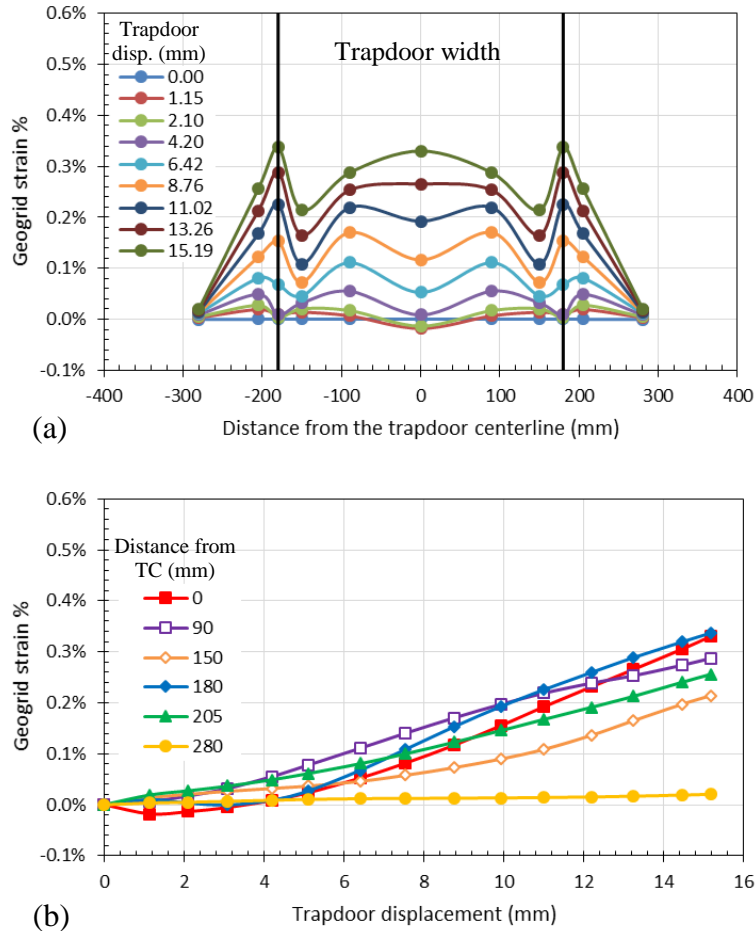


Figure 4.18 Measured strains of the biaxial geogrid during the trapdoor test (T7a): (a) the strain distribution in the lower geogrid layer and (b) the measured strain in the lower geogrid layer versus the trapdoor displacement

In these tests, the geogrids were stretched to the maximum tensile strain in the lower geogrid layer of about 0.35% at the trapdoor centerline and the trapdoor edges (i.e., 180 mm away from the trapdoor centerline) at the end of the trapdoor tests as shown in Figures 4.18, 4.20(a), and 4.21(a) as the trapdoor was lowered. The minimum strain in the lower geogrid layer was found within the stationary supports at the distance of 280 mm away from the trapdoor centerline.

Meanwhile, in the upper geogrid layer, the maximum tensile strain of about 0.27% was located at the trapdoor edges in all tests as shown in Figures 4.19, 4.20(b), and 4.21(b). However, at the trapdoor centerline, the upper geogrid layer underwent much smaller strain than that in the lower geogrid layer.

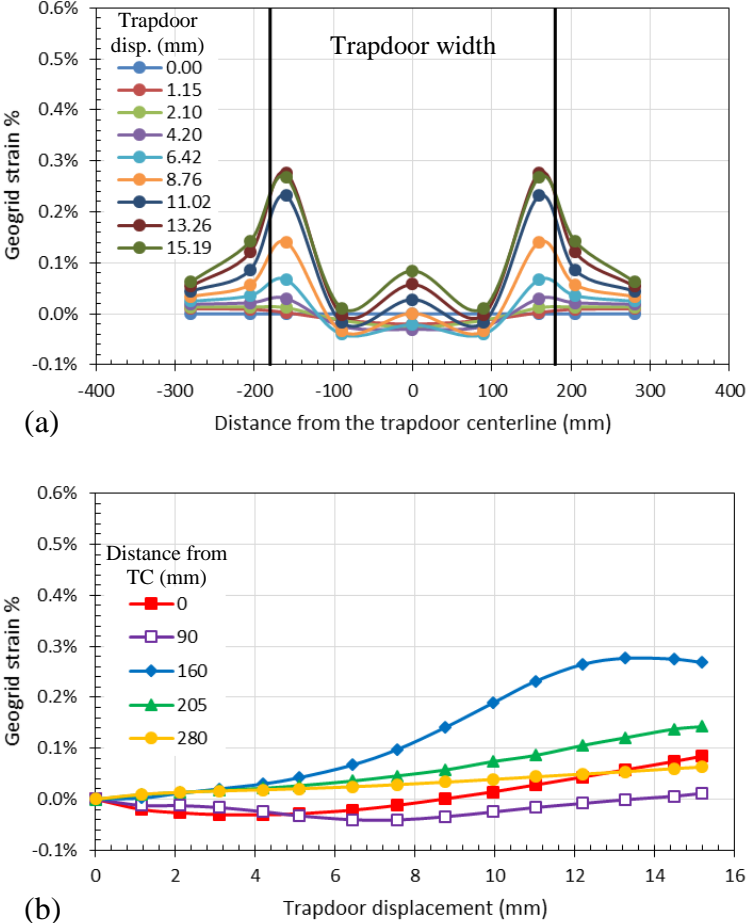


Figure 4.19 Measured strains of the biaxial geogrids during the trapdoor test (T7a): (a) the strain distribution in the upper geogrid layer and (b) the measured strain in the upper geogrid layer versus trapdoor displacement

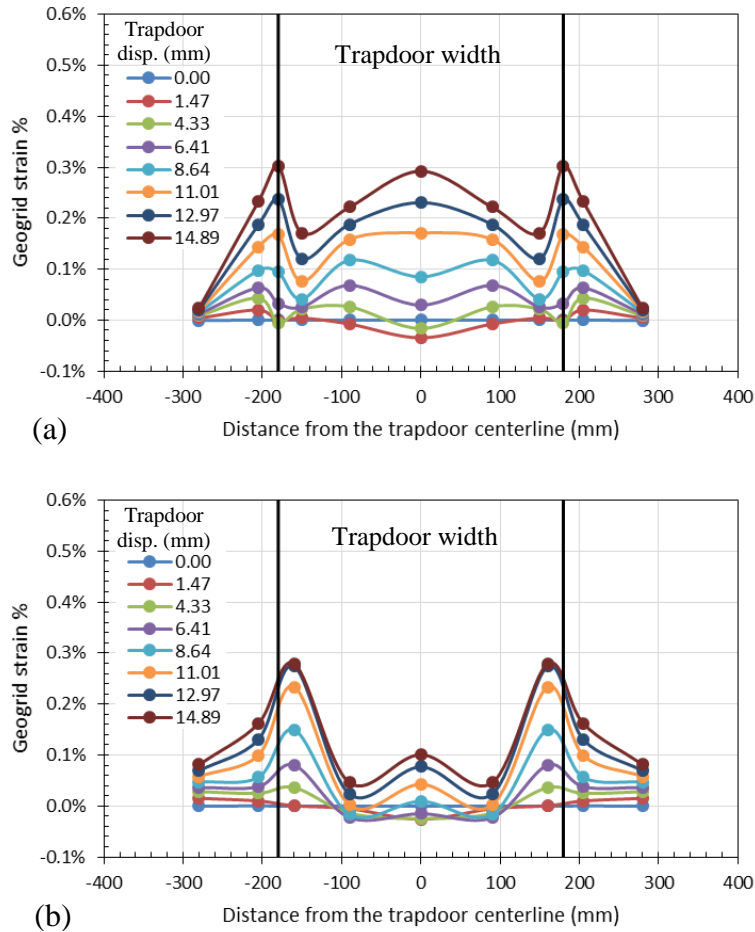


Figure 4.20 Measured strains of the biaxial geogrids during the trapdoor test (T7b): (a) the strain distribution in the lower geogrid layer and (b) the strain distribution in the upper geogrid layer

In other words, the existence of the maximum strain at the trapdoor centerline in the lower geogrid layer and the maximum strain at the trapdoor edges in the upper geogrid layer confirmed that the load transfer platform formed by double layers of geosynthetic reinforcement and the sand functioned as a beam. Similar results were obtained by Huang et al. (2005) in their numerical analysis of the three geosynthetic layer-reinforced embankment. Moreover, it is obvious that the geogrid strains in the double geosynthetic-reinforced tests were approximately half of those in the single geosynthetic-reinforced tests.

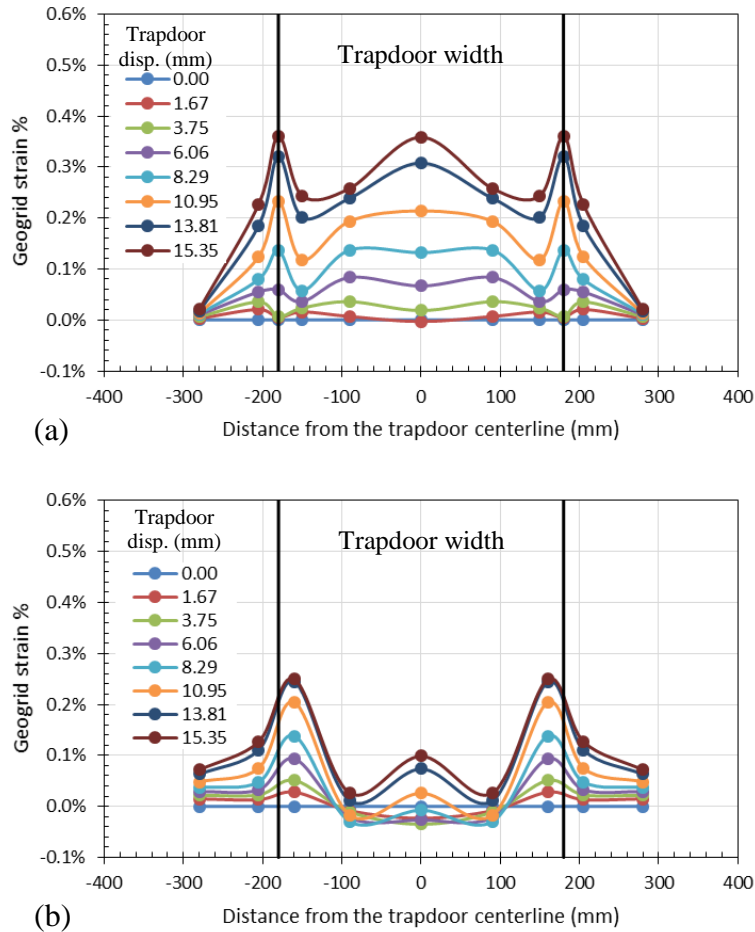


Figure 4.21 Measured strains of the biaxial geogrids during the trapdoor test (T13): (a) the strain distribution in the lower geogrid layer and (b) the strain distribution in the upper geogrid layer

#### 4.2 TRAPDOOR TEST UNDER SOIL SELF-WEIGHT AND FOOTING LOAD

For the purpose of investigating the effects of the footing load in addition to the soil self-weight on the soil arching mobilization, two trapdoor tests with an unreinforced embankment (T4 and T10) were carried out. After the embankment had been constructed in each test, a constant footing load was first applied and held throughout the trapdoor test. Trapdoor tests were conducted to the maximum trapdoor displacement of about 8.0 mm, which is similar to those in T3 and T9. The static footing pressure of 16.4 kPa was chosen based on the results of the loading tests (T3 and T9), which will be presented in Chapter 5, by considering a factor of safety of 3.0. Figure 4.22

shows the measured pressures above and besides the trapdoor during the embankment construction in T4 and T10.

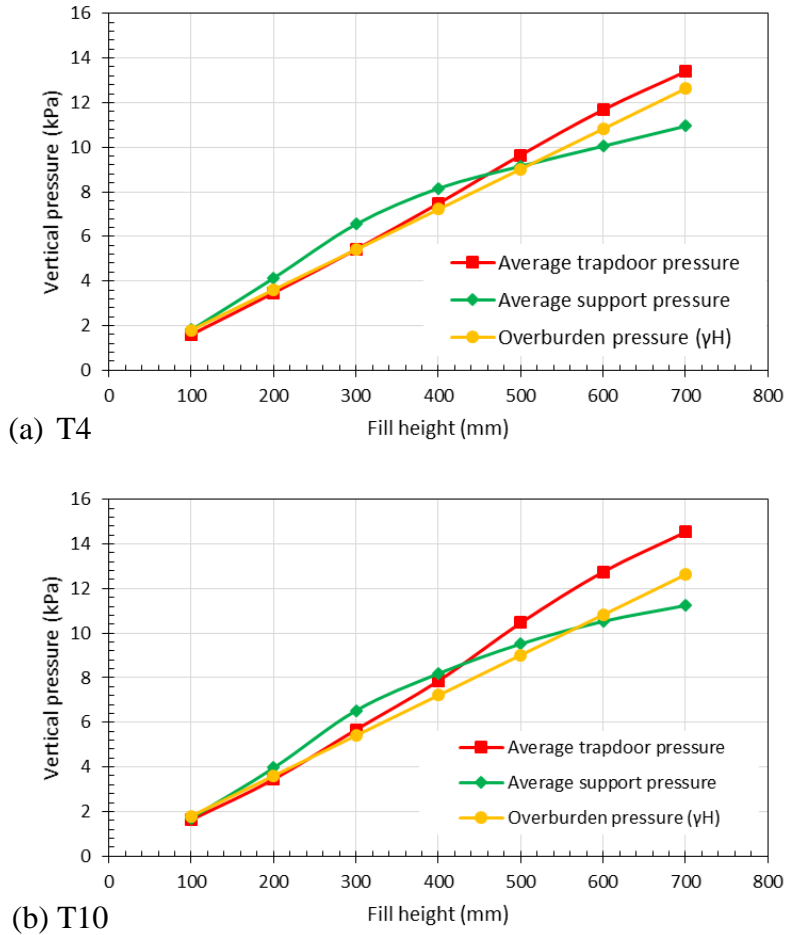


Figure 4.22 Measured pressures on and besides the trapdoor during the fill construction in the tests: (a) T4 and (b) T10

Figure 4.23 shows the vertical pressure versus trapdoor displacement results of the trapdoor tests in T4 and T10. The trapdoor test in T4 was conducted after a static footing pressure of 16.4 kPa was applied, while a cyclic footing pressure of the same magnitude at a frequency of 0.1 Hz was applied in T10 followed by the trapdoor test. The cyclic loading was applied for a total number

of 280 cycles (i.e., 30 cycles per each trapdoor lowering increment) throughout the trapdoor test as shown in Figure 4.24.

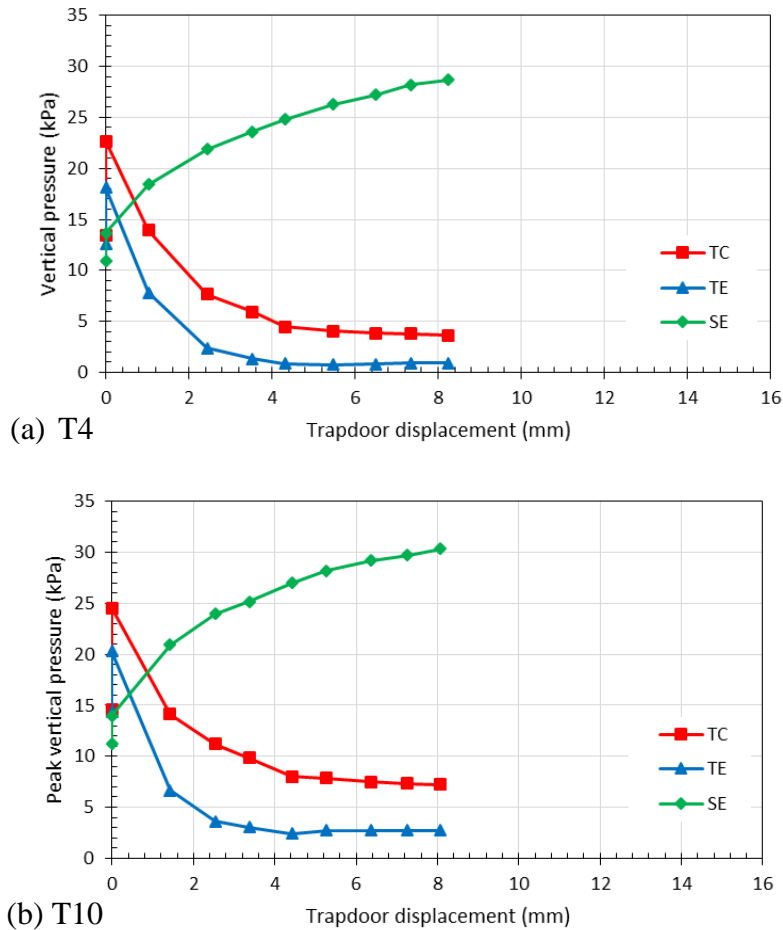


Figure 4.23 Measured pressures on and besides the trapdoor versus the trapdoor displacement in tests: (a) T4 and (b) T10

Different from the trapdoor tests under only soil self-weight, the pressures on the trapdoor in T3 and T9 sharply dropped to the minimum value with the trapdoor displacement as small as 2.0 mm. In both T4 and T10, however, the measured pressures on the trapdoor (TC and TE) sequentially decreased as the trapdoor was progressively lowered until they reached the minimum pressures at the end of the trapdoor test (i.e., at the trapdoor displacement of 8 mm) due to the soil

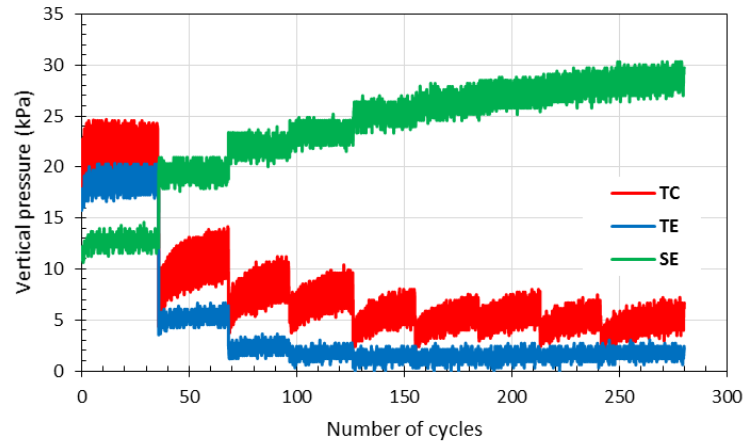


Figure 4.24 Measured pressures on and besides the trapdoor versus number of cycles in the trapdoor test (T10)

arching effect, which in turn induced a gradual increase in the pressure at SE. However, the applied footing load increased the measured pressures at TC and TE at the end of the trapdoor tests to 3.61 and 0.91 kPa in T4 and to 7.1 and 2.5 kPa in T10, respectively. In T3 or T9, the pressures were 2.4 kPa at TC and 1.2 kPa at TE. Soil arching was fully mobilized in both T4 and T10 with the soil arching ratios of 0.11 and 0.22, respectively. Since static and cyclic footing loads were applied in T4 and T10, respectively, the denominator of Equation 2.1 for calculating the soil arching ratio was determined based on the measured pressure during the tests. In other words, the soil arching ratios were calculated based on the average pressure on the trapdoor at the end of the trapdoor test divided by the average pressure on the trapdoor before the trapdoor test for each test (i.e., the average pressures at TC and TE at the trapdoor displacement of 0 mm and the applied footing pressure of 16.4 kPa as shown in Figure 4.25). Moreover, there was no sign of soil arching deterioration in both tests.

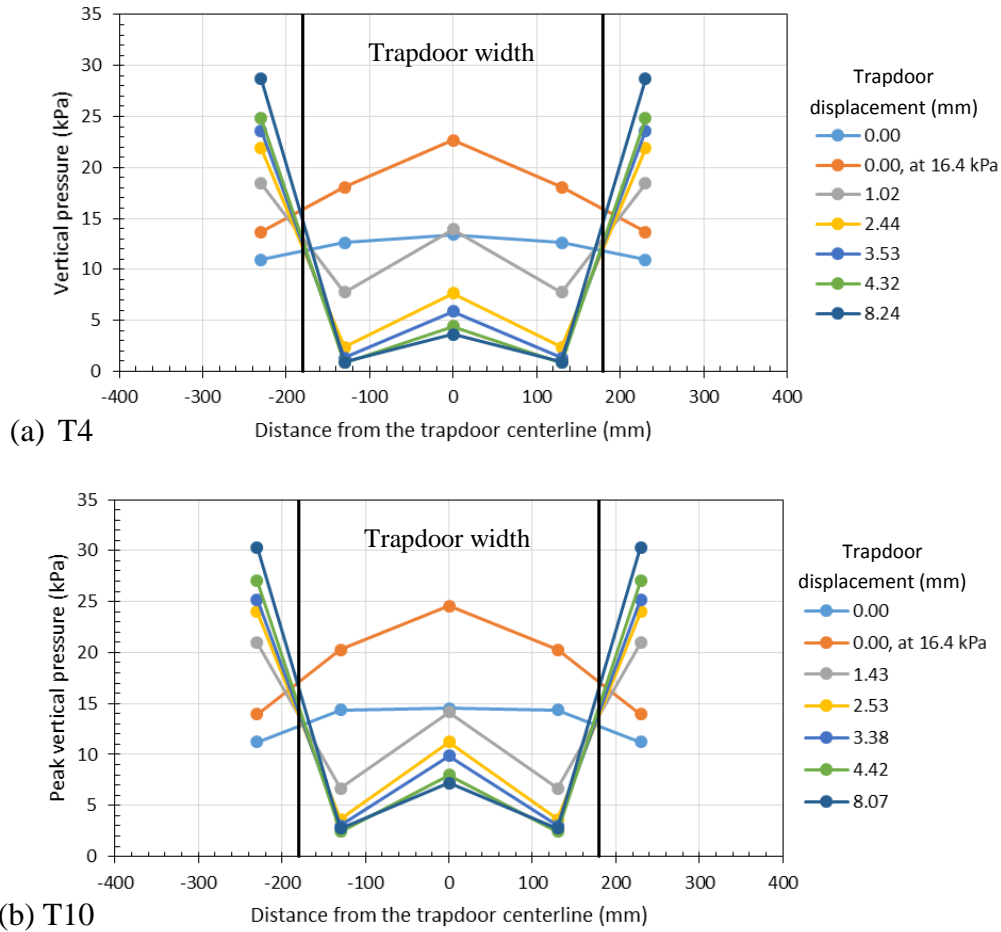


Figure 4.25 Cross-sectional distribution of the measured pressures during the trapdoor tests in:  
 (1) T4 and (b) T10

Furthermore, no differential settlement was found at the surface of the embankment at the end of the trapdoor test in T4 (under the static footing load). However, the cyclic footing load caused a visible differential settlement on the embankment surface at the end of the trapdoor test in T10, mostly because the initial settlement resulted from the footing load before the start of the trapdoor test. However, the equal settlement plane did not reach the surface of the embankment if the induced footing settlement before the trapdoor test had been subtracted from the total settlement. In the trapdoor tests of T4 and T10, the equal settlement planes were determined at 1.46S and 1.54S, respectively.

### 4.3 SUMMARY ON THE TRAPDOOR TESTS

This chapter presents the results of 12 trapdoor tests which were carried out after the construction of embankment fill to investigate the mobilization of soil arching under the soil self-weight and the soil self-weight with the footing load. Findings from these tests are summarized as follows:

- Since the trapdoor consisted of a steel plate underneath the wooden plate, it had slightly higher stiffness than the stationary supports with wooden plates only. Therefore, the pressure on the trapdoor was slightly higher than that on the stationary supports at the end of the construction in all tests. However, they both were close to the soil overburden pressure ( $\gamma H$ ).
- In all tests, lowering the trapdoor caused the pressure redistribution such that the measured pressures on the trapdoor at TC and TE decreased. At the same time, the pressure at SE increased as the trapdoor was progressively lowered due to the soil arching effects.
- In all tests, soil arching was fully mobilized at the arching ratios ranging from 0.13 to 0.27 at the end of the trapdoor tests.
- The trapdoor displacement caused the particle movement within the embankment fill and the differential settlement between the yielding soil mass and the unyielding soil mass. The equal settlement planes, which had no differential settlement, existed at a height,  $Z$ , from the trapdoor, ranging from 1.39S to 1.82S.
- Three trapdoor tests (T2, T3, and T9) were conducted at two different maximum trapdoor displacements in the **unreinforced embankment** tests under the soil self-weight in order to investigate the effects of the progressive trapdoor displacement on the soil arching mobilization.

- In the trapdoor test of T2 performed to the maximum trapdoor displacement of 15 mm, soil arching started to deteriorate under the soil self-weight as the trapdoor displacement increased more than 2.5% of its width (i.e., the trapdoor displacement of 9 mm). In both trapdoor tests of T3 and T9, soil arching deterioration was eliminated by reducing the trapdoor displacement to 8.0 mm.
- Four tests (T5, T6, T11, and T12) were conducted with a **single layer of geosynthetic reinforcement** under soil self-weight, in which the geosynthetic minimized the deterioration and help stabilize soil arching although the trapdoor was lowered to 15 mm.
- The mechanisms in which the geosynthetic helped stabilize soil arching were lateral confinement and tensioned membrane effect. Interlocking of geosynthetic-soil particles applied additional horizontal stress to the soil particles under loading and in turn increased the soil shear strength thus creating more stable soil arching. The vertical component of the tensioned membrane reduced the pressures on the trapdoor and subsequently increased the pressures on the stationary supports. Lateral confinement was more effective at the small displacement, while the tensioned membrane effect was more effective at the large displacement.
- Geosynthetic reinforcement lowered the equal settlement plane. Therefore, the geosynthetic not only helped stabilize soil arching but also kept the differential settlement far below the surface of the embankment.
- When both the uniaxial and the biaxial geogrids were utilized in the single geosynthetic-reinforced fill tests, the maximum strain (also tensile strain) was located at the edges of the trapdoor. However, the biaxial geogrid underwent a considerably higher tensile strain

at the trapdoor centerline than the uniaxial geogrid because it had a better interlocking mechanism due to the existence of more transverse bars than the uniaxial geogrid.

- Three tests (T7a, T7b, and T13) had **double layers of geosynthetic reinforcement**, which were 100 mm apart. Trapdoor tests under soil self-weight were performed to the trapdoor displacement of 15 mm. The measured pressures above and below the lower geosynthetic layer at TC, TE, and SE implied that double layers of geosynthetic reinforcement with the soil in between acted as a stiffened platform in minimizing the deterioration of soil arching.
- In these tests (T7a, T7b, and T13) , the geogrid was stretched as the trapdoor was lowered to reach the similar tensile strain in the lower geogrid layer of about 0.35% at the trapdoor centerline and the trapdoor edges at the end of the trapdoor tests. Meanwhile, in the upper geogrid layer, the maximum tensile strain of about 0.27% developed at the trapdoor edges. However, the upper geogrid layer underwent much lower strain than that in the lower geogrid layer at the trapdoor centerline. Since the maximum strain occurred at the trapdoor centerline in the lower geogrid layer and at the edges of the stationary supports in the upper geogrid layer, the double layers of geosynthetic reinforcement with the soil functioned as a beam.
- Two trapdoor tests (T4 and T10) with **unreinforced embankment** fill were carried out in order to investigate the effect of static and cyclic footing loading in addition to the effect of the soil self-weight on the soil arching mobilization. Trapdoor tests were conducted to a maximum trapdoor displacement of about 8.0 mm.
- In the trapdoor test (T4) conducted under the static footing load, no differential settlement occurred on the surface of the embankment at the end of the trapdoor test. However, the

cyclic footing load caused a visible differential settlement on the embankment surface at the end of the trapdoor test in T10, mostly because of the initial settlement under the footing load before the start of the trapdoor test. The equal settlement plane did not reach the surface of the embankment in T10 if the induced settlement before the start of the trapdoor test was subtracted.

## **CHAPTER 5 ANALYSIS OF LOADING TEST RESULTS**

Geosynthetic-Reinforced Pile-Supported (GRPS) embankments are mostly constructed for roadway applications on soft soils. They are subjected to differential settlement between the foundation soil and the supports during the construction and service life. Therefore, by the time when these embankments are ready for service, a considerable degree of soil arching are mobilized and responsible for the performance of the embankment system. Consequently, assessing the effects of traffic loading on the stability of soil arching, which has not well been investigated, is of great importance. Therefore, in this study, the effects of traffic loading were investigated by utilizing a static or cyclic footing load after soil arching was fully mobilized. Two baseline tests, T1 and T8, were conducted under static and cyclic loading without any trapdoor test in the unreinforced embankment. Then totally 12 tests after the trapdoor tests as described in Chapter 4 were subjected to both static and cyclic footing loading. Loading types and details were described in Section 3.5 in Chapter 3. This chapter presents the analysis and discussion of loading test results.

### **5.1 BASELINE TESTS**

Baseline tests were conducted under footing loading without any trapdoor test to provide bases for evaluating the effects of mobilized soil arching on redistribution of the applied pressure in other tests and the stability of soil arching under surface loading. After the embankment fill had been constructed in T1, a loading test was performed with a monotonic static footing load. Figure 5.1 shows the results of the loading test in T1, in which the pressure on the trapdoor centerline (TC) increased the most as compared with those at other locations (TE and SE). Figure 5.2 and 5.3 show the results of the loading test in T8 that was performed under an incremental cyclic footing load with 100 cycles applied for each loading increment (about 7 kPa).

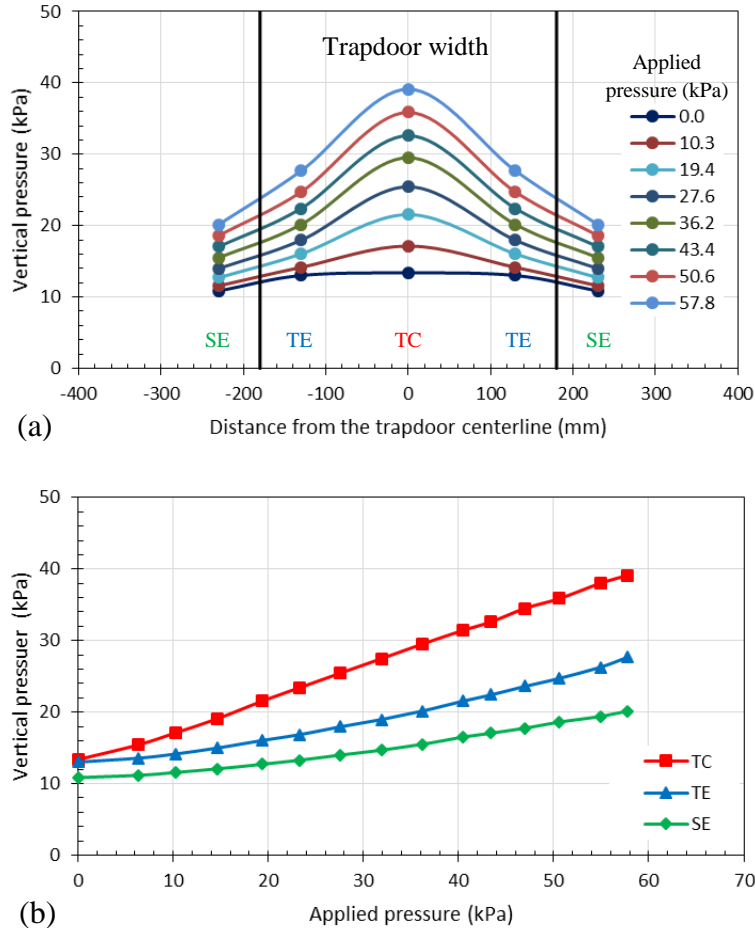


Figure 5.1 Measured pressures on and besides the trapdoor in the loading test of T1: (a) the cross-sectional distribution of pressure and (b) measured pressure versus the monotonic static footing pressure

In the loading test in T8, similar to that in T1, the pressure on the trapdoor centerline (TC) increased the most as compared with those at other locations (TE and SE). However, under the same applied pressure, the measured pressures at TC, TE, and SE in T8 were higher than those in T1 as shown in Figure 5.4 for the measured pressure at TC only. For instance, at the applied footing pressure of 50 kPa, the peak pressures at TC, TE, and SE in T8 were 42.4, 36.2, and 25.8 kPa, respectively. On the other hand, those in T1 were 35.8, 24.7, and 18.6 kPa, respectively. This behavior can be explained by the fact that the pressure under static loading was distributed onto a

wider area than that under cyclic loading. Soil densification that was associated with the application of cyclic loading would increase the soil friction angle. Consequently, the pressure distribution angle would be smaller with the increased number of load application. Giroud and Han (2004) proposed a method to account for the change in the distribution angle for roadway applications.

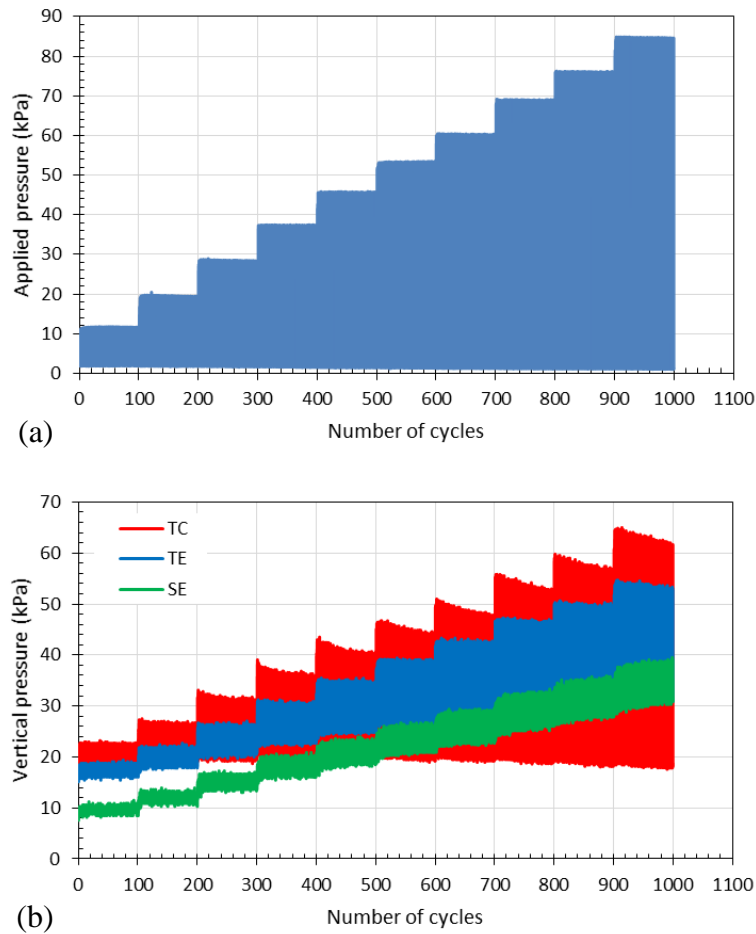
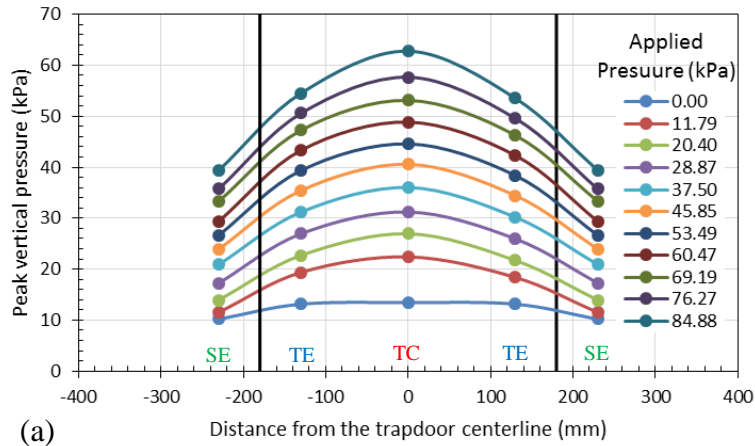
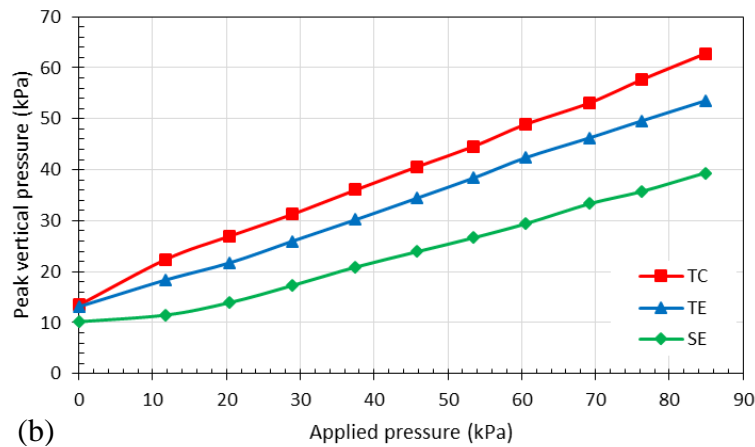


Figure 5.2 Applied and vertical pressures: (a) incremental cyclic footing pressure (b) measured pressures on and besides the trapdoor versus the number of cycles in the loading test of T8



(a)



(b)

Figure 5.3 Peak pressures on and besides the trapdoor in the loading test of T8: (a) along the trapdoor and the edges of the stationary supports and (b) the peak vertical pressure versus the applied pressure

Moreover, for the same reason mentioned earlier, the amplitudes for the measured pressures at TC were larger than those at other locations, TE and SE. The difference became even larger as the applied pressure increased as shown in Figure 5.2 (b). In addition, the maximum footing settlement at the cycle number of 100 versus the applied pressure in T8 is plotted in Figure 5.5 to show that the footing settlement increased much faster under the cyclic loading than that under static loading in T1.

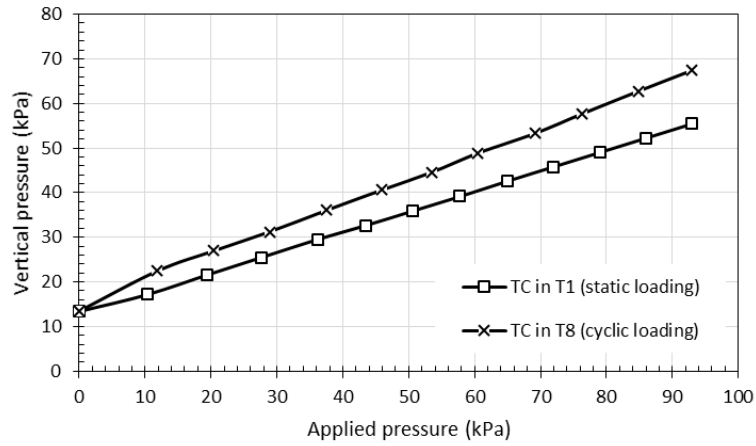


Figure 5.4 Measured pressures at the trapdoor centerline (TC) versus the applied pressure in both T1 and T8

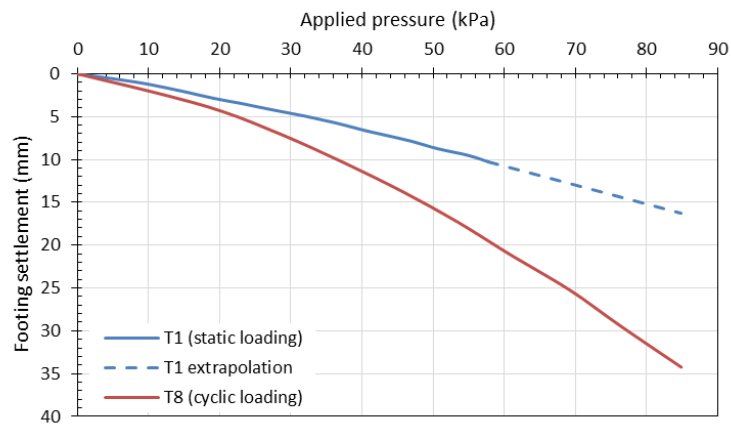
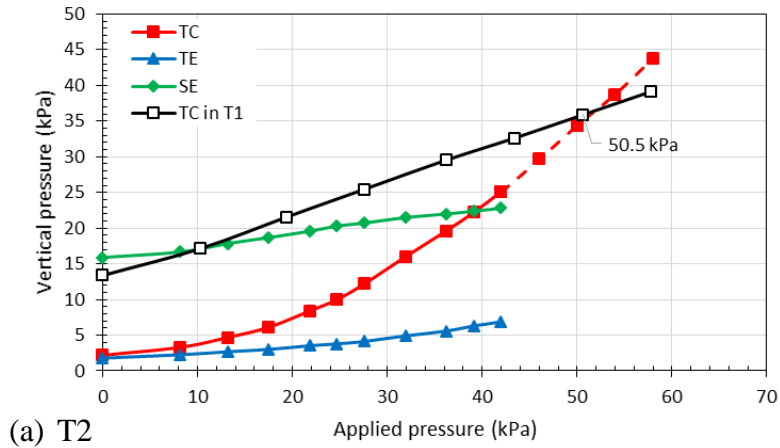


Figure 5.5 Measured footing settlements induced by static and cyclic footing pressures in T1 and T8

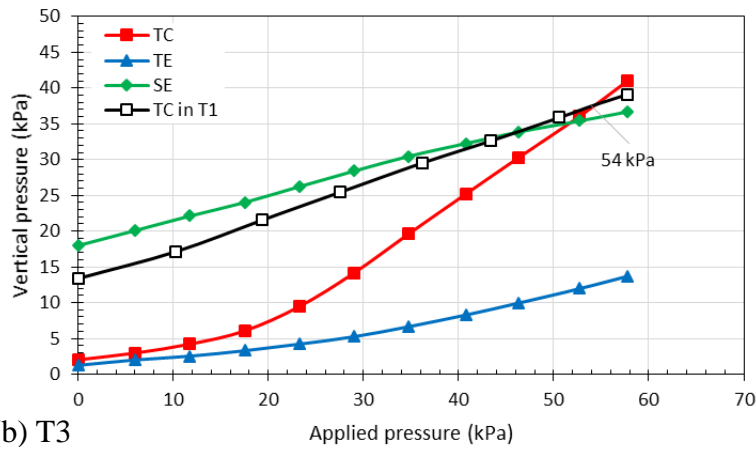
## 5.2 UNREINFORCED EMBANKMENT FILL

Five tests were conducted without reinforcement to study the stability of soil arching in the unreinforced embankments. In three tests (T2, T3, and T9), soil arching was mobilized under soil self-weight, while in other two tests (T4 and T10), soil arching was mobilized under the soil self-weight and the footing load. The trapdoor test stage in each test was discussed in Chapter 4. In the loading test stage, either static or cyclic loading was applied until soil arching deteriorates to the point when the pressures at TC and SE were equal. Loading test results presented in this section are compared with those of the baseline tests. Loading tests in T2, T3, and T4 under static footing loading are compared with the loading test results of T1, while the loading test results in T9 and T10 under cyclic footing load are compared with those in T8.

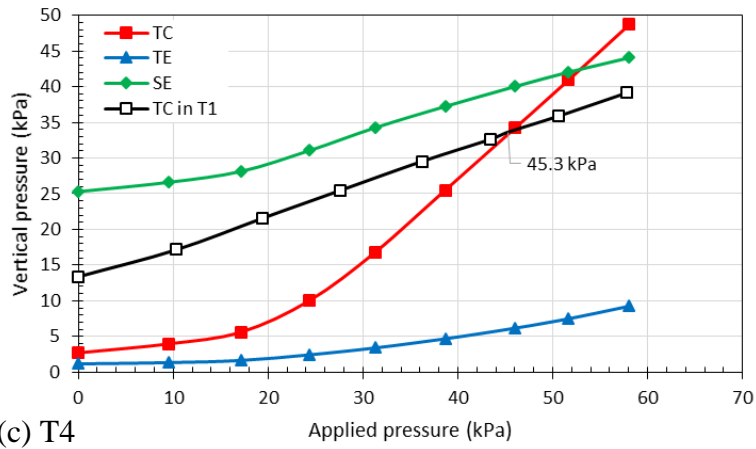
Figures 5.6, 5.7, and 4.8 present the measured pressures at the trapdoor center, edges, and the stationary supports during the loading tests in T2, T3, T4, T9, and T10. In these tests, the measured pressures on the trapdoor center (TC) increased most rapidly as compared with those at other locations. At this location, the slope of the pressure increase was flat at the beginning and then became steep with the applied pressure. However, the pressures on the edges of the stationary supports (SE) increased fast and then at a slow rate as the applied pressure increased. Also, the pressure at TE increased as the applied pressure increased.



(a) T2

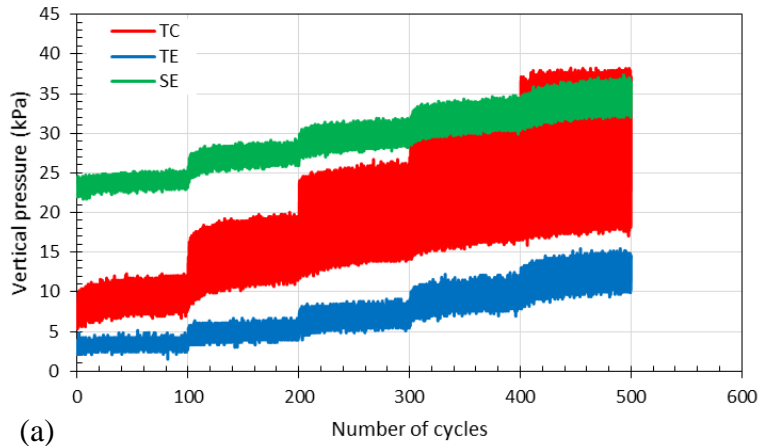


(b) T3

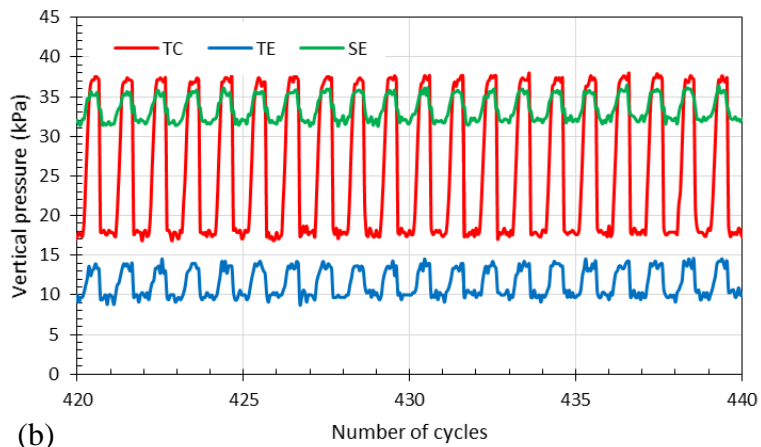


(c) T4

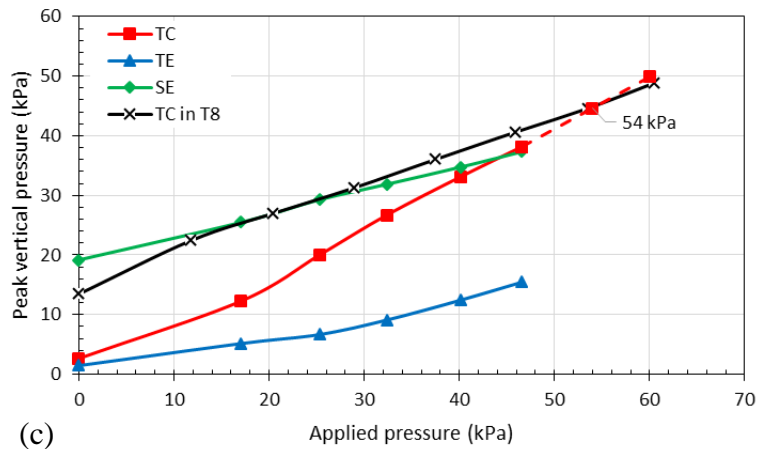
Figure 5.6 Measured pressures on and besides the trapdoor versus the monotonic static footing pressure in the loading test of the unreinforced fill tests: (a) T2, (b) T3, and (c) T4



(a)



(b)



(c)

Figure 5.7 Measured pressures on and besides the trapdoor in the loading test of the unreinforced fill test (T9): (a) the vertical pressure versus the number of cycles, (b) the results at the number of cycles from 420 to 440, and (c) the peak measured pressures versus the applied pressure

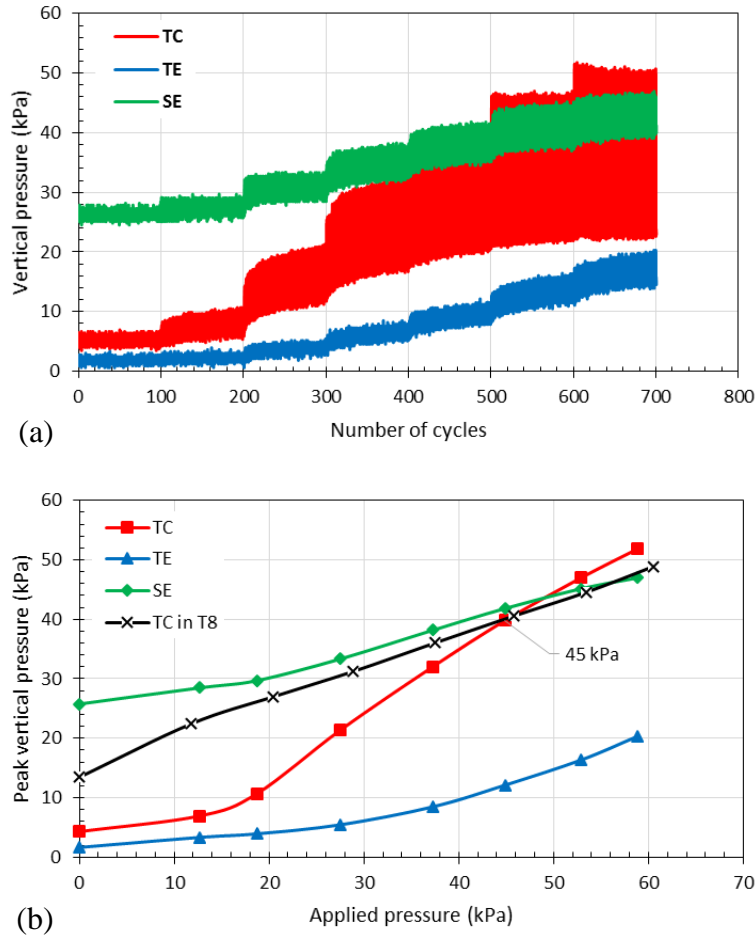


Figure 5.8 Measured pressures on and besides the trapdoor in the loading test of the unreinforced fill test (T10): (a) the pressure versus the number of cycles and (b) the measured peak pressure versus the applied pressure

The significant difference between these tests is the level of the measured pressure. For instance, as shown in Figure 5.6, the measured pressure at SE in T2 at the applied footing pressure of 40 kPa was 22.5 kPa after the trapdoor test was conducted to the maximum trapdoor displacement of 15.15 mm. However, the corresponding pressures in T3 and T4 were 32 and 38 kPa, respectively after the trapdoor tests were performed to the maximum displacement of about 8.0 mm. Therefore, the reduction of the trapdoor displacement by 7.0 mm mobilized more soil arching that helped transfer 42% more pressure to the stationary supports. This result indicates the

effect of progressive trapdoor displacement on the soil arching ability to transfer the load from the foundation soil (i.e., the soil above the trapdoor) to the stationary supports under static footing load. Also, the application of a constant static footing load during the trapdoor test in T4 did not affect the capability of soil arching. Furthermore, the measured pressures at SE in the loading tests in T9 and T10 at the applied footing pressure of 40 kPa were equal to 34.5 and 40 kPa, respectively. Therefore, the cyclic footing load did not affect the capability of soil arching on transfer the applied pressure to the stationary supports as compared to those of T3 and T4.

Moreover, the measured pressures at TC and SE were equal at different applied pressures. Under the static footing load in T2, T3, and T4, the measured pressures at TC and SE were equal at the applied pressures of 42, 51.5, and 53 kPa, respectively. Under the cyclic footing load in T9 and T10, however, the measured pressures at TC and SE were equal at the applied pressures of 44.2 and 48.8 kPa, respectively, after the application of 500 cycles.

Figure 5.9 presents the settlement of the embankment surface under the footing during the loading tests of the unreinforced embankments. Figure 5.9 (a) shows that as compared with T2 and T3, an increase of the trapdoor displacement by 7.0 mm caused 52% increase in settlement of the embankment surface at an applied static pressure of 50 kPa. In addition, at the same level of the applied pressure, an application of cyclic loading instead of static loading increased the settlement of the embankment surface by 60% as T3 is compared to T9 in Figure 5.9 (b). In T4 and T10, in which footing load was applied during the trapdoor test, the induced settlements under the footing during the loading tests were much lower than those in T3 and T9 due to the increase of soil modulus as shown in Figure 5.9 (c). Figure 5.9(c) also shows that a reduction in the embankment surface settlement of 78.6% and 64% at the applied pressure of 50 kPa were obtained as compared the settlements in T4 with T3 and T9 with T10, respectively.

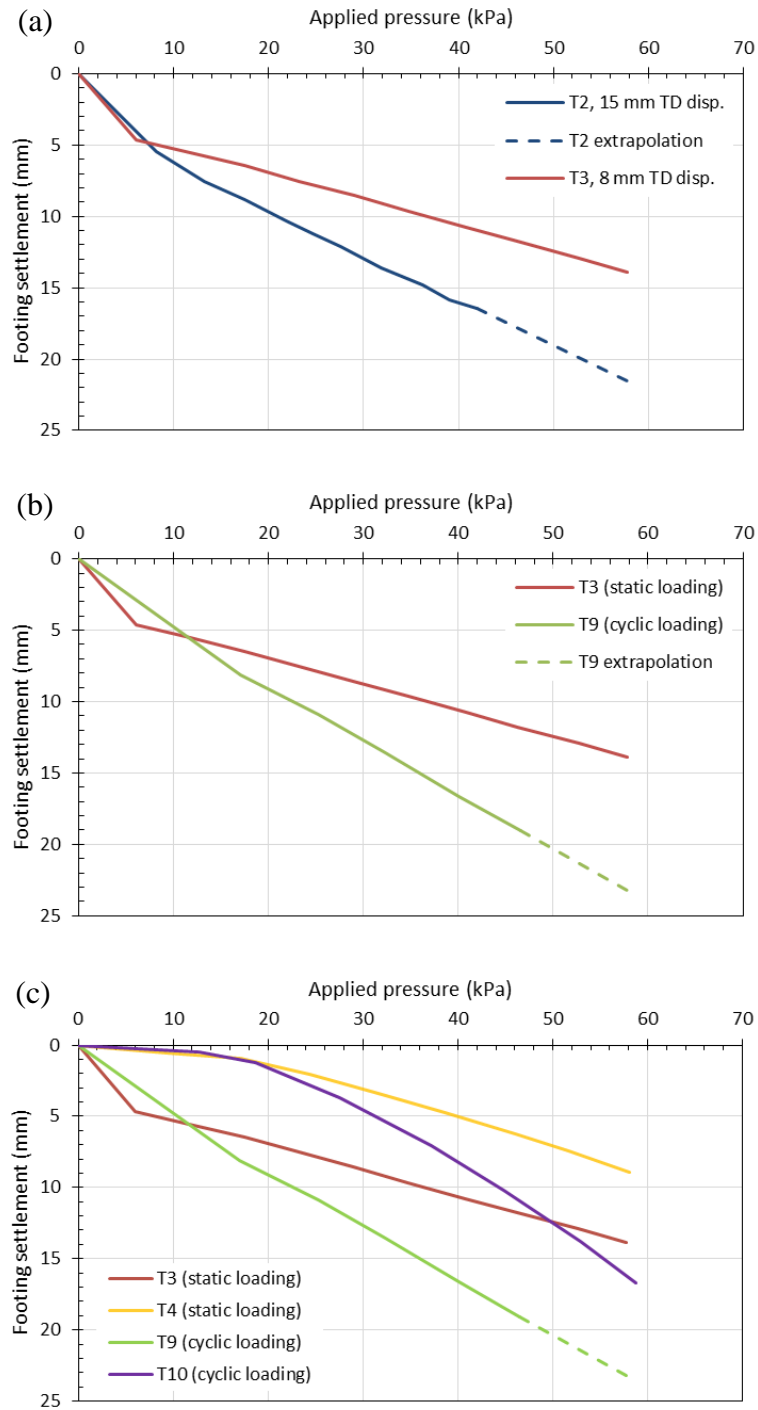


Figure 5.9 Measured footing settlements induced by static and cyclic footing loads in the loading test of the unreinforced fill tests (T2, T3, T4, T9, and T10) to evaluate the effects of: (a) trapdoor displacement, (b) loading type, (c) application of the footing load during the trapdoor tests

### ***Soil Arching Deterioration***

To assess the stability of soil arching or the deterioration of soil arching, the soil arching ratio,  $\rho$ , defined in Equation 2.1 was used.  $\rho = 0$  represents complete soil arching while  $\rho = 1$  represents no soil arching. Figure 5.10 shows the cross-sectional distribution of the measured pressures at the end of construction, the trapdoor test, and the loading test in T2 and T3. At the end of the trapdoor test, the measured pressures on the top of the trapdoor were relatively uniform; therefore, the soil arching ratio calculated based on the average pressure on the trapdoor is reasonable. However, when a localized footing load was applied, the pressure distribution on the trapdoor was not uniform; therefore, the soil arching ratio calculated based on the average pressure on the trapdoor is not reasonable anymore. To overcome this problem, the measured pressure at the center of the trapdoor (TC) was used as  $\sigma_v$  for calculation of the soil arching ratio. At the same time, the applied pressure,  $q$ , in Equation (2) was obtained based on the baseline tests, T1 for the tests performed under static loading and T8 for the tests performed under cyclic loading, for the location at the center of the trapdoor.

For the tests carried out for the unreinforced embankment fill, the soil arching ratios could be calculated without and with a footing load as presented in Table 5.1. Table 5.1 shows low soil arching ratios before loading because fully mobilized soil arching was reached. However, when the footing load was applied, the soil arching ratios increased for these tests as presented at the applied footing pressure of 50 kPa. The increase of the soil arching ratio indicates the deterioration of soil arching. Table 5.1 also shows that the increase of the soil arching ratio in T3 was less than those in T2 and T4. This comparison indicates the effects of the progressive trapdoor displacement as well as the static footing load on the soil arching mobilization and deterioration. However, the

cyclic footing load did not affect soil arching when the calculated soil arching ratios in T9 were compared with T3 and T10 with T4 after the application of the footing load.

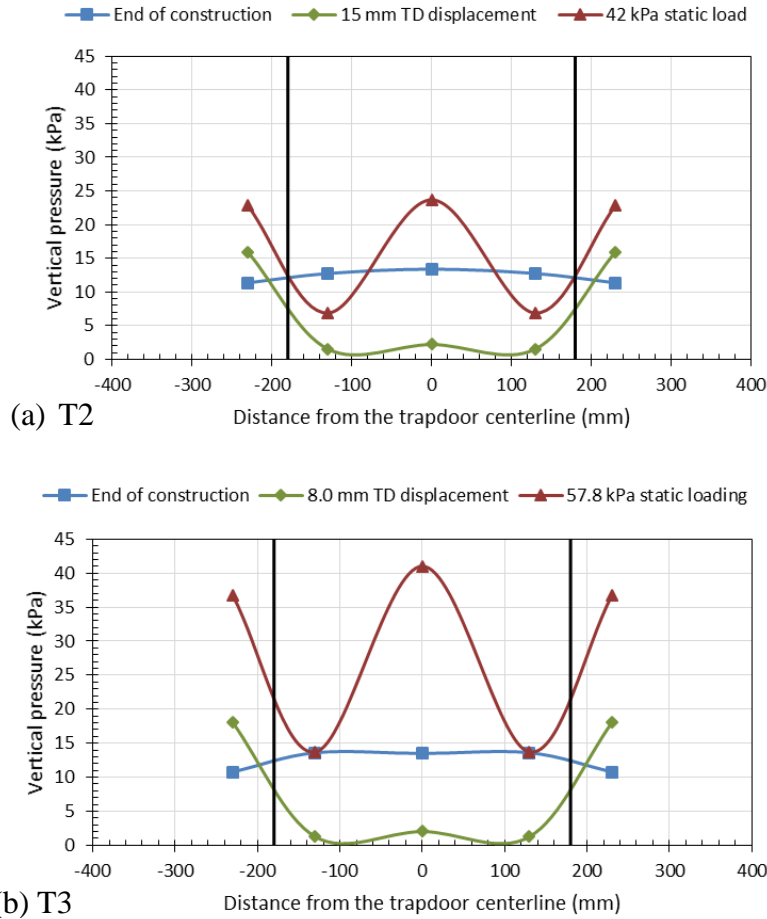


Figure 5.10 Cross-sectional distribution of the measured pressures at the end of construction, the trapdoor test, and the static loading test of the unreinforced fill tests: (a) T2 and (b) T3

When a soil arching ratio is equal to 1.0, soil arching disappears and full deterioration of soil arching happens. In this study, the applied footing pressure required to increase the soil arching ratio to 1.0 is defined as the Soil Arching Degradation Pressure (SADP). Table 5.1 shows that the SADP was equal to 54.0 kPa in both T3 and T9, while it was equal to 45.3 and 45.0 kPa in T4 and T10, respectively. Therefore, the application of the static or cyclic footing pressure during the soil

arching mobilization reduced the SADP by about 20%. Although applying a footing pressure of 16.4 kPa in T4 and T10 during the trapdoor test did not affect the mobilization of soil arching as discussed in Chapter 4, it increased the probability of the arching collapse during the service life.

Table 5.1 Soil arching ratios and degradation pressures in the unreinforced embankment tests

Test number	Max. trapdoor disp. (mm)	Loading type	$\rho$ before loading	$\rho$ at 50 kPa loading	SADP (kPa) at $\rho=1$	SADP reduction at $\rho=1$
T2	15.15	Static	0.14	0.98	50.5	6.93 %
T3	8.07	Static	0.13	0.94	54.0	<b>Baseline</b>
T4	8.24	Static	0.11	1.09	45.3	19.2 %
T9	8.47	Cyclic	0.16	0.95	54.0	0.0 %
T10	8.07	Cyclic	0.22	1.04	45.0	20.0 %

### 5.3 SINGLE GEOSYNTHETIC-REINFORCED FILL

Four tests were conducted with a single layer of geosynthetic reinforcement. Section 4.1.2 presented these trapdoor test results, to assess the benefit of geosynthetic inclusion on the stability of the soil arching. As described earlier in Chapter 4, two different types of reinforcement were utilized. A layer of uniaxial geogrid overlain by a layer of non-woven geotextile was used in T5 and T11, and a layer of biaxial geogrid overlain by a layer of non-woven geotextile was used in T6 and T12. In each of these tests, soil arching was first mobilized under soil self-weight during the trapdoor test stage. Subsequently, in the loading test stage, a footing pressure was applied to cause the deterioration of soil arching. The effect of each type of geosynthetic reinforcement on soil arching was investigated under both static and cyclic loading. Loading test results were compared with those of the baseline test to assess the effect on the stability of the soil arching (i.e., the soil arching degradation pressure); however, to evaluate the benefit of the geosynthetic reinforcement, they were compared with the results of the loading test in T2.

Figure 5.11 presents the measured pressures at the trapdoor center, edges, and the stationary supports during the loading tests in T5 and T6, which were conducted under monotonic static footing loading. Also, the peak pressures measured at TC, TE, and SE during each 100-cycle loading increment in both T11 and T12 were plotted and are presented in Figure 5.12. In these figures, the pressures at the trapdoor center, edges, and the stationary supports were measured at both above and below the geosynthetic reinforcement. At both levels, the measured pressures at TC increased most rapidly as compared with those at other locations, TE and SE. Also at TC, the

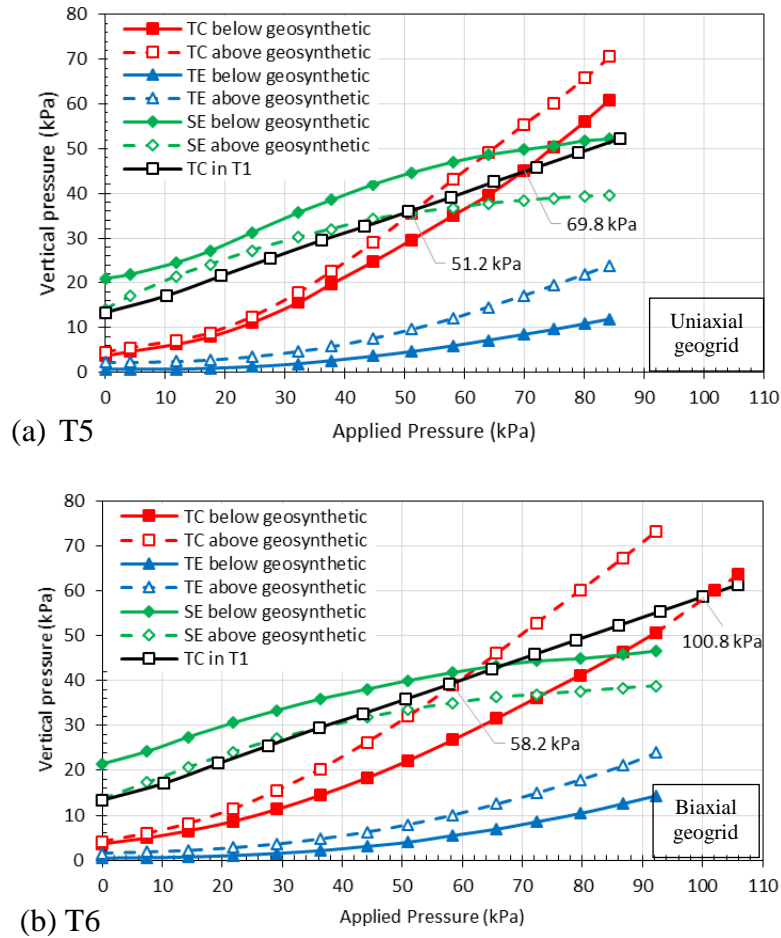


Figure 5.11 Measured pressures on and besides the trapdoor versus the monotonic static footing pressure in the single geosynthetic-reinforced tests: (a) T5 and (b) T6

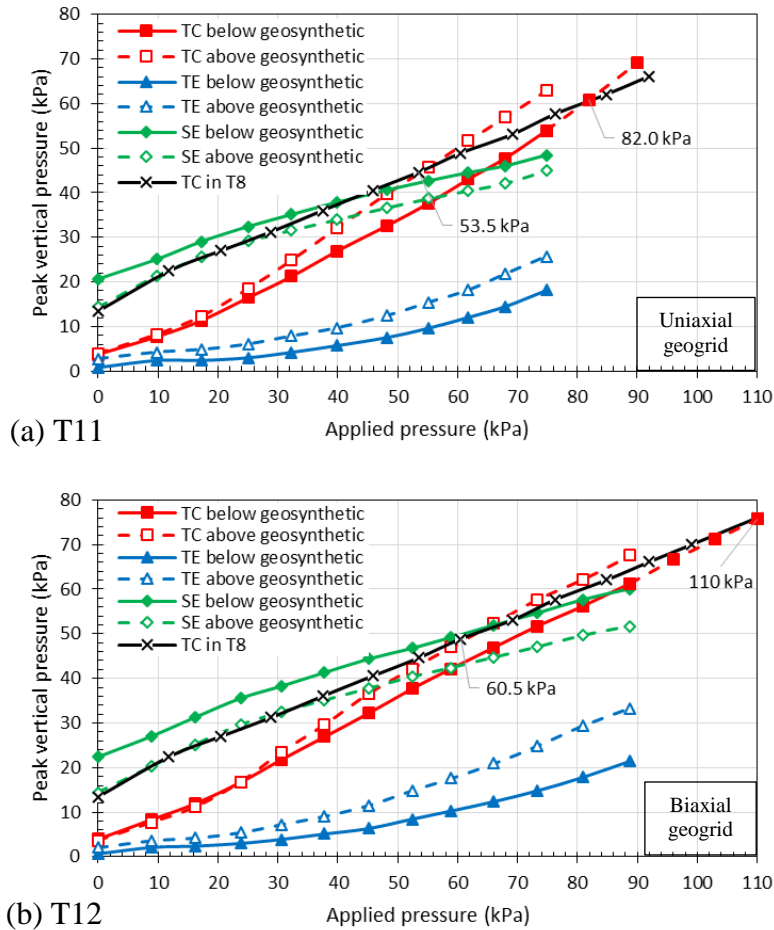


Figure 5.12 Measured pressures on and besides the trapdoor versus the incremental cyclic footing pressure in the single geosynthetic-reinforced tests: (a) T11 and (b) T12

slope of the pressure increase was flat at the beginning and then became steep with an increase of the applied pressure. However, the pressure on the edges of the stationary supports (SE) above and below the reinforcement increased fast and then at a slow rate as the applied pressure increased. In addition, the pressure at TE increased as the applied pressure increased. However, as the applied footing pressure increased, the geosynthetic carried more load so that the measured pressures at TC and TE below the geosynthetic were lower than those above the geosynthetic. However, the pressure at SE below the geosynthetic was higher than that above the geosynthetic because of the vertical component of the geosynthetic tension due to the tensioned membrane effect.

Moreover, the benefit of the geosynthetic reinforcement could be evaluated by comparing the results of the loading tests in T5 and T6 with those in T2. To illustrate this effect, the measured pressures below the geosynthetic at an applied static pressure of 50 kPa at TC, TE, and SE in T5 and T6, as well as those in T2 are shown in Figure 5.13. It can be seen that the biaxial geogrid reduced the pressure within the trapdoor area (especially in T6) by 59% at the center and 124% at the edges of the trapdoor. In other words, much smaller settlement in the foundation (soft) soil would be expected due to the reduction of the exerted pressure by using the geosynthetic. At the same time, the efficiency of the stationary supports (piles or columns) would be increased as the geosynthetic would transfer more load to the stationary supports. In T5 and T6, the percentages of the load increase applied to the stationary supports were 90% and 71%, respectively.

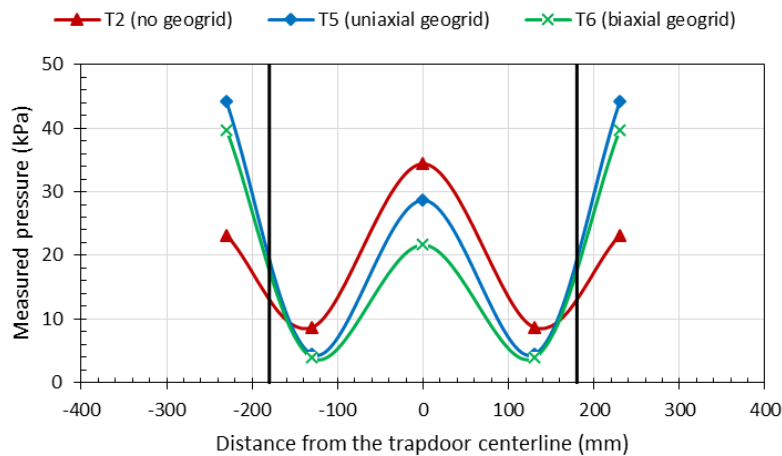


Figure 5.13 Cross-sectional distribution of the measured pressures at an applied static pressure of 50 kPa in T2, T5, and T6

Figures 5.14 and 5.15 present the settlement of the footing during the loading tests of the single geosynthetic-reinforced tests. It can be seen in Figure 5.4 (a) that the geosynthetic reinforcement reduced the settlement of the footing by 23.3% in T5 and 39.1% in T6 at an applied static pressure of 80 kPa. Also, the biaxial geogrid reduced the settlement of the footing by 12.8%

more than the uniaxial geogrid under the static footing load. However, under cyclic footing loading in T11 and T12, the biaxial geogrid slightly reduced the settlement of footing, by around 4.1% more than the uniaxial geogrid at an applied cyclic pressure of 80 kPa as presented in Figure 5.14 (b). In addition, at the same magnitude of the applied pressure, cyclic loading increased the settlement of the footing by 67.3% more than the static loading with the use of the uniaxial geogrid and 81.4% with the use of the biaxial geogrid as shown in Figure 5.15.

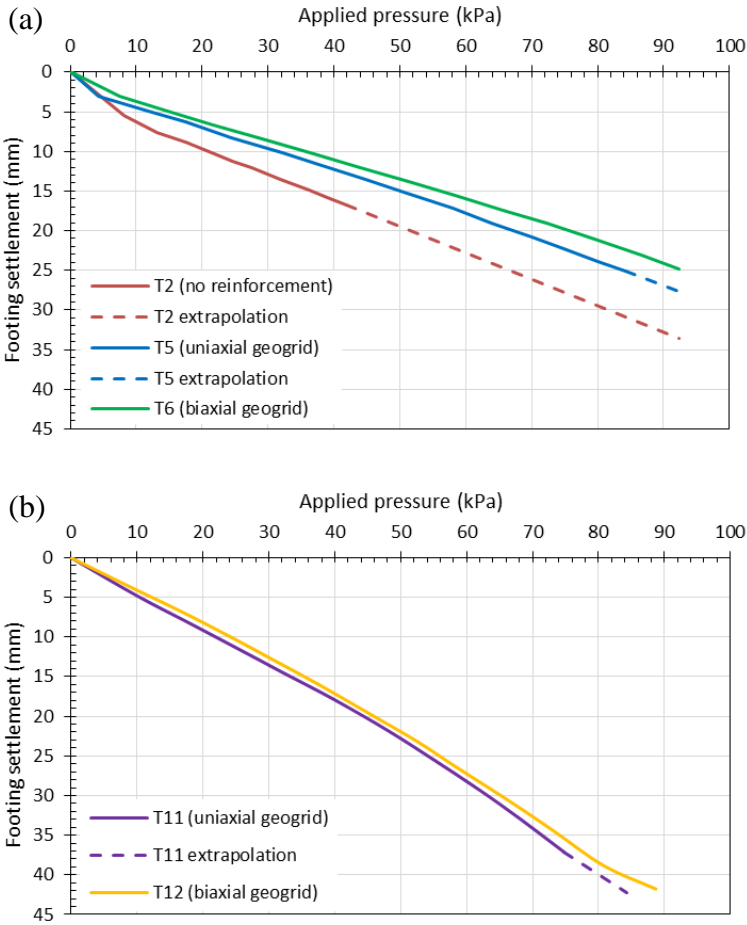


Figure 5.14 Measured footing settlements induced by the applied pressure in the single geosynthetic-reinforced tests (T5, T6, T11, and T12) to evaluate the effects of: (a) reinforcement type under static loading and (b) reinforcement type under cyclic loading

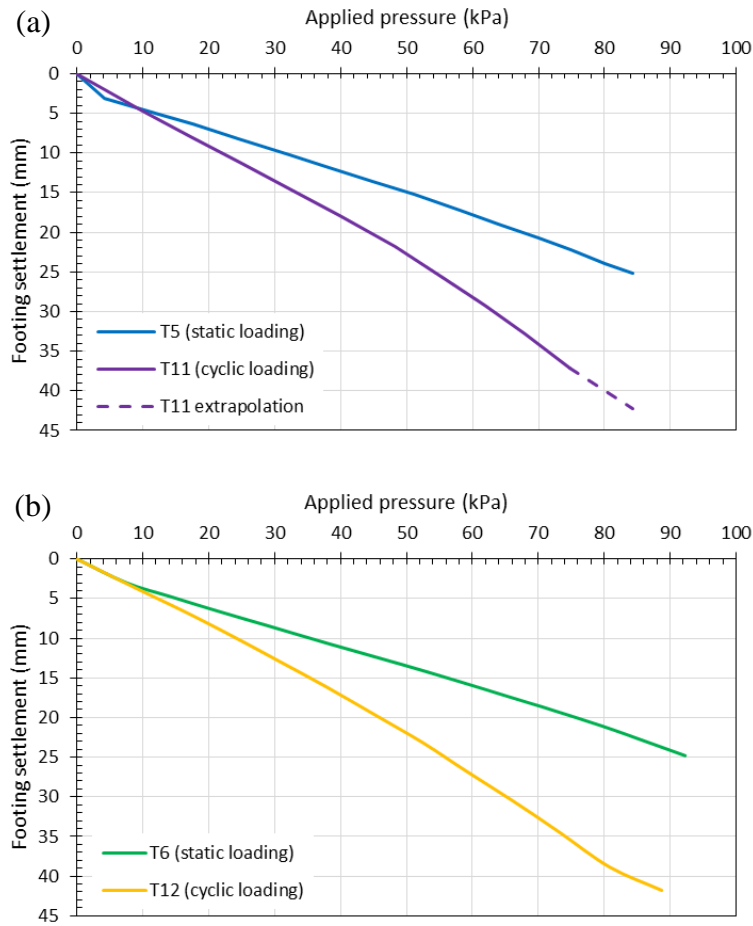


Figure 5.15 Measured footing settlements induced by the applied pressure in the single geosynthetic-reinforced tests (T5, T6, T11, and T12) to evaluate the effects of: (a) loading type with the uniaxial geogrid and (b) loading type with the uniaxial geogrid

As shown previously in Figures 5.11, 5.12, and 5.13, non-uniform pressures were measured on the trapdoor during the loading test of the single geosynthetic-reinforced sections. To assess the stability of soil arching using the soil arching ratio,  $\rho$ , the measured pressure at the center of the trapdoor (TC below the geosynthetic) was used as  $\sigma_v$  in Equation (2) for the calculation of the soil arching ratio. At the same time, the applied pressure,  $q$ , was obtained based on the baseline tests, T1, for the tests performed under static loading and T8 for the tests performed under cyclic loading, at the same location, TC.

Table 5.2 presents the soil arching ratios before the loading test as well as at the applied footing pressure of 50 kPa. When no footing load was applied, the soil arching ratios were found to be low because fully mobilized soil arching was reached. However, as the footing pressure was applied at 50 kPa, the soil arching ratios increased. The increase of the soil arching ratio indicates the deterioration of soil arching. Table 5.2 also shows that the increase of the soil arching ratio in the reinforced tests was less than that in the unreinforced test. This comparison proved the benefit of the geosynthetic reinforcement in maintaining soil arching stability. In addition, the cyclic footing load slightly increased the soil arching ratios in T11 and T12 as compared with those in T5 and T6.

Table 5.2 Soil arching ratios and degradation pressures in the single geosynthetic-reinforced tests and T2

Test number	Reinforcement type	Loading type	$\rho$ before loading	$\rho$ at 50 kPa	SADP (kPa) at $\rho=1$	SADP increase at $\rho=1$
T2	No geogrid	Static	0.14	0.98	50.5	<b>Baseline</b>
T5	Uniaxial geogrid	Static	0.19	0.81	69.8	38.2 %
T6	Biaxial geogrid	Static	0.14	0.61	100.8	99.6 %
T11	Uniaxial geogrid	Cyclic	0.18	0.84	82.0	17.5 % *
T12	Biaxial geogrid	Cyclic	0.17	0.79	110	9.13 % *

Note: \*SADP percentage increase for cyclic loading was calculated with respect to SADP under static loading

Table 5.2 shows that the SADPs were equal to 69.8 and 100.8 kPa under the static footing pressure in both T5 and T6, respectively, while the SADP was equal to 50.5 kPa in T2. In other words, the uniaxial geogrid increased the SADP by 38.2% while the biaxial geogrid increased the SADP by 99.6%. In the unreinforced tests, the SADPs under static and cyclic loading were the same; however, in the reinforced tests, the geosynthetic reinforcement further increased the SADP under cyclic footing load as compared with that under static loading by 17.5% and 9.13 % in T11 and T12, respectively.

Even though the geosynthetic underwent very small additional strains during the loading test as shown in Figures 5.16 and 5.17, the geosynthetic maintained the stability of the soil arching during the loading test, increased the SADP, and reduced the settlement of the embankment surface. Figure 5.17 also shows that the applied cyclic footing pressure induced more tensile strains along the geogrid than the static footing pressure. However, the geosynthetic underwent very small additional strains during the loading test because the trapdoor was not allowed to move. The addi-

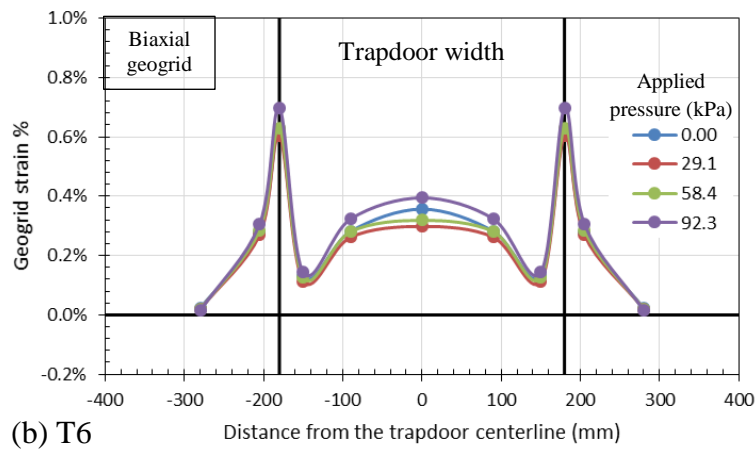
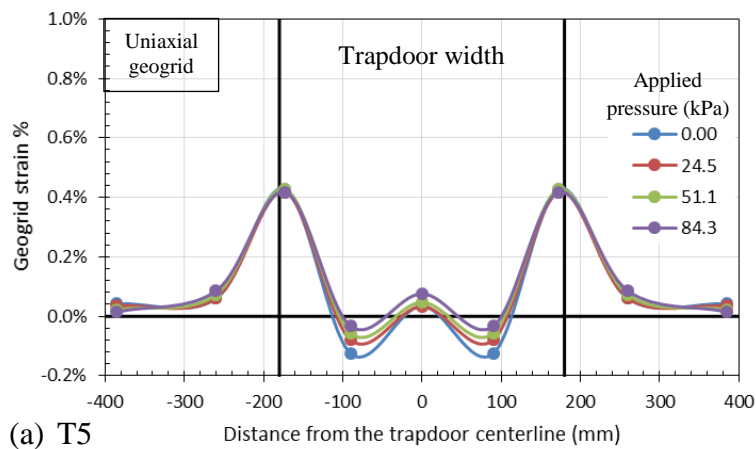


Figure 5.16 Strain distribution along the geogrid during the static loading tests in the single geosynthetic-reinforced tests: (a) T5 and (b) T6

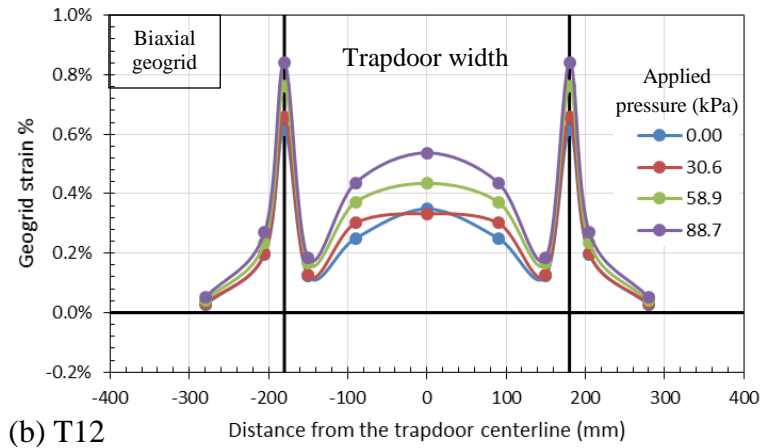
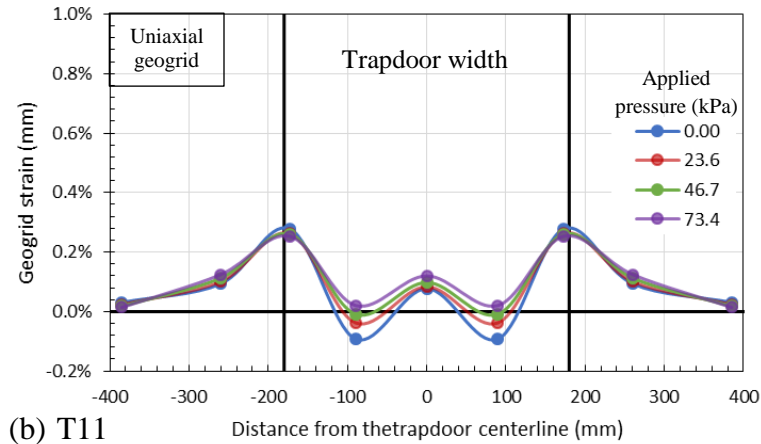


Figure 5.17 Strain distribution along the geogrid during the cyclic loading tests in the single geosynthetic-reinforced tests: (a) T11 and (b) T12

tional strains resulted from the compressibility of the embankment fill only under the applied pressure. Since the mobilization of the geosynthetic strength depends upon the strain level of the geosynthetic, which mostly gained during the trapdoor test; the soil arching degradation pressure would increase if more strain was allowed due to the deformation of the trapdoor during the loading test.

## 5.4 DOUBLE GEOSYNTHETIC-REINFORCED FILL

This section presents the results of three tests carried out with double layers of geosynthetic reinforcement to study the behavior of the load transfer platform (i.e., the beam effect) under footing loading. As described in Chapter 4, each layer of reinforcement consisted of a biaxial geogrid overlain by a non-woven geotextile. In each of these tests, soil arching was first mobilized under soil self-weight during the trapdoor test stage as discussed in Section 4.1.3. Subsequently, in the loading test stage, the static or cyclic footing pressure was applied until the measured pressure on the trapdoor center (TC) and the support edges (SE) were equal. Loading test results were compared with those of the baseline test to assess the stability of soil arching (i.e., SADP); however, the results of the loading test in T2, T6, and T12 were compared to evaluate the effect of the reinforcement type on soil arching.

Figure 5.18 presents the measured pressures during the loading test in T7a and T7b under monotonic static footing loading. Figure 5.19 presents the peak pressures during the loading test in T13, which was performed under incremental cyclic footing load. Each cyclic loading was applied for 100 cycles, during which the peak pressures at TC, TE, and SE in T13 were measured. Figures 5.18 and 5.19 show the pressures at the trapdoor center, edges, and the stationary supports above and below the lower geosynthetic reinforcement layer. Similar to the results of the single geosynthetic reinforced test, the measured pressure at TC increased most rapidly as compared with those at other locations, TE and SE. Also at TC, the slope of the pressure increase was flat at the beginning and then became steep with the applied pressure. However, the pressure on the edges of the stationary supports (SE) increased fast and then at a slow rate as the applied pressure increased. In addition, the pressure at TE slightly increased as the applied pressure increased. However, the measured pressures at TC below the geosynthetic reinforcement in T7a and T7b was higher than

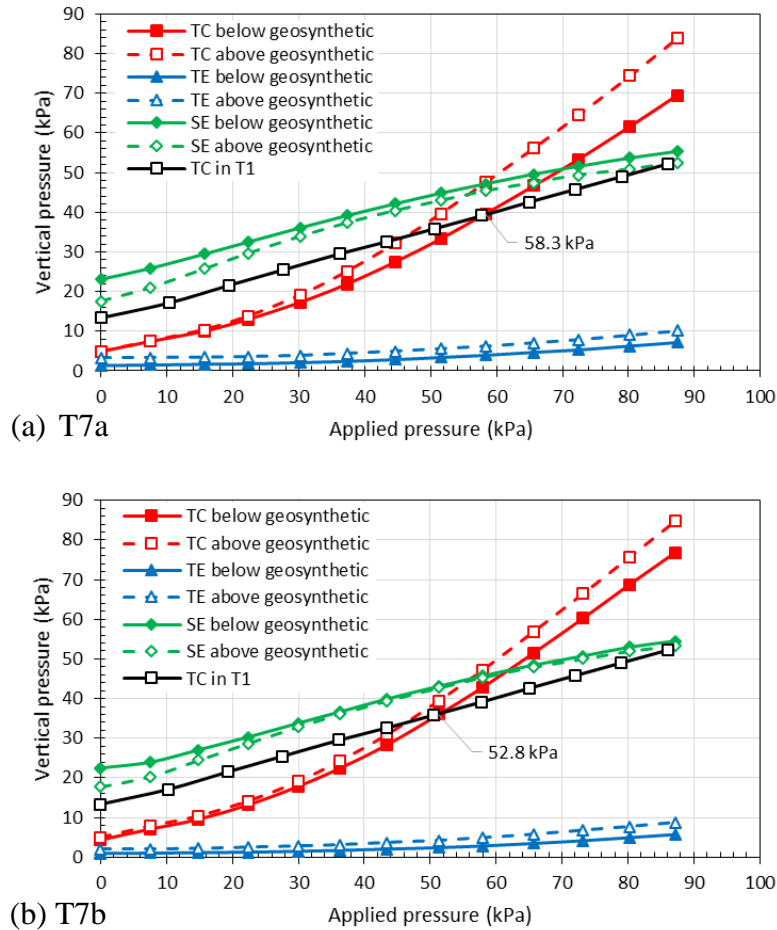


Figure 5.18 Measured pressures on and besides the trapdoor versus the monotonic static footing load in the double geosynthetic-reinforced tests: (a) T7a and (b) T7b

that in the single geosynthetic reinforced test (T6) as depicted in Figure 5.20. For instance, the measured pressures at the static footing pressure of 80 kPa in T7a and T7b were equal to 61.4 and 68.5 kPa, respectively, while the measured pressure in T6 was equal to 41.5 kPa. Moreover, as the applied footing pressure increased, the difference in the measured pressures above and below the lower layer of the geosynthetic reinforcement at TC, TE, and SE was less than that in the single geosynthetic reinforced test. This result indicates that the double geosynthetic reinforced fill did not sustain the applied pressure. It is believed that the trapdoor was not displaced enough during the trapdoor test stage to mobilize the geosynthetic strength with the presence of the upper

geosynthetic layer. Figures 5.21, 5.22, and 5.23 show the measured strains during loading in the double geosynthetic-reinforced tests T7a, T7b, and T13, respectively. Clearly, the geosynthetic did not mobilize much strain during the loading test; therefore the geosynthetic lacked the necessary strength to sustain the applied footing pressure.

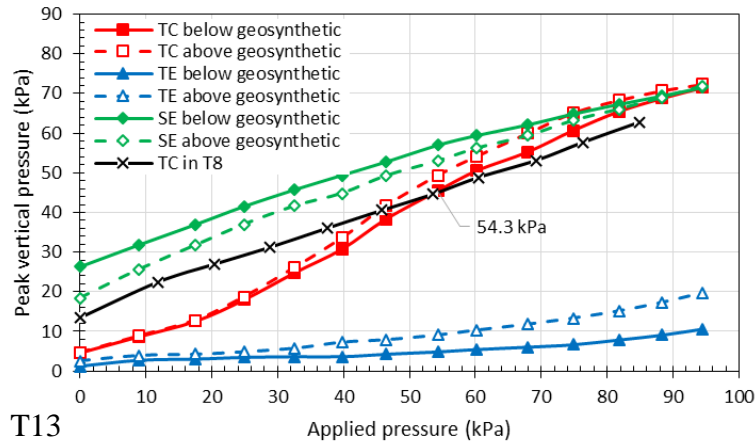


Figure 5.19 Measured pressures on and besides the trapdoor versus the incremental cyclic footing pressure in the double geosynthetic-reinforced test (T13)

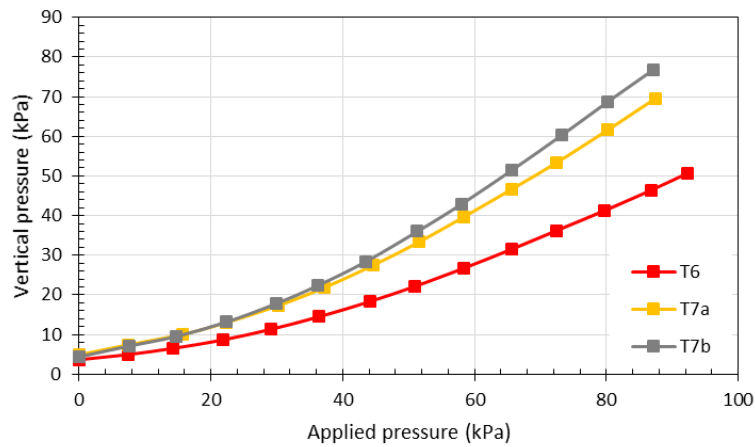


Figure 5.20 Measured pressures at TC below the lower geosynthetic layer in T7a and T7b compared to that in T6

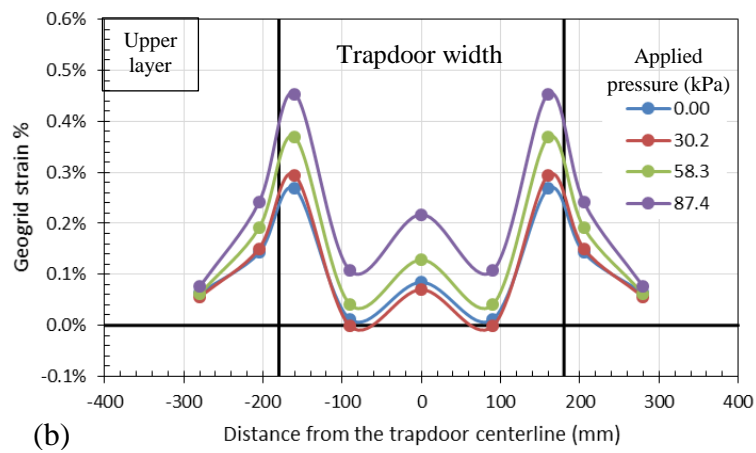
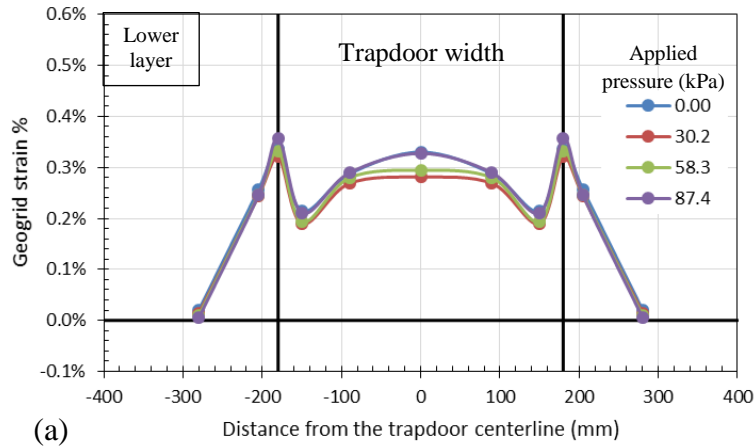


Figure 5.21 Strain distribution along the biaxial geogrids during the loading test in T7a: (a) the lower geogrid layer and (b) the upper geogrid layer

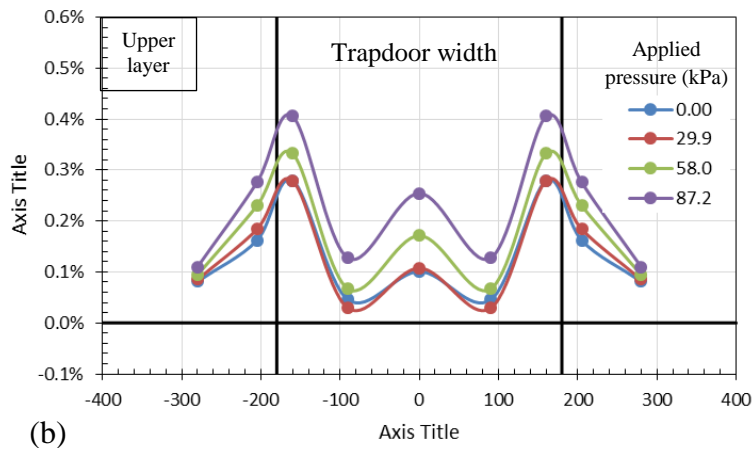
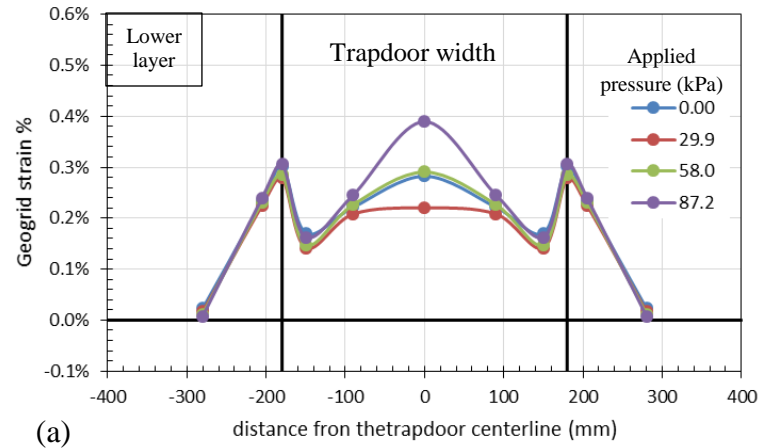


Figure 5.22 Strain distribution along the biaxial geogrids during the loading test in T7b: (a) the lower geogrid layer and (b) the upper geogrid layer

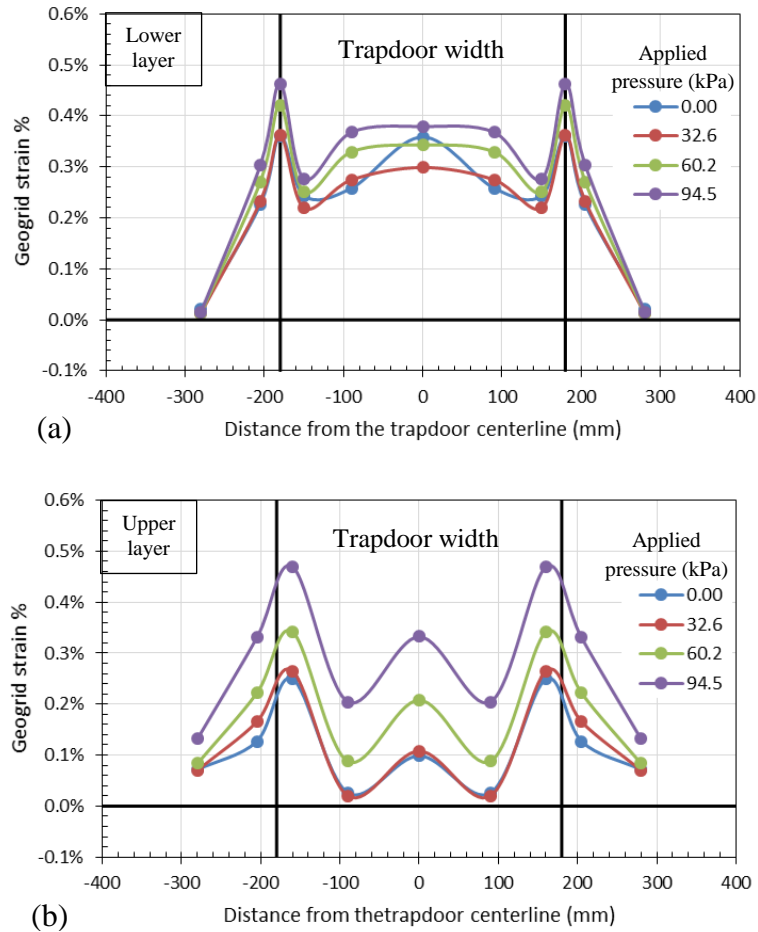


Figure 5.23 Strain distribution along the biaxial geogrids during the loading test in T13: (f) the lower geogrid layer and (e) the upper geogrid layer

Figure 5.24 presents the settlement of the footing during loading in the double geosynthetic-reinforced tests. Figure 5.24 (a) also compares the test results of T2, T6, T7a and T7b and shows that an additional layer of geosynthetic reinforcement further reduced the settlement of the footing by 23.0% in T7a and T7b as compared with T6 at an applied static pressure of 80 kPa. In other words, the use of double layers of the geosynthetic reinforcement reduced the footing settlement by 71% as compared with that without any reinforcement. However, the cyclic footing pressure in T13 only reduced the settlement by 5.5% by using double layers of geosynthetic as compared with the single layer of geosynthetic at an applied cyclic pressure of 80 kPa as presented

in Figure 5.24 (b). In addition, at the same magnitude of the applied pressure, cyclic loading increased the settlement of the footing by 108% as compared to static loading.

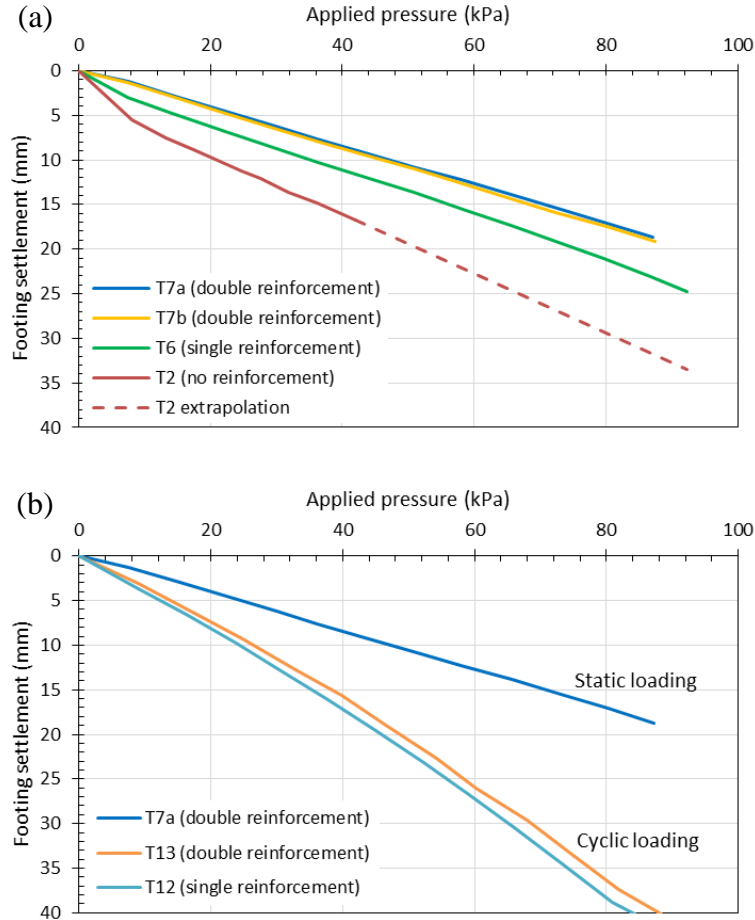


Figure 5.24 Measured footing settlement induced by the applied pressure in the double geosynthetic-reinforced tests (T7a, T7b, and T12) to evaluate the effects of: (a) reinforcement type under static loading and (b) reinforcement type and loading type

Table 5.3 presents the soil arching ratios before loading as well as at the applied footing pressure of 50 kPa. Without a footing load, the soil arching ratios at the end of trapdoor test were found to be low because fully mobilized soil arching was reached. However, when the applied footing pressure was 50 kPa, the soil arching ratios increased. The increase of the soil arching ratio indicates the deterioration of soil arching. Although double layers of geosynthetic reinforcement

were used in T7a, T7b, and T13, the increase of the soil arching ratios in these tests was more than those in the single geosynthetic reinforced tests (T6 and T12). Nevertheless, this increase was comparable to that in the unreinforced embankment. Table 5.3 also shows that the soil arching degradation pressures (SADPs) in T7a and T7b were 58.3 and 52.8 kPa static footing pressure, respectively, while SADP was equal to 54.3 kPa in T13. Even though the load transfer platform (beam effect) reduced the settlement of the footing, it had a negative effect on the stability of the soil arching under the footing loading. Such a system had three mechanisms including soil arching, the tensioned membrane or beam effect, and the stress concentration. The interaction between these three mechanisms is not well understood and needs further investigation. The numerical analysis would be adequate to assess the micromechanical features such as particle movements.

Table 5.3 Soil arching ratio and degradation pressure in the double geosynthetic-reinforced tests as well as T2, T6, and T12

Test number	Reinforcement type	Loading type	$\rho$ before loading	$\rho$ at 50 kPa loading	SADP (kPa) at $\rho=1$
T2	No Reinforcement	Static	0.14	0.98	50.5
T6	Single layer	Static	0.14	0.61	100.8
T7a	Double layer	Static	0.24	0.90	58.3
T7b	Double layer	Static	0.21	0.98	52.8
T12	Single layer	Cyclic	0.17	0.79	110
T13	Double layer	Cyclic	0.22	0.97	54.3

## 5.5 SUMMARY ON THE LOADING TESTS

In this chapter, the effects of traffic loading were investigated by utilizing a footing static or cyclic load after the soil arching was fully mobilized. Only two baseline tests were conducted under static and cyclic loading without any trapdoor test in the unreinforced embankment. Chapter 4 described twelve trapdoor tests under both static and cyclic footing loading. Findings from these tests are summarized as follows:

- In the **baseline tests**, the induced pressures over the box base (measured at TC, TE, and SE) under cyclic footing loading were higher than those under static footing loading.
- Five tests were conducted for the **unreinforced embankment**. Reduction of the trapdoor displacement by 7.0 mm in T3 mobilized more stable soil arching that increased the transferred pressure by 42% to the stationary supports at an applied pressure of 40 kPa. The cyclic footing load in T9 did not affect the capability of the soil arching on transferring the applied pressure to the stationary supports. Also, applying constant static and cyclic footing loading during the trapdoor tests in T4 and T10 did not affect the capability of the soil arching under the footing loading.
- By increasing the trapdoor displacement by 7.0 mm in T2 as compared with those in T3, the settlement of the footing increased by 52% at an applied pressure of 50 kPa . At the same level of the applied pressure, the applying cyclic loading instead of static loading increased the settlement of the footing by 60% as T3 compared to T9. However, mobilization of soil arching under the static and cyclic footing load, as in T4 and T10 respectively, reduced the induced settlement under the footing due to the pre-loading densification effect.
- The soil arching degradation pressure in both T3 and T9 was equal to 54.0 kPa, while in T4 and T10 it was equal to 45.3 and 45.0 kPa, respectively.
- Four tests were conducted with a **single layer of geosynthetic reinforcement** to assess the benefit of geosynthetic inclusion on the stability of the soil arching. In these tests, as the applied footing pressure increased, the geosynthetic carried some load so that the measured pressures at TC and TE below the geosynthetic were lower than those above the geosynthetic. The pressure at SE below the geosynthetic was higher than that above the

geosynthetic because of the vertical component of the geosynthetic tension due to the tensioned membrane effect.

- The biaxial geogrid reduced the applied pressure within the trapdoor area in T6 as compared with that of T2 by 59% at the center and 124% at the edges of the trapdoor at an applied static pressure of 50 kPa. At the same applied pressure, the geogrid increased the pressure transferred to the stationary supports by 90% and 71% in T5 and T6, respectively, as compared to T2.
- Geosynthetic reinforcement reduced the settlement of the footing by 23.3% in T5 and 39.1% in T6 as compared with that of T2 at an applied static pressure of 80 kPa. At the same applied pressure, cyclic loading increased the settlement of the footing by 67.3% using the uniaxial geogrid and 81.4% using the biaxial geogrid as compared with that by static loading.
- The SADPs in T5 and T6 were equal to 69.8 and 100.8 kPa under the static footing pressure, respectively, while the SADP in T2 was equal to 50.5 kPa. Therefore, the uniaxial geogrid increased the SADP by 38.2% while the biaxial geogrid increased the SADP by 99.6 %. This comparison proved the benefit of the geosynthetic reinforcement in maintaining the soil arching stability. Moreover, in the reinforced tests, geosynthetic reinforcement increased the SADP under cyclic footing loading as compared with that under static loading by 17.5% and 9.13 % in T11 and T12, respectively.
- Three tests were carried out with **double layers of geosynthetic reinforcement** to study the behavior of the load transfer platform (i.e., beam effect) under footing loading. An additional layer of geosynthetic reinforcement further reduced the settlement of the footing by 23.0% in T7a and T7b as compared with T6 at an applied static pressure of 80 kPa.

Also, the use of double layers of geosynthetic reinforcement reduced the footing settlement by 71% as compared with that without reinforcement. At the same magnitude of the applied pressure, the application of cyclic loading instead of static loading increased the settlement of the footing by 108%.

- The static SADPs in T7a and T7b were 58.3 and 52.8 kPa, respectively, while the SADP in T13 was 54.3 kPa. Even though the load transfer platform (i.e., the beam effect) reduced the settlement of the footing, it had a negative effect on the stability of the soil arching under the footing loading. It is believed that the trapdoor was not displaced enough during the trapdoor test stage to mobilize the geosynthetic strength with the presence of the upper geosynthetic layer in order to sustain the applied pressure.

## CHAPTER 6 CONCLUSIONS AND RECOMMENDATIONS

### 6.1 CONCLUSIONS

In this research, laboratory tests were conducted to assess the mobilization as well as the stability of soil arching under soil self-weight and surface loading. Trapdoor model tests under a plane strain condition were conducted to mobilize soil arching. Subsequently, static and cyclic footing loads were utilized to simulate traffic loading. The arching phenomenon associated with the unreinforced and geosynthetic-reinforced embankments was investigated. Based on the test results, the following main conclusions can be made:

1. Soil arching developed under soil self-weight as the trapdoor displacement increased in both unreinforced (and also under soil self-weight and surface loading) and reinforced embankments so that the pressure on the trapdoor decreased and that on the supports increased.
2. The progressive displacement of the trapdoor affected the mobilization of soil arching. Soil arching started to deteriorate under soil self-weight as the trapdoor displacement increased to more than 2.5% of its width. However, the use of geosynthetic reinforcement prevented the deterioration of soil arching although the trapdoor was displaced more than 4% of its width.
3. Reducing the trapdoor displacement by 7.0 mm resulted in more stable soil arching so that more applied pressure was transferred to the stationary supports under both static and cyclic footing loading. Also, the settlement of the footing decreased by 52% at an applied static pressure of 50 kPa.
4. The soil arching degradation pressures in the unreinforced tests under static and cyclic loading were the same and equal to 54.0 kPa. However, mobilization of soil arching under

static and cyclic footing loading reduced the soil arching degradation pressure to 45.0 kPa. Although the application of a footing load during the trapdoor test did not affect the mobilization of soil arching, it increased the probability of the arching collapse during the service life.

5. In the geosynthetic-reinforced embankment, the pressure below the geosynthetic continued decreasing as the trapdoor displacement increased. Due to the lateral restraint and the tensioned membrane effect, the geosynthetic helped transfer more embankment load onto the supports. This result implies that the geosynthetic prevented soil arching from deterioration under self-weight and helped maintain more stable soil arching.
6. Geosynthetic reinforcement lowered the equal settlement plane. Therefore, the geosynthetic not only helped stabilize soil arching but also kept the differential settlement far below the embankment surface.
7. The geosynthetic reduced the applied pressure within the trapdoor area by about 59% at the center and 124% at the edges of the trapdoor at an applied static pressure of 50 kPa as compared to those in the unreinforced embankment.
8. Geosynthetic reinforcement reduced the settlement of the footing by 23% - 39% as compared to that in the unreinforced embankment at an applied static pressure of 80 kPa. However, applying cyclic loading increased the settlement of the footing by about 67.3% - 81.4% as compared to applying static loading.
9. The geosynthetic reinforcement minimized the increase of the soil arching ratio under the static footing load as compared with the case without a geosynthetic. The soil arching degradation pressure was increased from the unreinforced embankment to the reinforced embankment by 38.2% and 99.6% using the uniaxial and biaxial geogrids, respectively.

10. Moreover, in the reinforced embankment tests, the geosynthetic reinforcement increased the soil arching degradation pressure under cyclic footing loading as compared to that under static loading by 17.5% and 9.13 % using the uniaxial and biaxial geogrids, respectively.
11. Double layers of geosynthetic reinforcement, as well as the soil in between, functioned as a beam since the maximum strain occurred at the trapdoor centerline in the lower geogrid layer and at the stationary supports edges in the upper geogrid lower.
12. The settlement of the footing in the double geosynthetic-reinforced fill decreased by 71% as compared to that without reinforcement at the applied static pressure of 80 kPa. Therefore, introducing an additional layer of geosynthetic reinforcement further reduced the settlement of the footing by 23.0% as compared to using the single geosynthetic layer.
13. The soil arching degradation pressure required for the double geosynthetic reinforced tests were lower than those in the single geosynthetic reinforced tests. Even though the load transfer platform (i.e., the beam effect) reduced the settlement of the footing, it had a negative effect on the stability of the soil arching under the footing loading.

## **6.2 RECOMMENDATIONS FOR FUTURE STUDY**

The following topics are recommended for future studies:

1. To investigate soil arching mobilization under a higher level of applied pressure, especially for cyclic loading during a trapdoor test since in this study the applied pressure was 8.2% of its ultimate bearing capacity.
2. To assess the soil arching degradation pressure by allowing the trapdoor to move during the loading test to simulate the behavior of foundation soil. When larger displacement is allowed, the geosynthetic would mobilize its higher strength and is expected to increase the soil arching degradation pressure.
3. To conduct a numerical analysis to study the interaction between the key load transfer mechanisms with multiple layers of reinforcement in the geosynthetic-reinforced pile-supported embankment, such as soil arching, tensioned membrane or beam effect, and stress concentration.

## REFERENCES

- Adachi, T., Kimura, M., and Tada, S. (1989). "Analysis on the preventive mechanism of landslide stabilizing piles." *Proceedings of the 3rd International Symposium Held In Niagara Falls, Canada, 8-11 May 1989*. Publication of: Elsevier Applied Science Publishers Limited, 15(3), 691-698.
- Agaiby, S. W., and Jones, C. J. (1995). "Design of reinforced fill systems over voids." *Canadian geotechnical journal*, 32(6), 939-945.
- Agaiby, S. W., and Jones, C. J. (1996). "Design of reinforced fill systems to support footings overlying cavities." *Geotextiles and Geomembranes*, 14(1), 57-72.
- Atkinson, J., and Potts, D. (1977). "Stability of a shallow circular tunnel in cohesionless soil." *Geotechnique*, 27(2), 203-215.
- Bell, A., Jenner, C., Maddison, J., and Vignoles, J. (1994). "Embankment support using geogrids with vibro concrete columns." *Proc., Proceedings, 5th International Conference on Geotextiles, Geomembranes, and Related Products*, 335-338.
- Bertin, Y. (1978). *A Centrifuge Study of the Collapse of Hemispherical Cavities in Soil.*, M.Sc. Thesis, University of Florida, Gainesville, Florida.
- Bhandari, A. (2010). *Micromechanical Analysis of Geosynthetic-Soil Interaction Under Cyclic Loading*. Ph.D. Dissertation, the University of Kansas.
- Bosscher, P. J., and Gray, D. H. (1986). "Soil arching in sandy slopes." *Journal of Geotechnical Engineering*, 112(6), 626-645.
- British Standard 8006, B. (2010). Code of Practice for Strengthened/Reinforced Soils and Other Fills." British Standard Institution, London, UK.

- Broms, B., and Wong, I. (1985). "Embankment piles." *Proc., Proceedings of 3rd International Geotechnical Seminar—Soil Improvement Methods*, Singapore: Nanyang Technological Institute, 167-178.
- Card, G., and Carter, G. (1995). "Case history of a piled embankment in London's Docklands." *Geological Society, London, Engineering Geology Special Publications*, 10(1), 79-84.
- Carlsson, B. (1987). "Reinforced soil, principles for calculation." *Terratema AB*, Linköping (in Swedish).
- Chen, H. L., Chen, S. E., and Kiger, S. A. (1991). "An experimental study of dynamic soil arching." *Proceedings of the 62nd Shock and Vibration Symposium*, (1), (Defense Nuclear Agency, Springfield, Virginia), 190-198.
- Chen, R., Chen, Y., Han, J., and Xu, Z. (2008). "A theoretical solution for pile-supported embankments on soft soils under one-dimensional compression." *Canadian Geotechnical Journal*, 45(5), 611-623.
- Collin, J. (2003). *NHI Ground Improvement Manual—Technical Summary# 10: Column Supported Embankments*. National Highway Institute, Arlington, Va.
- Dancygier, A., and Karinski, Y. (1999). "A simple model to assess the effect of soil shear resistance on the response of soil-buried structures under dynamic loads." *Engineering Structures*, 21(12), 1055-1065.
- Delmas, P. (1979). *Sols Renforcés par Géosynthétiques-Premières études.*, Ph.D. Dissertation, Université Scientifique et Médicale de Grenoble.
- Demerdash, M. A. (1996). *An Experimental Study of Piled Embankments Incorporating Geosynthetic Basal Reinforcement*. Ph.D. Dissertation, the University of Newcastle-upon-Tyne, 158 p.

- Einstein, H. H., and Schwartz, C. W. (1979). "Simplified analysis for tunnel supports." *Journal of Geotechnical and Geoenvironmental Engineering*, ASCE, 109(1), 15-39.
- Evans, C. H. (1983). *An Examination of Arching in Granular Soils.*, M.Sc. Thesis, Massachusetts Institute of Technology, 235p.
- Feld, J. (1948). "Early history and bibliography of soil mechanics." *Proc., communication présentée à Second International Conference on Soil Mechanics and Foundation Engineering*, Rotterdam, (1), 1-7.
- Finn, W. L. (1963). "Boundary value problems of soil mechanics." *Journal of Soil Mechanics and Foundation Division*, ASCE, 89(5), 39-72.
- Gabr, M., and Han, J. (2005). "Geosynthetic reinforcement for soft foundations: US perspectives." *International Perspectives on Soil Reinforcement Applications*. ASCE, 1-17.
- Gabr, M., and Hunter, T. (1994). "Stress-strain analysis of geogrid-supported liners over subsurface cavities." *Geotechnical & Geological Engineering*, 12(2), 65-86.
- Getzler, Z., Komornik, A., and Mazurik, A. (1968). "Model study on arching above buried structures." *Journal of Soil Mechanics & Foundations Div.*, 94(5), 1123-1142.
- Giroud, J. P. (1984). "Geotextiles and Geomembranes Definitions, Properties and Design: Selected Papers, Revisions and Comments." Industrial Fabrics Association International, 404p.
- Giroud, J., Bonaparte, R., Beech, J., and Gross, B. (1990). "Design of soil layer-geosynthetic systems overlying voids." *Geotextiles and Geomembranes*, 9(1), 11-50.
- Giroud, J., and Han, J. (2004). "Design method for geogrid-reinforced unpaved roads. I. Development of design method." *Journal of Geotechnical and Geoenvironmental Engineering*, 130(8), 775-786.

- Gourc, J., and Villard, P. (2000). "Reinforcement by membrane effect: Application to embankments on soil liable to subsidence." *Proc., Proceedings of the 2nd Asian Geosynthetics Conference*, (1), 55-72.
- Han, J. (1999). "Design and construction of embankments on geosynthetic reinforced platforms supported by piles." *Proceedings of 1999 ASCE/PaDOT Geotechnical Seminar*, 66-84.
- Han, J. (2015). *Principles and Practice of Ground Improvement*, John Wiley & Sons, Hoboken, New Jersey, USA, June, 432p.
- Han, J., and Bhandari, A. (2009). "Evaluation of geogrid-reinforced pile-supported embankments under cyclic loading using discrete element method." *Proc., US-China Workshop on Ground Improvement Technologies*, 73-82.
- Han, J., Bhandari, A., and Wang, F. (2011). "DEM analysis of stresses and deformations of geogrid-reinforced embankments over piles." *International Journal of Geomechanics*, 12(4), 340-350.
- Han, J., and Gabr, M. (2002). "Numerical analysis of geosynthetic-reinforced and pile-supported earth platforms over soft soil." *Journal of geotechnical and geoenvironmental engineering*, ASCE, 128(1), 44-53.
- Han, J., Wang, F., Xu, C., and Al-Naddaf, M. (2016). "Fully-mobilized soil arching versus partially-mobilized soil arching." *2016 International Conference on Transportation Infrastructure and Materials*, July 16-18, 2016, Xi'an, China.
- Handy, R. L. (1985). "The arch in soil arching." *Journal of Geotechnical Engineering*, 111(3), 302-318.

- Harris, G. (1974). "A sandbox model used to examine the stress distribution around a simulated longwall coal-face." *Proc., International Journal of Rock Mechanics and Mining Sciences & Geomechanics Abstracts*, Elsevier, 325-335.
- Helwany, S. M., and Chowdhury, A. (2000). *Dynamic Lateral Earth Pressure on Underground Structures*. Research Report, submitted to Air Force Office of Scientific Research, 68p.
- Hewlett, W. (1984). *The Analysis and Design of Bridge Approach Support Piling*. Part I project report, Cambridge University Engineering Department.
- Hewlett, W., and Randolph, M. (1988). "Analysis of piled embankments." *Ground Engineering*, 21(3), 12-18.
- Holmberg, S. (1979). "Bridge approaches on soft clay supported by embankment piles." *Geotechnical Engineering*, 10(1).
- Holtz, R., and Massarsch, K. (1976). "Improvement of the stability of an embankment by piling and reinforced earth." *Proc., Sechste Europaeische Konferenz Fuer Bodenmechanik und Grndbau, (1)*.
- Huang, J., Han, J., and Collin, J. G. (2005). "Geogrid-reinforced pile-supported railway embankments-three dimensional numerical analysis." *Journal of Transportation Research Board*, 1936, 221-229.
- Jang, D., and Montero, C. (1993). "Design of liner systems under vertical expansions: an alternative to geogrids." *Proceedings of Geosynthetics, Canada Vancouver, BC:[sn], (3)*, 1487-1510.
- Janssen, H. (1895). "Versuche über getreidedruck in silozellen." *Zeitschr. d. Vereines deutscher Ingenieure*, 39(35), 1045-1049.

- Jones, C., Lawson, C., and Ayres, D. (1990). "Geotextile reinforced piled embankments." *Proc., of the 4th International Conference on Geotextiles: Geomembranes and Related Products*, Rotterdam, 155-160.
- Kempfert, H., Göbel, C., Alexiew, D., and Heitz, C. (2004). "German recommendations for reinforced embankments on pile-similar elements." *Proc., EuroGeo3-third European Geosynthetics Conference, Geotechnical Engineering with Geosynthetics*, Deutsche Gesellschaft für Geotechnik, Munich, Germany, 279-284.
- Kezdi, A. (1975). "Lateral earth pressure." *Foundation engineering handbook*, Van Nostrand Reinhold company, New York, 197-220.
- Koutsabeloulis, N., and Griffiths, D. (1989). "Numerical modelling of the trap door problem." *Geotechnique*, 39(1), 77-89.
- Ladanyi, B., and Hoyaux, B. (1969). "A study of the trap-door problem in a granular mass." *Canadian Geotechnical Journal*, 6(1), 1-14.
- Low, B., Tang, S., and Choa, V. (1994). "Arching in piled embankments." *Journal of Geotechnical Engineering*, 120(11), 1917-1938.
- Magnan, J. P. (1994). "Methods to reduce the settlement of embankments on soft clay: a review." *Proc., Vertical and Horizontal Deformations of Foundations and Embankments*, ASCE, 77-91.
- Marston, A. (1930). "The theory of external loads on closed conduits in the light of the latest experiments." *Highway Research Board Proceedings*, (9).
- McNulty, J. W. (1965). *An Experimental Study of Arching in Sand*. Rep. No.I-674, US Army Engineer Waterways Experiment Station, Corps of Engineers, Vicksburg, Mass.,170.

- Miki, H. (1997). "Design of deep mixing method of stabilization with low improvement ratio." *Proc., of the first seminar on ground improvement in highways*, Bangkok, Thailand, 197-204.
- Reichman, O., and Smith, S. C. (1990). "Burrows and burrowing behavior by mammals." Chapter 5, in *Current Mammalogy*, H.H. Genoways (ed.), Plenum Press, New York and London, 197-244.
- Reid, W., and Buchanan, N. (1984). "Bridge approach support piling." *Piling and ground treatment*, Thomas Telford Publishing, 267-274.
- Russell, D., and Pierpoint, N. (1997). "An assessment of design methods for piled embankments." *Ground Engineering*, 30(10), 39-44.
- Spangler, M. (1964). "Protection of underground structures by arch action associated with the imperfect ditch method of construction." *Proc., of the Symposium on Soil-Structure Interaction*, the University of Arizona, Tucson, Arizona, 531-546.
- Spangler, M., and Handy, R. (1973). "Loads on underground conduits." *Soils Engineering*, New York, (3), 658-686.
- Terzaghi, K. (1936). "Stress distribution in dry and in saturated sand above a yielding trap-door." *Proceedings of First International Conference on Soil Mechanics and Foundation Engineering*, Cambridge, Massachusetts, 307-311.
- Terzaghi, K. (1943). *Theoretical Soil Mechanics*, John Wiley & Sons, New York, 66-76.
- Tsur-Lavie, Y., Denekamp, S., and Fainstein, G. (1988). "Surface subsidence associated with long wall mining: Two and three dimensional boundary element model." *Geological Society, London, Engineering Geology Special Publications*, 5(1), 225-231.

- Wang, F., Han, J., Miao, L.-C., and Bhandari, A. (2009). "Numerical analysis of geosynthetic-bridged and drilled shafts-supported embankments over large sinkholes." *Geosynthetics International*, 16(6), 408-419.
- Wang, M., Feng, Y., and Jao, M. (1996). "Stability of geosynthetic-reinforced soil above a cavity." *Geotextiles and Geomembranes*, 14(2), 95-109.
- Wu, T., and Leonards, G. (1985). "Characterization of soil arching above buried conduits." *Advances in Underground pipeline engineering*, ASCE, 396-407.

# APPENDICES

## APPENDIX A TRAPDOOR TEST RESULTS

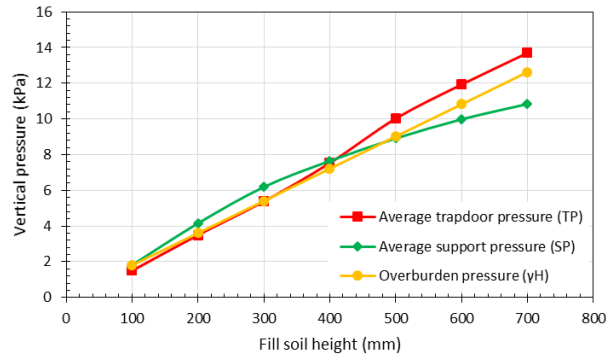


Figure A.1 Measured pressures on and besides the trapdoor during the fill construction in T9

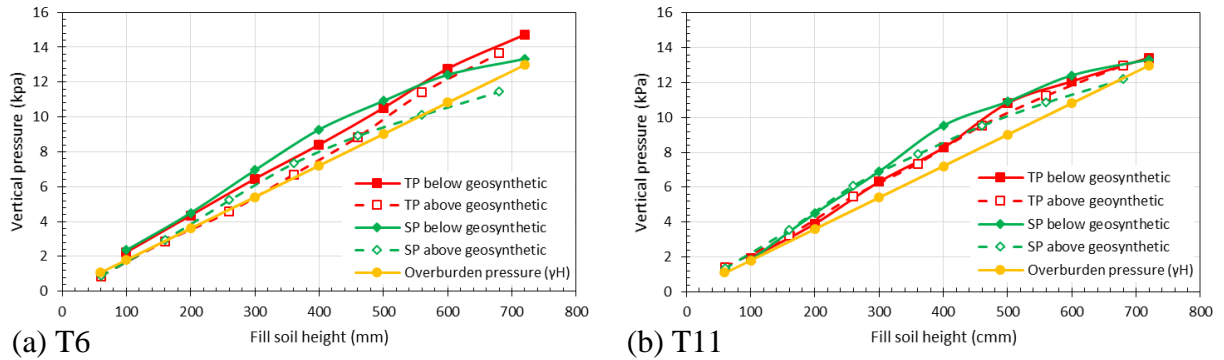


Figure A.2 Measured pressures on and besides the trapdoor during the fill construction in the single layer of geosynthetic-reinforced tests: (a) T6 and (b) T11

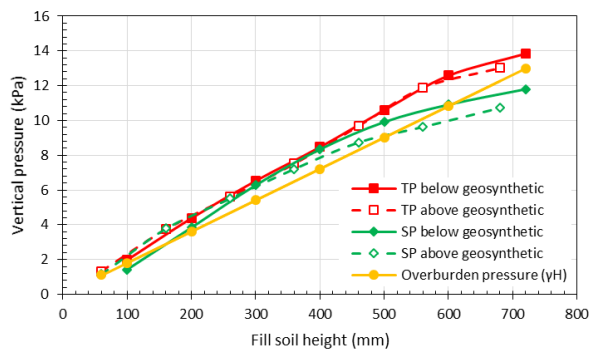


Figure A.3 Measured pressures on and besides the trapdoor during the fill construction in the double layer of geosynthetic-reinforced test in T7b

## APPENDIX B LOADING TEST RESULTS

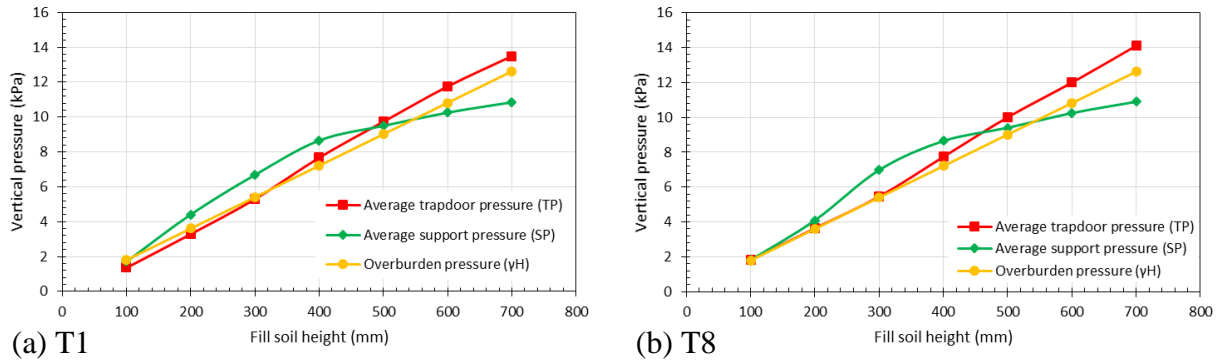


Figure B.1 Measured pressures on and beside the trapdoor during the fill construction of the baseline tests: (a) T1 and (b) T8

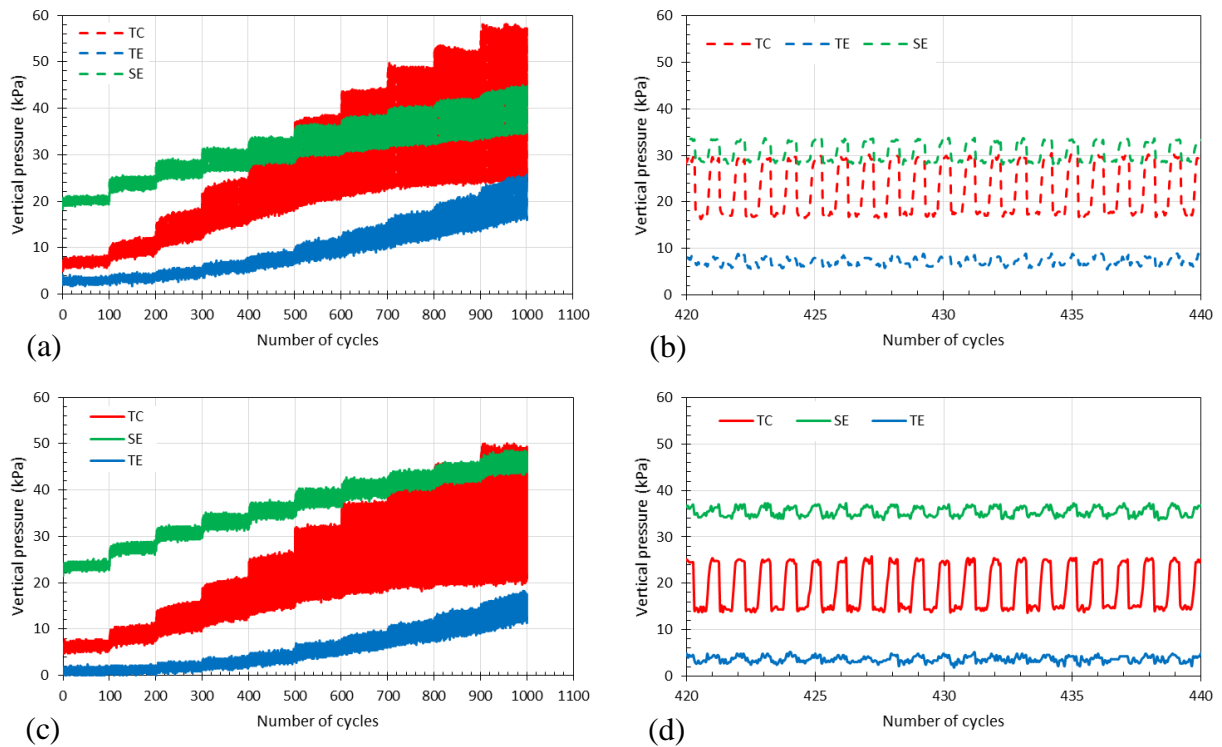


Figure B.2 Measured pressures over and beside the trapdoor versus the number of cycles in the loading test T11 (a) above the geosynthetic, (b) enlargement of (a) for the cycles No. 420 to 440, (c) below the geosynthetic, and (d) enlargement of (c) for the cycles No. 420 to 440

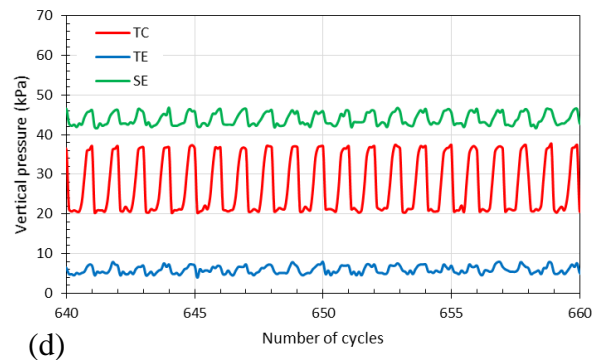
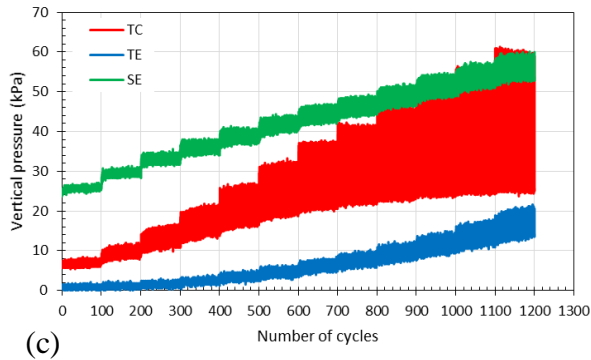
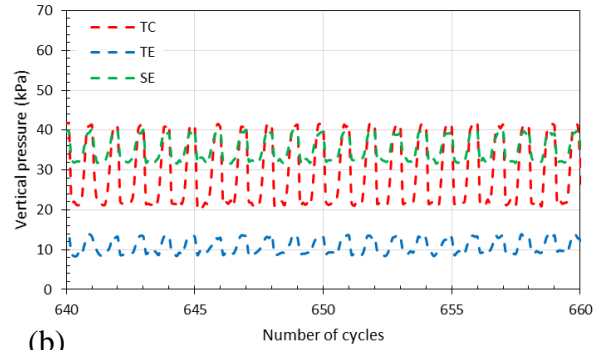
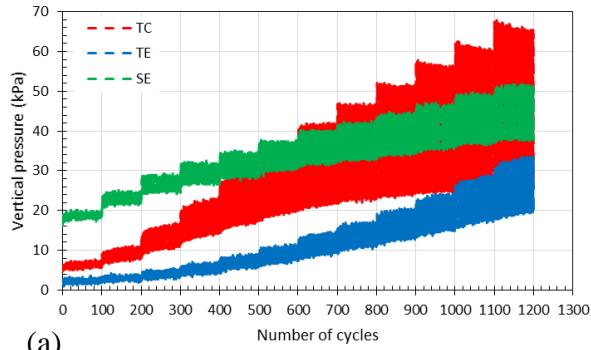


Figure B.3 Measured pressures over and besides the trapdoor versus the number of cycles in the loading test T12 (a) above the geosynthetic, (b) enlargement of (a) for the cycles No. 640 to 660, (c) below the geosynthetic, and (d) enlargement of (c) for the cycles No. 640 to 660

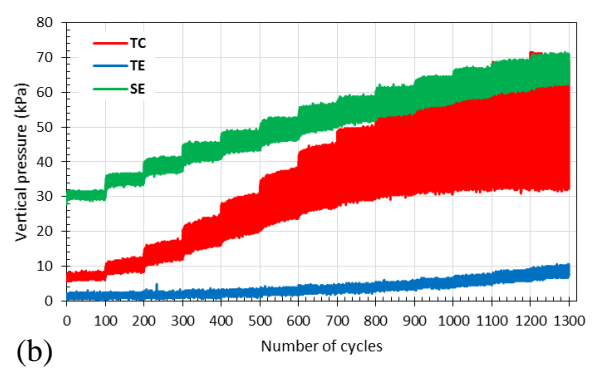
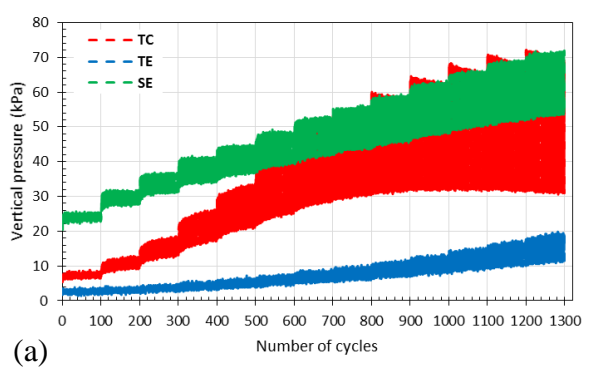


Figure B.4 Measured pressures over and besides the trapdoor versus the number of cycles in the loading test T13 (a) above the geosynthetic and (b) below the geosynthetic